Study into the Synthesis, Characterisation and Applications of Vanadium-based Metal Organic Frameworks, using 1, 2, 4, 5-Benzenetetracarboxylic Acid

A thesis submitted in the fulfilment of the requirements for a degree of:

Master of Science

To

Rhodes University

RHODES UNIVERSITY

By

Wesley Feldmann

March 17, 2016

ABSTRACT:

This study focussed on the synthesis, characterisation and catalytic application of synthesised vanadium-based Metal-Organic Frameworks using 1,2,4,5-benzenetetracarboxylic acid as a ligand. A number of synthetic methods were tested in multiple attempts to synthesise a V-MOF, these included; ambient, gel, reflux and solvothermal methods of synthesis. Two products of interest were identified, an ambient synthesis produced a vanadium-based complex with the empirical formula: $V_2O_2(Na_2H_2B4C)\cdot 6H_2O$ (RU-V2) and a solvothermal synthesis produced a MOF with the empirical formula: $V_2O_2(H_2O)_2(B4C)$ (RU-V1). Both products were characterised using elemental analysis, infrared spectroscopy, thermogravimetric analysis, differential scanning calorimetry and X-ray powder diffraction.

The catalytic activity of these products was tested, alongside the activity of the solid decavanadate ion, for the conversion of cyclohexene to cyclohexene oxide. The decavanadate ion was included to determine if the ion was catalytically active in the solid state, to potentially be used in the construction of a future MOF or V-complex. The reaction for the conversion of cyclohexene to cyclohexene oxide was chosen, as it has been previously conducted using a V-MOF and was found to be successful. The product of the reaction, the epoxide: cyclohexene oxide, is a very useful precursor for a number of reactions involved in the pharmaceutical industry, so developing catalysts which are able to convert cyclohexene to the epoxide with high yields and selectivities are well sought after in industry.

The results of the catalytic reactions were varied, as the materials exhibited high yields and selectivities to the epoxide, but these results were only obtained when water was present in the reaction mixture. Water was able to bring about the cleavage of the bonds between the metal and ligand in a highly coordinated framework, at a faster rate than other solvents, such as decane. This ultimately leads to the structural decomposition of the entire complex or framework, depending upon the reaction time. The use of water was a double edged sword in that it was required to initiate the catalytic reaction, but was also the reason that the catalytic materials were noted to decompose over time. The solid decavanadate ion was only noted to exhibit homogeneous activity by dissolving into the small volume of water present in the reaction mixture.

The study proved that using a multidentate ligand such as 1,2,4,5-benzenetetracarboxylic acid yielded products which were highly coordinated in nature and would therefore not have large open spaces associated with them, which is commonly observed with other MOFs. Instead the closed nature of the synthesised complexes and frameworks offered a different environment for catalytic reactions, where the small pores/channels had a controlling and inhibiting effect on the reaction. The conversion of cyclohexene to the

epoxide is accompanied with a number of undesired side products, so when using the synthesised closed-natured MOF, it was found that there was a greater selectivity for the epoxide over other potential products. This indicates that close natured MOFs may find application in catalytic reactions which require high selectivities for a particular product.

ACKNOWLEDGEMENTS:

I would like to acknowledge the following people and organisations for their help throughout the duration of this thesis. The time spent answering my numerous questions and general help given is greatly appreciated.

- Prof G. M. Watkins for his advice, supervision and guidance over the course of this thesis.

- Mr F. Chindeka and Mr H. Keulder for their assistance in the operation, maintenance and repair of the equipment used, ranging from CHNS analyses to pH meters.

- Mr A. Adriaan and Mr H. L. R. Douglas for their assistance with any glass-blowing that was required and any other odd jobs that needed completion.

- The Center for Nanotechnology Innovation (NIC) for allowing me to use their XRPD equipment and specifically Dr J. Britton for his assistance in the running of the equipment.

- Mr M. Randall (Rhodes Electron Microscopy Unit) for teaching me to use the SEM and aiding in the acquisition of the images.

- Dr N. Richoux for allowing me to use the GC-MS in the Zoology Department for my catalytic studies.

- Mrs B. Tarr, Mrs B. L. Ah Yui and Mrs G. Cobus for their help with all administrative matters.

- Dr C. Veale and Dr R. Klein for their advice and aid with all things catalytic.

- Mr U. Mpiti, Mr S. Hulushe, Mr I. Hodgson and all my other lab-mates from F5 and F12 for their constant company, assistance and support with any issues faced.

- Rhodes Chemistry Department, all my colleagues and friends, for providing me with ideas for my study, interesting conversation and general support.

- My family and friends for their support of me and my thesis, specifically my mother Mrs J. M. Feldmann for her assistance with formatting and editing.

- The National Research Fund (NRF) for the funding of my Masters studies.

TABLE OF CONTENTS

LIST OF FIGURES:

LIST OF TABLES:

LIST OF APPENDICIES:

LIST OF INSTRUMENT APPENDICES:

LIST OF ABBREVIATIONS:

B2C and BDC = 1,4 – Benzenedicarboxylic acid (H_2B2C).

B3C and BTC = 1,3,5 – Benzenetricarboxylic acid (H_3B3C).

B4C and BTEC = 1,2,4,5 – Benzenetetracarboxylic acid (H_4B4C).

RU-V1 = $[V^{IV}_2O_2(H_2O)_2(B4C)]$ (Solvothermal Product).

RU-V2 = $V_2O_2(Na_2H_2B4C)\cdot 6H_2O$ (Ambient Product).

MIL-47 = V-MOF used by Van Der Voort et al for catalytic applications.

MIL = Materials Institute Lavoisier.

COMOC = Center for Ordered Materials, Organometallics and Catalysis, Ghent University.

HKUST = Hong Kong University of Science and Technology.

1. INTRODUCTION

1.1 Metal-Organic Frameworks

Metal organic frameworks (MOFs) are a class of crystalline compounds, which have gained research attention since the late 1990s [1]. MOFs are infinite lattice structures, which are built up from metal centres and organic ligands, which coordinate to one another to form a repeating unit and ultimately build up to an infinite network [1-2]. Metals act as centres or vertices, to which the ligands can bind and each metal has their own coordination preference, which depends on factors, such as their size and the number of electrons in their valence shell [1-3]. Ligands branch out from the metal centres, linking the entire structure together. With the great number and variety of ligands, each with their own specific structure and number of coordination sites, this ultimately leads to a huge number of potential structures which the MOFs can adopt, this is referred to in more detail in the following sections [1-2].

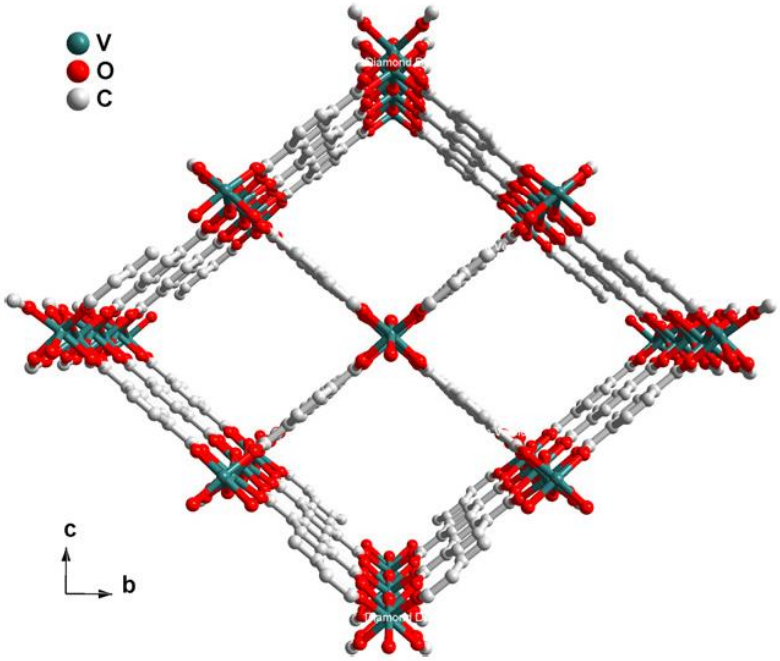

Figure 1: MIL-47, an example of the structure of a MOF [4].

Figure 1 is used to show an example of the general structure of a MOF, where one can observe the metal centres, in this case vanadium octahedra, coordinated together via an organic ligand or linker, 1,4-benzenedicarboxylic acid.

When searching into the literature on work completed in the field of MOFs, one can gain an idea of the number of MOFs synthesised and applied in various areas of chemistry. The most common metals reported in literature are copper and zinc, owing to their versatility of co-ordination [1][5]. The most common ligands used are benzene carboxylates, specifically 1,4-benzenedicarboxylic acid, as these ligands tend to form relatively strong coordination bonds, owing to the oxygen donor group of the carboxylic acid, and are structurally rigid, owing to the inclusion of the benzene ring in their structure. These are the most common starting materials which have made up the most studied MOFs, but there has still been a substantial amount of research into synthesising MOFs using different types of starting materials to create a unique framework and study its properties. Alternate ligands have been used in synthesis to build a more flexible framework. Nitrogen donor ligands have been used [6-7] and the use of two ligands has been attempted to build up unique structural frameworks [6]. A number of bimetallic MOFs have been synthesised and studied [8-10].

The frameworks can be designed to be 1, 2 or 3 dimensional in structure, with 2 and 3 dimensional structures most often designed to be porous, which is the key property of MOFs. When porous, their structure will contain spaces or voids which act to greatly enhance the surface area of the framework [1-2]. Arguably, the most important ability of the pores is the inclusion of smaller molecules, referred to as 'guest molecules' and gives MOFs application into a wide range of different fields [1-4]. 3 Dimensional structures can have 2 dimensional planes stacked on top of one another; this can allow the pores to be stacked and can create channels which are able to propagate through the MOF. The pores and channels are generally uniform in size and shape due to the structure of the MOF being highly ordered and the fashion in which binding occurs. The pores have the ability to be designed by selecting the starting materials which have the potential to form pores with dimensions suitable for a specific application and can therefore be said to be 'tunable' [1-4]. These void areas are often filled by solvent molecules, which can often be integral to the structural integrity of the framework, as their removal may cause structural collapse [1].

Most MOFs, however, do not collapse upon the removal of the initial solvent molecules, so can be defined as displaying 'permanent microporosity'. This is important for almost all applications, as it allows for continuous desorption and re-absorption of a molecule of interest from the pores or channels [1-2].

Due the structure and porosity associated with MOFs, one can readily compare them to the well-known alumina-silicate structures known as Zeolites. Zeolites are highly porous alumina-silicate minerals which are completely inorganic in structure and have a number of applications [11]. Zeolites have the advantage in that their structures are incredibly rigid and strong, leading to them being used in a number of reactions which are carried out under harsh condition, such as elevated temperatures and pressures. Zeolites have disadvantages however, as they only exhibit a certain number of pore sizes, due to their fixed tetra- and octahedral co-ordination of Si and Al, these are generally small, never reaching sizes greater than a nanometer [11]. This restricts them to the inclusion of relatively small molecules, which limits the amount of reactions that they can find application in, as a storage material or a catalyst. MOFs are more flexible than zeolites and can be synthetically produced with a specific purpose in mind, so they can be potentially 'tuned' for a wider range of applications [1].

Pore size, shape and structure of the MOF are largely dependent on the structure of the ligand. Two Examples of previously mentioned common ligands used in the syntheses of MOFs will be shown, the carboxylates; 1,4-benzenedicarboxylic acid (H_2B2C) and 1,3,5-benzenetricarboxylic acid (H_3B3C).

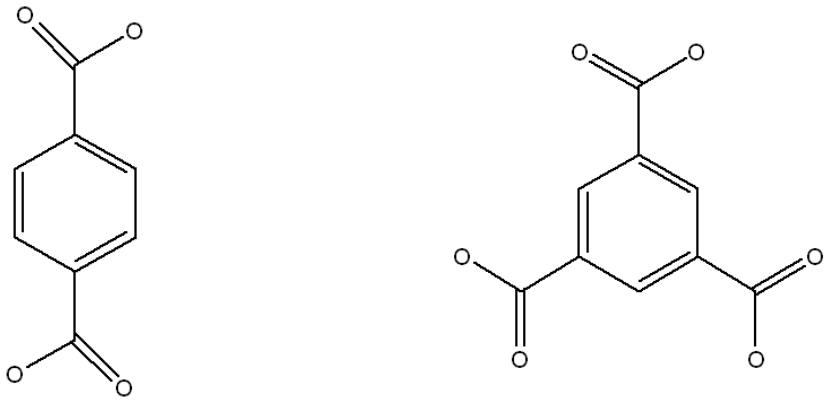

Figure 2: The structures of 1,4-Benzenedicarboxylic Acid (H_2B2C) and 1,3,5-Benzenetricarboxylic Acid (H_3B3C).

H_2B2C has a linear structure, so the angle between the co-ordination sites of the carboxylic acid functional groups is 180° and H_3B3C has a triangular or trigonal structure, so the angle between the carboxylic acid functional groups is 120°. This simple difference leads to major differences in terms of the possible pore sizes and shapes that can occur within a MOF. For H_2B2C the pores are generally square or cubic in shape, whereas for H_3B3C the pores are expected to have hexagonal shaped pores. This is also highly dependent on the oxidation state and coordination number of the metal.

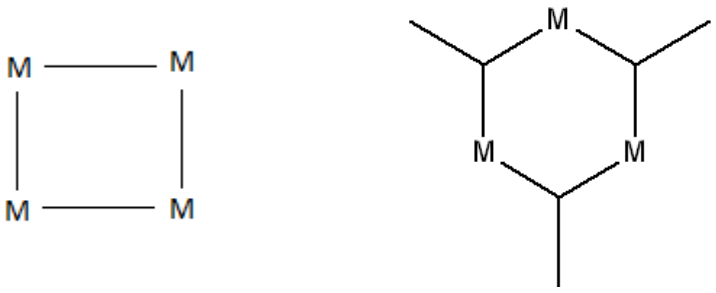

Figure 3: Basic pore shapes depending on Metal to Ligand coordination.

Ligands with a larger number of functional groups tend to have a larger number of coordination sites and this increases the structural complexity of the MOF that they are able to form. These frameworks tend to be highly coordinated and are termed as 'closed frameworks'. Frameworks can also have pores which overlap into one another, leading again to a 'closed framework', which lacks any substantial pore volumes, or has particularly small pore volumes [12]. Ligands with a lower number of coordination sites generally tend to produce MOFs with more open structures, leading to larger pore sizes and volumes.

Similarly, the choice of metal or metal oxide and its oxidation state, coordination number and geometry, will ultimately determine how the ligand/s are able to coordinate to it. The coordination number of a metal is dependent of the oxidation state and can range from 2 to 7. With such a large number of potential coordination sites associated with the metal and a large number of ligands with alternating geometries, the number of possibilities for creating a MOF with a unique structure is truly enormous [1][13].

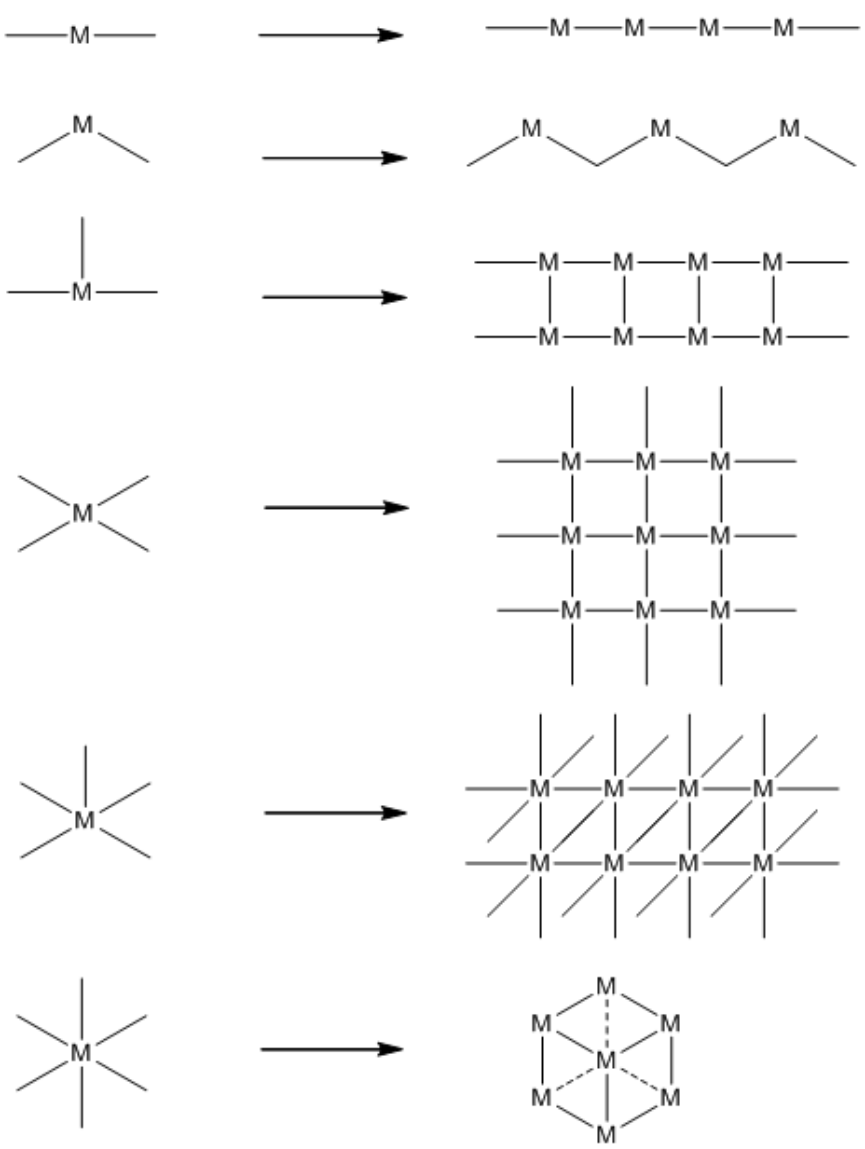

Figure 4: Examples of coordination geometry and the structures it can produce.

The geometric structures shown in Figure 4 are some of the most basic structures possible for the geometries of the metals shown. There are a multitude of other more complex structures that are possible, which are often able to propagate in 3 dimensions, especially when the coordination number is high [12-13].

An important factor to the structure of a MOF is the conditions under which it is synthesised. Zeolites have been synthesised using solvothermal methods, which employ high temperatures and pressures, resulting in a strongly bound and stable framework [11]. The solvothermal synthetic technique has been very successful for MOFs as well, resulting in

the most stable and crystalline of structures [1-3][12-13]. The solvothermal method involves elevated temperatures and pressures, in which the metal and ligand are forced into close proximity, allowing coordination to occur via alternate kinetic pathways, often yielding a strongly bound structure [1][13]. Most MOFs have been synthesised using this method, but other methods of synthesis have been successful, these can be listed as ambient precipitation, gel, microwave assisted, ultrasonic syntheses and mechanochemical methods of synthesis [14-19]. Within each synthetic method stated above, a number of factors can be further altered to bring about subtle changes to the structure. These factors include; altering the pH value under which the synthesis is completed at, as this may alter the coordination preference of the ligand used, altering the molar ratios of metal to ligand, altering the temperature and finally altering the solvent used for the synthesis [1][20]. All these factors can and are used, in attempts to synthesize a novel MOF with a unique structure and properties.

1.2 Applications of Metal-Organic Frameworks

MOFs have received a great deal of attention over the past two decades, as they have a variety of specific applications which different industries find useful. The major applications include; gaseous and liquid absorption, separation and purification, heterogeneous catalysis and sensory applications [1]. All these applications make use of the porous nature and large surface areas which MOFs exhibit.

1.2.1 Gas and Liquid Absorption, Separation and Purification

The first and most popular application where MOFs find use is in gas storage, which drew the initial attention to this class of coordination polymers. Most MOFs have been shown to exhibit large surface areas, upon which gas molecules can undergo physisorption, via van der Waals interactions, within the pores of the framework [1]. With such large surface areas, the materials are able to accommodate vast quantities of guest molecules per unit of MOF [1]. The storage of hydrogen using a MOF is a specific application, which has gained a great deal of attention, mainly due to the fact that fuel cells are a promising alternative to petroleum-based fuels [1][21]. Hydrogen is highly flammable and relatively hazardous to transport in a pressurised vessel, but whilst contained within a MOF, the molecules are separated and bound to pores, thereby removing the gases flammable and explosive nature [21]. The MOFs which have shown the most promising uptake of hydrogen have been Cu and Zn MOFs, e.g. a Cu-MOF (HKUST-1) and a Zn-MOF (MOF-177) exhibit the ability to uptake a remarkable quantity of hydrogen of up to 7.5 wt%, but only at temperatures near 77 K and pressures of 70 bar [22]. The conditions at which the maximum amount of hydrogen is stored is a limiting factor for MOFs at the moment, as maintaining the low temperature would

require a costly cooling method, so designing a MOF which can uptake the same quantity of hydrogen, but at a higher temperature would be ideal.

MOFs find application in the absorption of CO_2, which is of great importance as CO_2 is a well-known greenhouse gas, so having materials that are able to absorb CO_2 effectively before it is released into the atmosphere is beneficial to the environment. One of the MOFs which has shown the greatest ability to absorb CO_2 is MOF-177, as a cylinder filled with MOF-177 is able to hold 9 times the amount of a cylinder filled with pressurised CO_2[23]. The CO_2 molecules are known to exhibit a negative quadruple moment, so have been found to be bound to the positive metal centres [24], which gives an idea as to where the gas molecules are most concentrated within the MOF. MOFs containing flexible ligands are often able to be referred to as 'breathing' frameworks. 'Breathing' frameworks are able to exhibit slight structural changes when absorbing a guest molecule, which often increases the selectivity for a specific molecules, which has been commonly observed with the absorption of CO_2 [1][25-28]. V-MOFs are not able to compete with Cu and Zn MOFs in their ability to absorb hydrogen, instead V-MOFs have shown a remarkable ability to absorb CO_2 and nitrogen. A number of V-MOFs have been investigated to determine their ability to absorb CO_2 [25-28]. The most research has been focussed towards MIL-47, (see Figure 1; pg. 1), by functionalising it with different groups, particularly the OCH_3 group, which has shown absorptions of 5.9 mmol/g at 0 °C and 1 bar, which is amongst the highest of reported absorption values for those specific conditions thus far [28].

Gaseous and liquid separation and purification takes advantage of the guest inclusion properties of MOFs to remove an unwanted molecule from a solution or mixture. A MOF can be designed to be very selective for a certain compound, based on; polarity, size and shape [1]. A mixture will be exposed to the crystalline material, which will selectively absorb the compounds of interest, depending on the nature of the pores and their size, thereby separating the compound from the mixture and isolating it within the MOF. An example of a MOF being used as a separation material has been the absorption and separation of xylene isomers. Xylene isomers have proven to be difficult to separate from one another in high yields, as they only differ in terms of the position of their methyl substituents around the benzene ring. MOFs MIL-47 (V-MOF) and MIL-53 (Al-MOF) are capable of separating these isomers into yields of up to 40 wt% at 70°C, under mild pressures of 0.005 bar, which significantly exceeds that of standard zeolitic materials [1][29]. The mild pressures are required to ensure that the xylene isomers undergo molecular packing into the pores of the MOFs, which acts to greatly increase the selectivity for the particular xylene isomer which is undergoing the packing [1][29].

Using MOFs in this way can also be generally beneficial to the environment, as MOFs can act as a filter to absorb hazardous or toxic components, from the waste before being released.

1.2.2 Heterogeneous Catalysis

Heterogeneous catalysis is an application where Zeolites have found a great deal of application. MOFs are similar to Zeolites, in terms of their porous nature, so are also finding increased application as heterogeneous catalysts. Heterogeneous catalysts are widely sought after for industrial reactions, due to their ability to be regenerated to their initial structure, allowing for repeated use in the reaction of interest [1]. Zeolites are the most notable catalysts which are used in industrial reactions and have a number of advantages, such as; large surface areas, with well-defined pore sizes and high thermal stability, but have limited possibilities for structural alteration and functionalisation [1][11][30].
MOFs have the advantage of having the high surface areas, due to their porous nature, allowing a larger volume for the reactants to interact within the MOF and on its external surface when compared to non-porous heterogeneous catalysts. Pore and channel size are important for catalysis and MOFs have the advantage of having tunable pore sizes and great variety of functionalisation possibilities and thus have the potential to be used in a greater variety of reactions [1-3][30].

There are factors which limit the potential of MOFs as catalysts, the major being their inability to withstand the elevated temperatures and pressures which are often associated with industrial reactions [30]. This is due to the strength of the covalent bond between silica and oxygen, found in zeolites, which is stronger than the carbon to oxygen bond generally found in MOFs [11]. The second factor is that MOFs have shown that their metal centres that are coordinatively saturated to the ligand, which means that there are no immediate sites upon which catalytic conversion may occur [30-31]. This can be circumvented in several ways, as MOFs often have solvent molecules coordinated to the metal centre [4][30-32], which can be removed, opening up a vacant site for catalytic conversion to occur. Another option is for a labile bond between the metal and ligand, to detach, opening up a possible coordination site for catalysis. This process is, however, difficult to control, as the detachment of too many bonds may cause structural collapse of the MOF, which is most often observed when water is present, as it aids in the weakening of the metal to ligand bonds. This will be discussed in detail in Chapter 4 of this study.

MOFs are however able to bring about catalytic activity in a number of different ways, due to having inorganic and organic components within their structure. The most common method is direct coordination to the metal centre, e.g. vanadium catalysts and MOFs are generally in the V^{IV} state and are oxidised to the V^{V} state by the addition of an oxidant, which initiates catalytic conversion to the product [4][33]. The metal is not always limited to a single centre, but can be in the form of a cluster [34], chain [4] or sheet [35]. These options result in a higher concentration of metal centres per unit cell of the MOF, increasing the overall catalytic activity. MOFs containing two different metals are bimetallic and offer

interesting catalytic properties, as one metal may be integral to maintaining the structure of the framework, having no free co-ordination sites, whereas the other is coordinatively unsaturated and has free sites for catalysis [34]. An additional possibility is that both metals can be involved in catalysis, but follow two different reaction pathways.

The ligand is another way in which catalysis can be brought about, as conversion is able to occur via the catalytically active functional group, but the ligand as a whole, is still able to coordinate to the metal and create a strong bond. Viable ligands in this regard are rare and most often two ligands are used in unison to synthesise the MOF. There have been a few MOFs studied, which have shown catalytic activity through their ligand groups, e.g. 1, 3, 5-benzenetricarboxylic acid and tris[N-(4-pyridyl)amide] showed great activity and recyclability in a Knoevenagel condensation reaction when incorporated into a cadmium-based MOF [36].

The final way in which MOFs can aid in catalytic processes, is to simply act as an environment in which the reactants can react with one another. This is the least studied of the methods by which catalysis can occur, as any porous material has the ability to restrict the reactants to a confined environment, but MOFs may have an advantage, due to their tunable pore sizes [30-31].

1.2.3 Application as Sensors

MOFs find application in sensory devices as they are able to elicit a response due to a certain change that occurs within the structure of the MOF. The changes that MOFs are able to show and detect can be a result of a number of different processes. The first of these processes is known as solvatochromatism, which is simply the uptake of the guest molecule of interest, which in turn, brings about a colour change to the MOF. The colour change is due to either a symmetry change of the hybridized metal orbitals (in terms of valence bond theory) or a change in the polarity of the guest molecule [37-38]. This shifting causes a difference between the ground and excited states of the MOF, either increasing or decreasing the energy required to excite an electron to the next orbital. These differences between the ground and excited states are what determine the colour of the complex, so depending on the difference in energy, the colour will either shift more to the red or blue regions of the spectrum [37-38]. The second and most common process by which MOFs can be used as sensory materials takes advantage of luminescence-based sensing [39]. This involves either the use of aromatic or conjugated ligand groups, which are able to exhibit luminescence or by incorporating a lanthanide ion, which are well known to exhibit luminescence [39]. The luminescence process is either centred around the metal or ligand, or possibly a combination of both, as the ligand can transfer charge to the metal or vice versa [40]. Luminescence can also occur without the structure being emissive at all, in this process

the MOF uptakes a luminescent compound and in so doing there may be π-π interactions between the guest molecule and the ligand, which can be measured as the signal [40-41].

1.2.4 Other Applications

With the interest into MOFs growing over the past few decades, there have been a number of new applications where MOFs have found use.

An interesting application is in the field of drug synthesis and design, where the framework can be used to provide a limiting environment upon which drugs of a particular size may be synthesised. MOFs are also able to temporally contain a particular drug and deliver it to the area of interest within the body, thereby protecting it from metabolic processes, which would otherwise have broken it down. The limiting factor at the moment is the pores sizes available, as these tend to be small in comparison to what may be required for drug delivery [1][42].

Biomedical imaging is another area where MOFs have begun to find application. This is particularly interesting as gadolinium-based chelates are generally used as contrast agents in biomedical imaging techniques, such as MRI. This procedure works via the attachment of the chelate onto the diseased tissue, which allows for better sensitivity of up to 35% in the image, as the gadolinium chelates act as a contrast to the soft tissue, creating a clearer image [1]. Gd-MOFs have been developed to follow a similar function, but are limited due to the fact that the frameworks break down over time and under the physiological conditions, releasing Gd^{3+} ions, which are harmful and potentially can cause nephrogenic systematic fibrosis (NSF) [1].

1.3 Vanadium Chemistry with Selected Oxygen Donor Ligands

Vanadium acquired its name from the name of the Norse god of beauty, Vanadis, due to the strong colour changes it exhibits when changing between oxidation states in solution.

Table 1: Colours of vanadium at the various oxidation states.

Oxidation state	**Ion**	**Colour**
+5	VO_3^- or VO_2^+	Amber
+4	VO^{2+}	Blue
+3	V^{3+}	Green
+2	V^{2+}	Violet

Vanadium is a hard transition metal with a silver/grey colour and an atomic number of 23. It cannot be found in its pure form in nature, only stabilised in combination with other

elements, such as oxygen, in the form of compounds [43]. These compounds can be subjected to separation processes which results in the isolation of the pure metal, but this will immediately oxidise in air, causing a thin layer of vanadium oxide to coat the surface of the pure metal. Vanadium is a d^5 element, having 5 electrons in its valence orbital. It has 4 stable oxidation states, being; +5, +4, +3 and +2, which gives it the ability of forming an array of different compounds [43-46]. Vanadium compounds find use in a number of different industries, with the major application being in alloys. Due to the hardness of vanadium, it is used as an additive to increase the strength of steel alloys, this is due to vanadium being able to form very stable carbides and nitrites [43-46].

Vanadium, as with many other metals, forms metal oxides in an oxidative environment, such as the Earth's atmosphere. There are two major vanadium oxides, which are of particular interest to this study, the; vanadate and vanadyl ions. These compounds only differ in the charge associated with the vanadium centre and therefore form alternate metal oxides [43-46].

V-species are able to coordinate to one another, via oxo-bridging, to form larger, more complex species, which are known as polyoxometalates (POMs). Vanadium is one of the few metal's that is able to form POMs, this is due to its stability at high oxidation states and being a group 5 transition metal. It is generally observed that only group 5 and 6 transition metals are able to form POMs effectively [47]. A well-known V-POM is the decavanadate ion (see Figure 6; pg. 12) which will be discussed in detail in Chapter 4. The decavanadate ion forms from smaller vanadate ions bonded together under specific pH conditions to build up the large $V_{10}O_{28}$ structure, with its associated counter ions and water molecules [43].

1.3.1 The Vanadate Ion

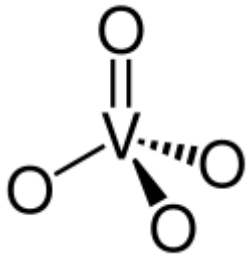

Figure 5: The basic orthovanadate ion, which has a tetrahedral geometry [48].

The vanadate ion contains a vanadium centre, which is in the 5+ oxidation state. There are a number of different vanadate compounds, which can become large and highly coordinated as the more basic vanadate compounds can coordinate to one another via edge and corner sharing, as shown below [49-51].

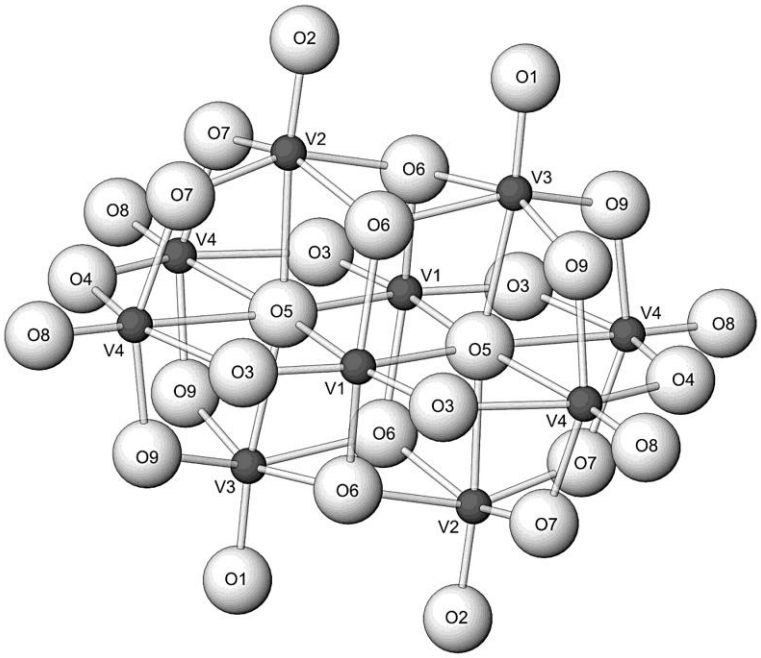

Figure 6: $V_{10}O_{28}^{6-}$ "Decavanadate", formed via edge and corner sharing of the VO_6 octahedra [52].

Vanadate compounds generally contain an oxoanion (the V-O species) bound to a counter ion, a cation, e.g. Na^+ or K^+, which balances the molecule to a neutral charge. The anion and cation are bound ionically to one another to form a stable and neutral compound, e.g. $NaVO_3$. The vanadates which will be used in this study are known as 'metavanadates', which are slightly different to the previously mentioned vanadates, as they are not distinct units, but are repeating units which bind together to form a chain.

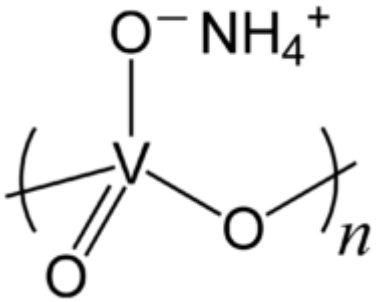

Figure 7: Ammonium Metavanadate [53].

There are two metavanadate metal salts of interest that are being used in the synthesis of a vanadium based MOF, namely; sodium metavanadate ($NaVO_3 \cdot 4H_2O$) and ammonium metavanadate (NH_4VO_3).The vanadium is in the 5+ oxidation state for both metal salts. Compounds synthesised will be compared to determine if the presence of different counter ions will have an effect on the product.

1.3.2 The Vanadyl Ion

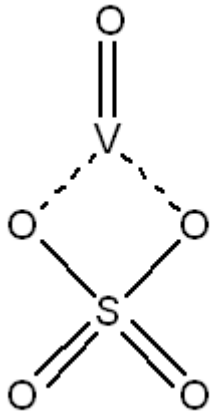

Figure 8: Vanadyl Sulphate.

The vanadyl cation is light blue in colour and is a single vanadium centre doubly bound to an oxygen ($[VO]^{2+}$), giving the molecule a 2+ charge. The vanadyl ion is one of the most stable diatomic ions known and is able to form a wide range of complexes [43-45]. The difference between the vanadyl and vanadate ions is that the vanadyl is a cation and the vanadate is an anion, so this may lead to differences in the structure of the products. The vanadyl cation must be ionically bound to an anion, e.g. Cl_2^{2-} or SO_4^{2-}, to maintain a neutral charge. The metal salt used in this study, is vanadyl sulphate ($VOSO_4 \cdot xH_2O$). Vanadyl sulphate is a well-known compound of vanadium, it is dark blue in colour and is hygroscopic, with the vanadium being 4+ oxidation state [43-45].

1.3.3 Speciation of Vanadium

There are a number of different factors that can often work together to effect the speciation of vanadium, they can be listed as; pH, concentration of vanadium, temperature, pressure, oxidation due to the atmosphere [43-45]. In this study, the effects of pH, temperature, pressure and oxidation due to the atmosphere were focussed on to see to see their effects on the formation of V-species.

Vanadates are the dominant species at the 5+ oxidation state. When the V^{5+} ion is in an aqueous medium, there are a number of V-species which can form depending on the pH of the solution, concentration of vanadium and ionic strength of the solution.

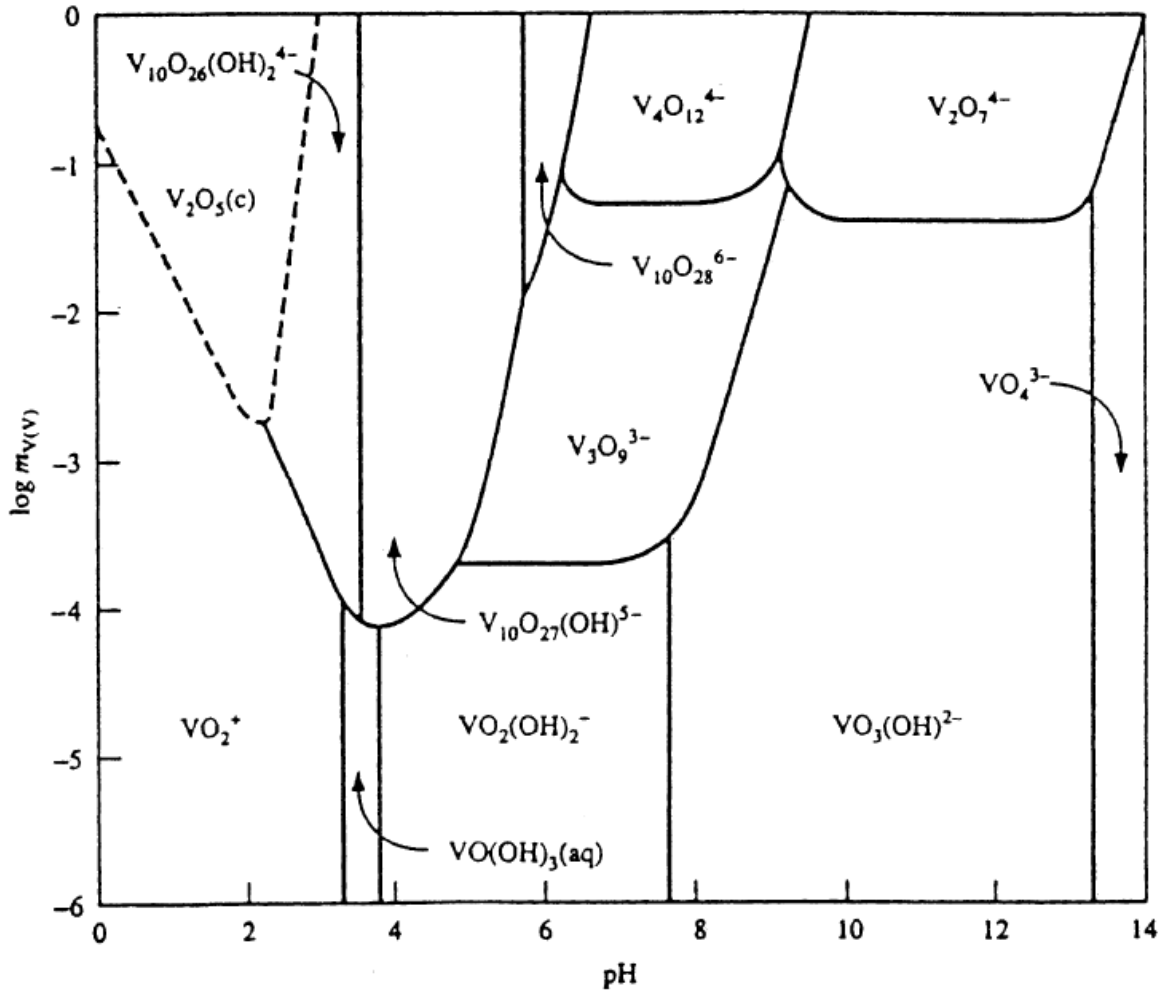

Figure 9: The Pourbaix diagram of vanadium, which shows the speciation as a function of pH and potential at 25°C and an ionic strength of 1M [33].

Potential will not be investigated in this study, so when one observes Figure 9 at the potential of 0, one is able to focus on the effect of pH. This study was restricted to pH values lower than 6, which will be discussed later in detail in Chapter 2. From pH 1 to 3 one can observe that the V_2O_5 species is present. At pH values of 2.5 – 3, the exact identification of the dominant species is slightly more ambiguous, the dashed line indicates that the exact point where the shift from the V_2O_5 species to the decavanadate species, $V_{10}O_{26}(OH)_2^{4-}$ occurs is unknown. From a pH value of 3 – 6 the dominant V-species are the decavanadate ions, with varying degrees of deprotonation.

V^{4+} dissolves in water to form the vanadyl ion, but the ion is only stable enough to remain in solution when the pH value is sufficiently low; below 3.5. Increasing the pH above this value will result in the formation of various vanadates, such as 'deca' and orthovanadates [43]. When a ligand is introduced into solution and the pH value is altered, the V-species that were originally unstable at the altered pH value, may be stabilised by bonding to the ligand and forming a stable molecule, thus allowing them to be present in solution in the form of a complex [43-45].

1.3.4 Benzenetetracarboxylic Acid:

1, 2, 4, 5 - Benzenetetracarboxylic acid (H_4B4C) was the ligand chosen to build a possible metal organic framework/s, as it has a stable and rigid structure, due to the benzene ring and the presence of the 4 carboxylic acid groups, through which coordination may occur.

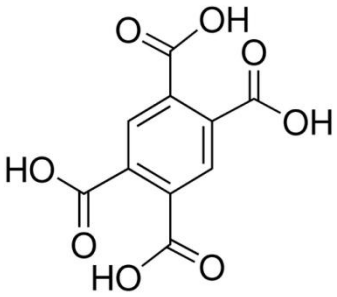

Figure 10: 1,2,4,5-Benzentetracarboxylic Acid [54].

Coordination can occur via the carboxylic acid groupings through two possible coordination sites, the carbonyl group and the OH group. The carbonyls have two lone pairs, which can be donated to form a bond, the OH groups can be deprotonated to the oxygen, which has lewis acid character and will bond to a metal with relative ease.

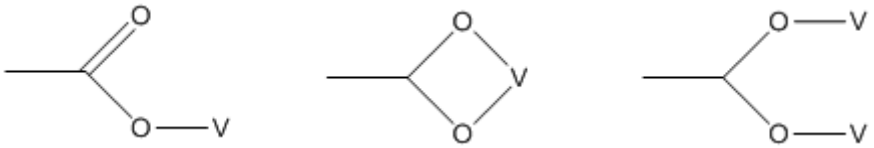

Figure 11: Possible coordination between the metal and ligand.

Figure 11 shows the potential coordination routes between the metal and the carboxylic acid groups, which can be identified as; unidentate, bidentate or bridging routes [55].

1.4 A Review of Vanadium-based Metal-Organic Frameworks

The use of vanadium as the metal centre in the synthesis of metal organic frameworks has been limited when compared to other, more popular divalent metals, such as copper and nickel. Vanadium has received an increased amount of attention in this regard over the past 5 to 10 years. 12 coordination complexes have been termed as V-MOFs, which have been reviewed in terms of synthesis, structure and have been investigated for potential applications. Van Der Voort et al has recently released a review on the synthesised V-MOFs [56], which aided in the compilation of this table.

Table 2: A list of the synthesised V-MOFs [56].

No.	MOF name:	Metal unit:	Ligand unit:	Reference:
1	MIL-47	{V-O-V} chains	BDC	[57]
2	MOF-48	{V-O-V} chains	DMBDC	[58]
3	MIL-59	Oxido-centred vanadium trimers	Isophthalic acid	[59]
4	MIL-68	{V-O-V} chains	BDC	[60]
5	MIL-60	{V-O-V} chains	BTEC	[61]
6	MIL-61	{V-O-V} chains	BTEC	[61]
7	MIL-71	{V-O-V} chains	BDC	[62]
8	COMOC-2	{V-O-V} chains	BPDC	[63]
9	COMOC-3	{V-O-V} chains	NDC	[64]
10	MIL-100	Oxido-centered vanadium trimers	BTC	[65]
11	MIL-101	Oxido-centred vanadium trimers	BDC	[66]
12	$[V^{IV}_2O_2(H_2O)(B4C)]$ (RU-V1)	{V-O-V} chains	BTEC	[33]

BDC = 1,4-Benzenedicarboxylic acid
DMBDC = 2,5-Dimethylbenzenedicarboxylate

BTEC = 1,2,4,5-Benzenetetracarboxylic acid
BPDC = Biphenyl-4,4-dicarboxylate
NDC = 2,6-Naphthalenedicarboxylate
BTC = 1,3,5-Benzenetricarboxylic acid

MIL =Materials Institute Lavoisier
COMOC = Center for Ordered Materials, Organometallics and Catalysis, Ghent University.

Table 2 shows the names, and structural motifs of the 12 vanadium coordination complexes, which have specifically been assigned as MOFs, via a literature review. An addition has been made the table of published V-MOFs, namely; no. 12 $[V^{IV}_2O_2(H_2O)_2(B4C)]$ which will be shortened to RU-V1 for the remainder of the thesis. RU-V1 has not been specifically

described as a MOF, but exhibits all the properties of a MOF. The complex exhibits porosity through its cavities and channels, has a large surface area and is crystalline, with a known structure.

All of the previously reported V-MOFs were synthesised using solvothermal conditions, which will be discussed with the parameters displayed in Chapter 2. Subjecting the previously discussed vanadium species to the elevated temperatures and pressures yields two V-O species; {V-O-V} chains and oxido-centered vanadium trimers.

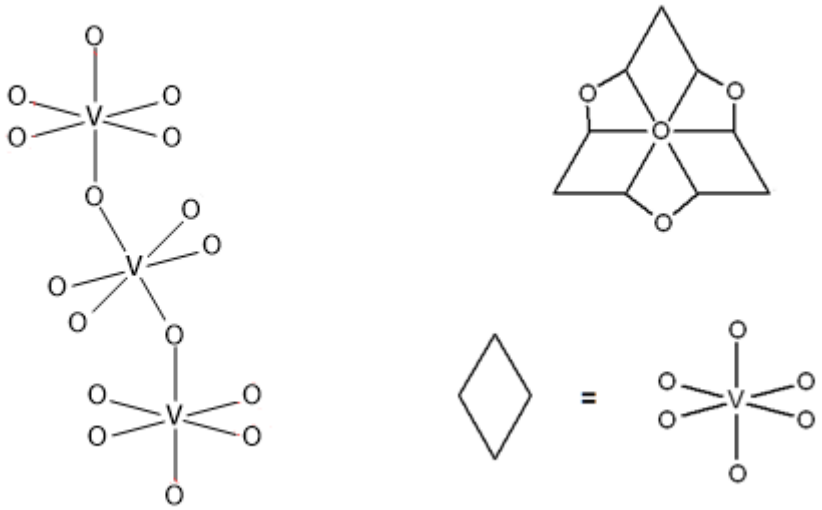

Figure 12: Two-dimensional representations of the V-O-V corner sharing chains and oxido-centered trimers.

Figure 12 shows a basic diagram of the V-O-V chains, which are tilted vanadium octahedra connected into chains via the axial -OH bonds. V-OH-V chains are expected when the V-centres are in the 3+ oxidation state. The deprotonation of the hydrogen from the OH yields V-O-V chains, which in turn oxidises the V-centres to the 4+ oxidation state [59][64-65]. The oxido-centered trimers are slightly more complex, as three vanadium octahedra now share bridging oxygen between their axial, creating a trimer. The equatorial positions are stabilised and bound together via O-O bridges. A ligand is able bind to the V-O-V chain at the equatorial positions, possibly linking a number of chains to create a repeating structure. The trimers can be linked together due to the ligand replacing the O which bridges between the equatorial positions of the trimer, thereby also creating a repeating structure.

MIL-47 was the first V-MOF to be synthesised and characterised [57], and is the most studied to date, with a comprehensive study completed into its catalytic activity for the conversion of cyclohexene to the epoxide [4]. This will be comparatively discussed with the results of this study in Chapter 4. In the initial study done on the V-MOF [57], two structures were described and compared, MIL-47as (V^{III}(OH)(BDC).*x*(BDC) (*x*= ±0.75) and MIL-47 (V^{IV}O(BDC)).

MIL-47as describes the 'as synthesised' product, which analysed directly after synthesis with no additional purification procedure, so free ligand is expected to be trapped within the pores. MIL-47 is the product after undergoing calcination in a tubular furnace at 573K, which releases the trapped ligand from the pores and confirmed that the structure exhibited permanent porosity after the removal of the free ligand, with a surface area 930 m^2/g [57]. The structure of the MIL-47 is shown in Figure 1 (pg. 1) and one can observe that it has rhomboidal shaped pores which propagate through the structure as channels. The pore sizes were compared between MIL-47as (7.9 Å x 12.0 Å) and MIL-47 (10.5 Å x 11.0 Å), where the pore size of MIL-47 is shown to be greater, which was expected, as the free ligand and any interactions it had with the framework, had been removed [57]. An interesting note was that the V-centres in MIL-47as were in the 3+ state, but after calcinations, were found to be in the 4+ state for MIL-47, this was due to the deprotonation of the OH groups which bridge the VO octahedra together, which replaces the V-OH-V chains, with V-O-V chains. Guest inclusion studies proved that the structure of MIL-47 exhibited significant flexibility, being able to expand and contract depending on the guest molecules to be included, such as; trimethylbenzene and 2-methyl-1-propanol [57]. Finally the structure's magnetic properties were investigated as using organic linkers, such as BDC, which contain delocalised π electrons, allowing for long range electronic interactions between the metal centres within the MOF. MIL-47as was found to exhibit antiferromagnetic behaviour at a temperature of T_N = 95K and MIL-47 at a temperature of T_N = 75 K [57]. The difference between MIL-47 and MIL-47as is due to the V^{3+} - V^{3+} interactions of MIL-47as being stronger, this is due to there being more delocalised electrons associated with the metal centres and more ligand available [57].

MOF-48 was synthesised using DMBDC as a ligand instead of BDC, which yielded a product with the same structure as MIL-47, but the ligand is functionalised with two methyl groups, which were found to point into the pores of the structure [58]. MOF-48 was also found to exhibit permanent porosity and flexibility of its structure. MOF-48 and MIL-47 were both used in a study [58] to compare their effectiveness in catalytically converting methane (CH_4) to acetic acid (CH_3CO_2H). It was initially found that MIL-47 exhibited the greatest conversion of acetic acid (70%), but had a lower selectivity (9%), whereas MOF-48 had lower conversion (48%), but had a higher selectivity (38%) due to its pores being more hydrophobic [58]. The study proceeded to use carbon monoxide (CO) instead of methane, with this change the selectivity of the reaction increased to 100% for both MOFs, for acetic acid, as methyl trifluoroacetate (MFTA) was found to no longer form as the minor product of the reaction. The yield for MIL-47 is reduced (33%), whereas the yield increases slightly for MOF-48 (49%) [58]. Both MOFs were found, as confirmed, via XRPD, to be able to maintain their structural stability after the reactions and required little in the way of regeneration [58].

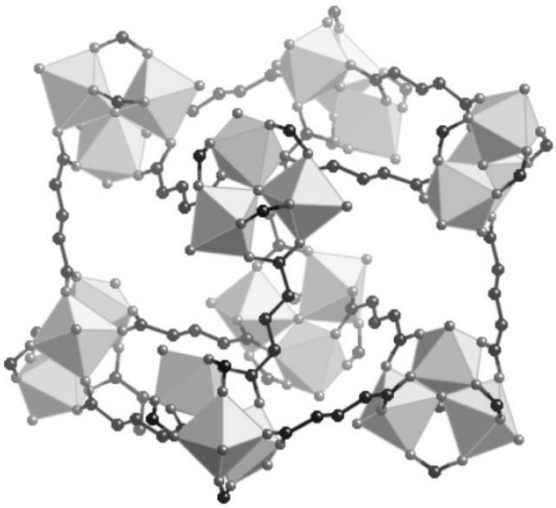

Figure 13: A structural unit of MIL-59 [59].

MIL-59 has the formula $[V^{III}(H_2O)]_3O(O_2CC_6H_4CO_2)_3 \cdot (Cl,9H_2O)$ and was the first V-MOF to be synthesised using 1,3-benzenedicarboxylic acid and vanadium oxido-centred trimers [59]. Figure 13 shows a structural unit of MIL-59, where one is able to observe the oxido-centred trimers connected to one another via the ligand, to create a cuboidal structural unit. One should note that the water molecules and chloride ions have been omitted and the carbons shown, are only those involved in the shortest pathways between the trimers, which may give the illusion that the pores are larger than they actually are. MIL-59 was found to be paramagnetic at all temperatures with an experimental Curie constant of 1.05 [59].

MIL-68 has a formula of $V^{III}(OH)\{O_2C\text{-}C_6H_4\text{-}CO_2\}.(HO_2C\text{-}C_6H_4\text{-}O_2H)_x(DMF)_y(H_2O)_z$ and has been synthesised in a similar way to MIL-47, but instead of using water as the solvent, *N*,*N*-dimethylformamide (DMF) was used [60]. DMF has a major impact on the pore size and shape, as two pores of different sizes are present to the single pore size of MIL-47. MIL-68 exhibits large hexagonal pores and small triangular pores involved in linking the hexagonal pores together [60]. The hexagonal pores are larger than the rhomboidal pores present in MIL-47 and the overall surface area is lower (603 m^2/g). Upon removal of the guest molecules, the structure was shown to exhibit permanent porosity [60].

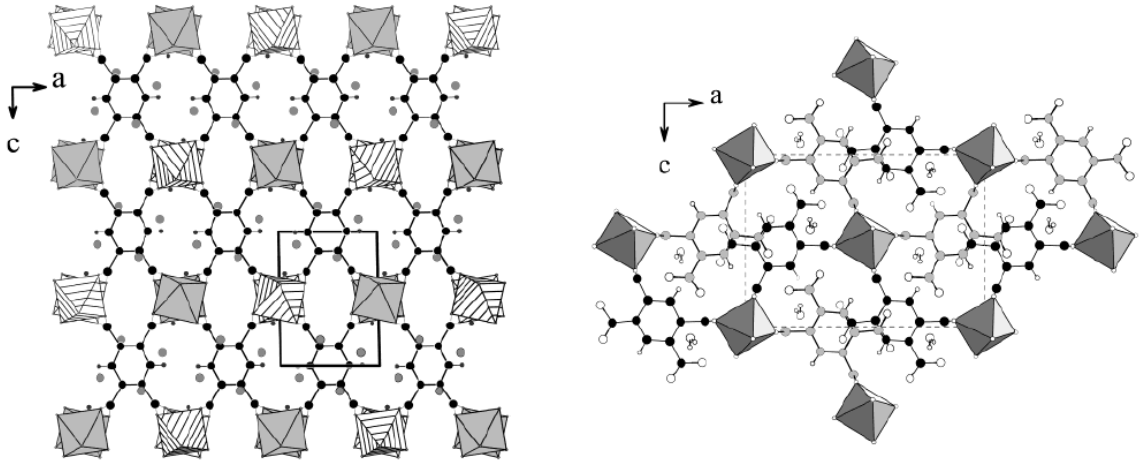

Figure 14: The structures of MIL-60 (left) and MIL-61 (right) [61].

V-MOFs: MIL-60 with formula: $((V^{III}(OH))_2[C_6H_2(CO_2)_4]\cdot 4H_2O)$ and MIL-61 with formula: $(V^{III}(OH)[_2(O_2C)C_6H_2(COOH)_2]\cdot H_2O)]$, are important as they were both synthesised using BTEC [61], which is the ligand used in this study. The only difference between the synthetic procedures of MIL-60 and 61 was that the molar ratios of the metal and ligand were altered, M:L = 5:1 for MIL-60 and 1:1 for MIL-61. From Figure 14, one can observe that MIL-60 is coordinated through all four of its carboxylic acid groups to vanadium in an octahedral geometry [61]. MIL-61 is more complex as it is only bound through two carboxylic acid groups, leaving two of the terminal carboxylates directed into the pores. This is due to the excess ligand present when using a M:L molar ratio of 1:1 [61]. This leads to a partial stacking of the ligands over one another, so the pore size of MIL-61 is expected to be far lower than that of MIL-60, but these properties were not specifically noted in the study [61]. The magnetic properties of the V-MOFs were investigated and it was found that MIL-60 exhibited paramagnetism, in a similar fashion to MIL-59, and MIL-61 was found to be antiferromagnetic at a temperature of T_N = 55 K. MIL-61 has a unique structure with a large number of delocalised π electrons, so with continued investigation, could lead to a material with unique magnetic properties in the future [61].

MIL-71 has a formula of $V^{III}_2(OH)_2F_2\{O_2C\text{-}C_6H_4\text{-}CO_2\}\cdot H_2O$ and the objective of the study was to synthesise the MOF with a two-dimensional inorganic subnetwork [62]. An inorganic subnetwork refers to positions of the inorganic molecules (the metal centres) with relation to each other within the MOF and can be zero dimensional (clusters and trimers), one dimensional, (chains) or two dimensional, which indicates that they are chains coordinating to form sheets [62]. In the previous study with MIL-47, the inorganic subnetwork was one dimensional, as the VO octahedra propagated through the MOF as a chain [57]. MIL-71 has a two-dimensional framework, in that the VO octahedra are able to coordinate to each other via a fluorine atom, linking them through two axes instead of just one.

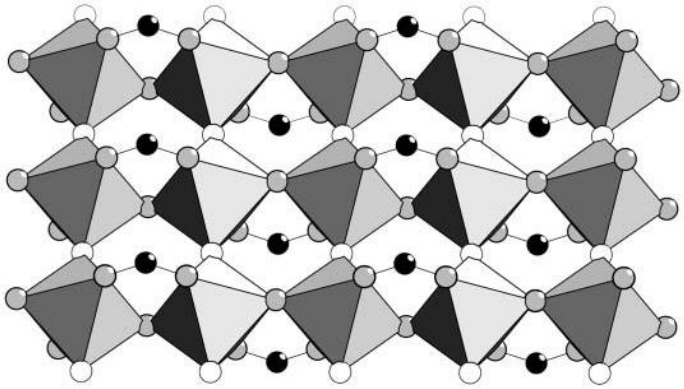

Figure 15: The structure of the oxyfluorinated octahedra sheets of the inorganic subnetwork. Grey circles = oxygen, white circles = fluorine and black circles = carbon [62].

Figure 15 shows how the addition of fluorine is able to form a two-dimensional inorganic subnetwork, as the fluorine replaces one of the oxygens in the equatorial position, linking two a subsequent chains together. The two dimensional inorganic subnetwork was originally in the V^{3+} oxidation state, but after calcination was irreversibly converted to the V^{4+} oxidation state, similar to what was observed for MIL-47as and MIL-47, where the V-OH-V chains were replaced with V-O-V chains [57][62]. This process caused the pores to become completely hydrophobic, preventing rehydration and caused permanent porosity [62]. The presence of a two-dimensional inorganic framework was thought to be advantageous, as it should increase the amount of interelectronic interactions between the inorganic centres. This MOF was found to exhibit antiferromagnetic properties at a lower temperature (T_N = 20 K) than the previous (MIL-47), due to the functionalisation of phenyl rings by carboxylate groups, which possibly reduces the strength of the magnetic coupling [62].

COMOC-2 has the formula: $V^{IV}O$(BPDC) and was incorporating BPDC as the ligand, to extend the pore sizes [63]. BPDC can be regarded as BDC with and extra benzene moiety and it was found that the pore sizes have been enlarged due to this fact (18.9 Å x 19.4 Å) [63]. COMOC-2 was able to be synthesised under solvothermal conditions and using micro-assisted synthesis. An extension to the reaction time (24 hrs) or an increase in temperature (160°C) formed the same product, but was found to exhibit a mixed valency of V^{IV}/V^{III} [63]. COMOC-2 (V^{IV}) and COMOC-2 (V^{IV}/V^{III}) were compared to one another in terms of their sorption properties and it was found that COMOC-2 (V^{IV}) was able to exhibit significant flexibility and breathing when absorbing CO_2 and CH_4, at various temperatures and pressures, which COMOC-2 (V^{IV}/V^{III}) was not able to exhibit [63]. COMOC-2 (V^{IV}) was noted to show similar isotherms for CO_2 and CH_4 at temperatures of 303 K and 35 bar, but when changing the temperature to 265 K, the structure was more selective for CO_2 and with 28 bar, with the pores being calculated to be almost completely filled, based off nitrogen porosimetry data [63].

COMOC-3 has the formula: $V^{IV}(OH)(O_2C\text{-}C_{10}H_6\text{-}CO_2)\cdot H_2O$, and used NDC as the ligand, which yielded a product with a structure that was similar to that of COMOC-2 [64]. Instead of 2

successive benzene rings bound together, as observed with BPDC, naphthalene was the central unit of the ligand NDC, which lead to a greater overall structural rigidity for COMOC-3 [64]. Similarly to COMOC-2, the MOF was able to be synthesised using either solvothermal or microwave-assisted syntheses. The 'as synthesised' product was found to be in the V^{3+} state and after calcination was converted into the V^{4+}. The objective of the study was to investigate the catalytic activity of the V-MOF in the epoxidation reaction of cyclohexene to cyclohexene oxide [64]. The catalytic results were comparable to that of MIL-47 [4], as COMOC-3 was able to convert cyclohexene to the epoxide with a high selectivity (82%), but slightly reduced conversion (38%) after 7 hours. It was also found to be completely reusable, only requiring washing and calcinations between successive runs, with a negligible amount of vanadium leached (0.62%) into solution [64].

MIL-100(V) has a formula of $V_3O(H_2O)_2X[C_9H_3O_6]_2.yH_2O$, where $X=(Cl^-)_{1-z}$ $(C_9H_5O_6)_z^-$, y=3 and z=0.3 and was synthesised using BTC as the ligand, with vanadium oxido-centred trimers as the inorganic subnetwork [65]. In contrast to what was found with MIL-59 [59], the oxido-centred trimers bind to BTC to create what are known as 'super-tetrahedra'.

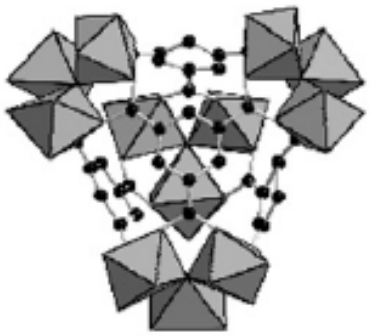

Figure 16: An example of a super-tetrahedra [65].

The super-tetrahedra connect to one another via corner sharing to create 'cages' with large cavities of 25 – 29 Å in diameter [65]. Similarly to the previously discussed COMOC-2 MOF [63], vanadium centres were found to be in a mixture of both V^{III} and V^{IV}, due to the number of coordinatively unsaturated sites and the different environments present within the MOF. Having coordinatively unsaturated vanadium centres may be a great advantage in the application of catalysis, as this would mean that the MOF would not have to undergo a bond dissociation from the metal centre, instead having a free coordination site available, which would aid in structural stability over repeated runs. MIL-100 was tested for its capacity to uptake CO_2 and CH_4, where it was determined that, similarly to COMOC-2, four times as much CO_2 could be adsorbed compared to CH_4[65]. This was determined to be due to the quadruple moment of CO_2, which induces specific interactions, such as Van der Waals forces and hydrogen bonds, between CO_2 and the pore of MIL-100, as the pore was found to be polar in nature [65].

V-MIL-101 has a formula of $[V_3OCl(DMF)_2(BDC)_3]\cdot 3.1DMF\cdot 10H_2O\cdot 0.1BDC$ and V-MIL-101-NH_2 $=[V_3OCl(DMF)_2(BDC\text{-}NH_2)_3]\cdot 2.8DMF\cdot H_2O\cdot 0.1BDC\text{-}NH_2$ [66]. The ligands used were BDC and 2-amino-1,4-benzendicarboxylic acid and the metal species were found to be the oxido-centred trimers, also found in MIL-59 and MIL-100. The structure was somewhat similar to that of MIL-100, with super-tetrahedra connecting to one another to create larger cages or pores, which were found to have a completely different structure due to the inclusion of a new ligand and the solvent used for the synthesis being DMF instead of water. The pore size was found to be smaller than that of MIL-100 with a diameter of 12 – 16 Å [66]. The objective of this study was to characterise the structures of the MOFs and enquire into their gas sorption properties. The MOFs were found to have moderate thermal stability (V-MIL-101 = 320°C and V-MIL-101-NH_2 = 240°C) and were able to significantly absorb N_2 and CO_2, but only under an inert atmosphere of argon [66]. A similar characteristic to what was found in MIL-100, was that V^{III} and V^{IV} centres were both present again due to the coodinatively unsaturated nature of the MOF, which may be an advantage for the application of catalysis.

The final V-MOF to be discussed has the formula $[V^{IV}{}_2O_2(H_2O)_2C_6H_2(COO)_4)]$ or shortened to RU-V1. RU-V1 was synthesised using BTEC and VO-octahedra to yield a highly coordinated MOF with the four carboxylic acid groups bound to a total of six V-O octahedra [33].

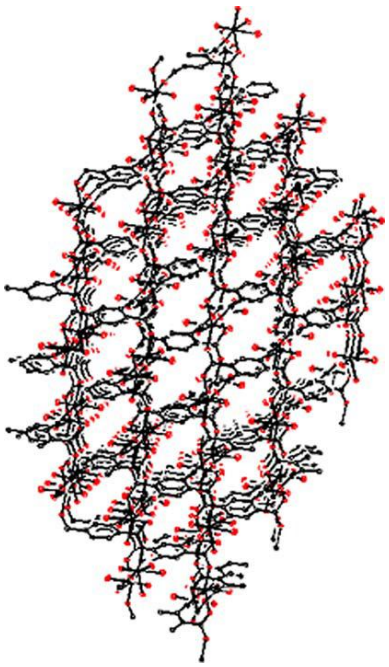

Figure 17: The bulk structure of RU-V1, showing the pores and channels which propagate through the framework [33].

The major difference between this MOF and the previously mentioned MOFs is that the VO-octahedra are not in a chain but are single clusters. The pore sizes are expected to be smaller than that of MIL-47, due to the structure being more highly coordinated, unfortunately the actual pore sizes were not noted in the study [33]. This MOF will be

discussed in greater detail in Chapters 3 and 4, as it is one of the materials which has been applied to the application of catalysis of cyclohexene to the epoxide, cyclohexene oxide.

1.5 Aims of the Study

The aims of the study were threefold:

- To synthesise a V-MOF/s using 1,2,4,5-benzenetetracarboxylic acid as a ligand, novel or otherwise.
- To fully characterise the synthesised V-MOF/s.
- To apply a V-MOF/s to the application of the catalysis for the conversion of cyclohexene to cyclohexene oxide.

References:

1. Farrusseng, D. *Metal-Organic Frameworks: Applications Form Catalysis to Gas Storage*. Wiley-VCH, 2011.
2. Yaghi, O. M.; Roswell, J. L. Metal-Organic Frameworks: A New Class of Porous Materials. *Micropor. Mesopor. Mat.* **2004**, 3-14.
3. Yaghi, O. M.; Long, J. R.; Zhou, H. Introduction to Metal-Organic Frameworks. *Chem. Rev.* **2012**, *112*, 673-674.
4. Van Der Voort, P.; Van Speybroek, V.; Leus, K.; Vandichel, M.; Liu, Y.; Muylaert, I.; Musschoot, J.; Pyl, S.; Vrielinck, H.; Callens, F.; Marin, G. B.; Detavernier, C.; Wiper, P. V.; Khimyak, Y. Z.; Waroquier, M. The Coordinatively Saturated Vanadium MIL-47 as a Low Leaching Hetergeneous Catalyst in the Oxidation of Cyclohexene. *J. catal.* **2012**, *258*, 196-207.
5. Kitagawa, S.; Kitaura, R.; Noro, S. Functional Porous Co-ordination Polymers. *Angew. Chem. Int. Edit.* **2004**, *43* (18), 2334-2375.
6. Li, Y.; Yan, C.; Wu, Z.; Zhu, C. Synthesis and Magnetism of μ-tetracarboxylato-bridged Dinuclear Oxovanadium(IV) Complexes. *Syn. React. Inorg. Met.* **2005**, *35*, 319-324.
7. An, J.; Geib, S. J.; Rosi, N. L. High and Selective CO_2Uptakein a Cobalt Adeninate Metal-Organic Framework Exhibiting Pyrimidine and Amino-decorated Pores. *J. Am. Chem. Soc.* **2010**, *132* (1), 38-39.
8. Khan, M.; Tabussum, S.; Doedens, R. A Novel Cationic Heteropolyoxovanadium(IV) Cluster Functionalized with Organic Ligands: Synthesis and Characterization of the Fully Reduced Species $[Mn^{II}V^{IV}_6O_6\{(OCH_2CH_2)_2N(CH_2CH_2OH)\}_6]Cl_2$. *Chem. Commun.* **2003**, 532-533.
9. Fischer, R. A.; Pöppl, A.; Sternemann, C.; Bertmer, M.; Kuttatheyil, A. V.; Jee, B.; Schneemann, A.; Yusenko, K.; Meilikhov, M.; Kozachuk, O. A Solid-Solution Approach to mixed Metal Metal-Organic Frameworks – Detailed Characterization of Local Structures, Defects and Breathing Behaviour of Al/V Frameworks. *Eur. J. Inorg. Chem.* **2013**, 4546-4557.
10. Walton, R. I.; Millange, F.; Dent, A. J.; Grenéche, J.; Daturi, M.; Vimont, A.; Campo, B. C.; Clet, G.; Breeze, M. I. Isomorphous Substitution in a Flexible Metal-Organic Framework: Mixed-Metal, Mixed-Valent MIL-53 Type Materials. *Inorg. Chem.* **2013**, *52*, 8171-8182.
11. Suib, S. L.; Ma, Y.; Tong, W.; Zhou, H. A Review of Zeolite-like Porous Materials. *Micropor. Mesopor. Mater.* **2000**, *37*, 243-252.
12. Tranchemontagne, D. J.; Mendoza-Cortes, J. L.; O'Keeffe, M.; Yaghi, O. M. Secondary Building Units, Nets and Bonding in the Chemistry of Metal-Organic Frameworks. *Chem. Soc. Rev.* **2009**, *38* (5), 1257-1283.
13. Kitagawa, S.; Kitaura, R.; Noro, S. Functional porous co-ordination polymers". *Angew. Chem. Int. Edit.* **2004**, *43* (18), 2334-2375.

14. Zhuang, J. L.; Ceglarek, D.; Pehuraj, S.; Terfort, A. Rapid Room-Temperature Synthesis of Metal-Organic Framework HKUST-1 Crystals in Bulk and as Oriented and Patterned Thin Films. *Adv. Funct. Mater.* **2011**, *21* (8), 1442-1447
15. Khan, N. A.; Haque, E.; Jhung, S. H. Rapid Syntheses of a Meal-Organic Framework Material $Cu_3(BTC)_2(H_2O)_3$ Under Microwave: A Quantitative analysis of Accelerated Syntheses. *Phys. Chem. Chem. Phys.* **2010**, *12* (11), 2625-2631.
16. Choi, J. S.; Son, W. J.; Kim, J.; Ahn, W. S. Metal-Organic Framework MOF-5 Prepared by Microwave Heating: Factors to be Considered. *Micropor. Mesopor. Mater.* **2008**, *116*, 727-731.
17. Li, Z. Q.; Qiu, L. G.; Xu, T.; Wu, Y.; Wang, W.; Wu, Z. Y.; Jiang, X. Ultrasonic Synthesis of the Microporous Metal-Organic Framework $Cu_3(BTC)_2$ at Ambient Temperature and Pressure: An Efficient and Environmentally Friendly Method. *Mater. Lett.* **2009**, *63* (1), 78-80.
18. Yang, H.; Orefuwa, S.; Goudy, A. Study of Mechanochemical Synthesis in the Formation of the Metal-Organic Framework $Cu_3(BTC)_2$ for Hydrogen Storage. *Micropor. Mesopor. Mater.* **2011**, *143* (1), 37-45.
19. Van Der Voort, P.; Leus, K.; Couck, S.; Vandichel, M.; Vanhaelewyn, G.; Liu, Y.; Marin, G. B.; Van Driessche, I.; Depla, D.; Waroquier, M.; Van Speybroeck, V.; Denayer, J. F. M. Synthesis, characterisation and sorption properties of NH_2-MIL-47. *Phys. Chem. Chem. Phys.* **2012**, *14*, 15562-15570.
20. Zou, X.; Samain, L.; Yun, Y.; Wan, W.; Platero-Prats, A.; Su, J.; Carson, F. Framework isomerism in vanadium metal-organic frameworks: MIL-88B(V) and MIL-101(V). *Crys. Growth. Des.* **2013**, *13*, 5036-5044.
21. Hwang, J.; Park, C.; Choi, K.; Cha, M. H.; Ahuja, R.; Kim, D. W.; Kim, D. O.; Sagong, K.; Joung, U. G.; Jeong, H.; Ihm, J. Hydrogen Storage Enhancement via Transition Metal Decoration on Metal-Organic Frameworks: A First Principles Study. *World Scientific* **2012**, *7* (6), 1250044-1 to 124044-11.
22. Panella, B.; Hirscher, M.; Pütter, H.; Müller, U. Hydrogen adsorption in metal-organic frameworks: Cu-MOFs and Zn-MOFs compared. *Adv. Funct. Mater.* **2006**, *16* (4). 520-524.
23. Millward, A. R.; Yaghi, O. M. Metal-organic frameworks with exceptionally high capacity for storage of carbon dioxide at room temperature. *J. Am. Chem. Soc.* **2005**, *127* (51), 17998-17999.
24. Palomino, G. T.; Cabello, C. P.; Rumori, P. Carbon dioxide adsorption on MIL-100(M) (M=Cr, V, Sc) metal-organic frameworks: IR spectroscopic and thermodynamic studies. *Micropor. Mesopor. Mater.* **2014**, *190*, 234–239.
25. Van Der Voort, P.; Biswas, S.; Couck, S.; Denysenko, D.; Bhunia, A.; Grzywa, M.; Denayer, J. F. M.; Volkmer, D.; Janiak, C. Sorption and breathing properties of difluorinated MIL-47 and Al-MIL-53 frameworks. *Micropor. Mesopor. Mater.* **2013**, *181*, 175–181.

26. Yot, P. G.; Zhong, C.; Ma, Q.; Haines, J.; Yang, Q.; Ghoufi, A.; Devic, T.; Serre, C.; Dmitriev, V.; Marin, G. Large breathing of the MOF MIL-47 (V^{IV}) under mechanical pressure: a joint experimental-modelling exploration. *Chem. Sci.* **2012**, *3*, 1100-1104.
27. Lieb, A.; Leclerc, H.; Devic, T.; Serre, C.; Margiolaki, I.; Mahjoubi, F.; Lee, J.; Vimont, A.; Daturi, M.; Chang, J. MIL-100(V) – A mesoporous vanadium metal organic framework with accessible metal sites. *Micropor. Mesopor. Mater.* **2012**, *157*, 18–23.
28. Van Der Voort, P.; Biswas, S.; Vanpoucke, D. E. P.; Verstraelen, T.; Vandichel, M.; Couck, S.; Leus, K.; Liu, Y.; Waroquier, M.; Van Speybroeck, V.; Denayer, J. F. M. New Functionalized Metal-Organic Frameworks MIL-47-X (X = -Cl, -Br, $-CH_3$, $-CF_3$, -OH, $-OCH_3$): Synthesis, Characterization, and CO_2 Adsorption Properties. *J. Phys. Chem. C.* **2013**, *117*, 22784-22796.
29. De Vos, D. E.; Alaerts, L.; Kirschhock, C. E. A.; Maes, M.; van der Veen, M. A.; Finsy, V.; Depla, A.; Martens, J. A.; Baron, G. V.; Jacobs, P. A.; Denayer, J. F. M. Selective absorption and separation of xylene isomers and ethylbenzene with microporous vanadium (IV) terephthalate MIL-47. *Angew. Chem. Int. Ed*. **2007**, *46*, 4293 –4297.
30. Garcia, H.; Alvaro, M.; Dhakshinamoorthy, A. Metal-organic frameworks a heterogeneous catalysts for oxidation reactions, *Catal. Sci. Technol.* **2011**, *1*, 856-867.
31. Garcia, H.; Corma, A.; Llabrés i Xamena, F. X. Engineering Metal-Organic Frameworks for Heterogeneous Catalysis. *Chem. Rev.* **2010**, *110* (8), 4606-4655.
32. Cevik, S.; Poyraz, M.; Sari, M. A Novel Three Dimensional Organic-Inorganic Hybrid Based Porous Phase: Synthesis and Characterization of Reduced Oxovanadium Pyromellitate, $[V^{iv}_2O_2(H_2O)_2(C_6H_2(COO)_4)]$. *J. Chem. Crystallogr.* **2007**, *37*, 497-502.
33. Weckhuysen, B. M.; Keller, D. E. Chemistry, Spectroscopy and the Role of Supported Vanadium Oxides in Heterogeneous Catalysis. *Catal. Today.* **2003**, *78*, 25-46.
34. Mishra, L.; Prajapati, R.; Kimura, K.; Raghavaiah, P. Metal-Organic Frameworks (MOFs) Constructed from Zn^{II}/Cd^{II}-2,2'-Bipyradines and Polycarboxylic Acids: Synthesis, Characterisation and Microstructural Studies. *Polyhedron.* **2009**, *28*, 600-608.
35. Gomez-Lor, B.; Gutiérrez-Puebla, E.; Iglesias, M.; Monge, M. A.; Ruiz-Valero, C.; Snejko, N. $In_2(OH)_3(BDC)_{1.5}$ (BDC = 1,4-benzenedicarboxylic acid): An In(III) supramolecular 3D Framework with Catalytic Activity. *Inorg. Chem.* **2002**, *41* (9), 2429-2432.
36. Hasegawa, S.; Horike, S.; Matsuda, R.; Furukawa, S.; Mochizuki, K.; Kinoshita, Y.; Kitagawa, S. Three-Dimensional Porous Coordination Polymer Functionalized with Amide Groups Based on Tridentate Ligand: Selective Sorption and Catalysis. *J. Am. Chem. Soc.* **2007**, *29* (9), 2607-2614.
37. Lu, Z. Z.; Zhang, R.; Li, Y. Z.; Guo, Z. J.; Zheng, H. G. Solvatochromic Behaviour of a Nanotubular Metal-Organic Framework for Sensing Small Molecules. *J. Am. Chem. Soc.* **2011**, *133* (12), 4172-4174.
38. Beauvais, L. G.; Shores, M. P.; Long, J. R. Cyano-Bridged Re6Q8 (Q = S, Se) Cluster-Cobalt(II) Framework Materials: Versatile Solid Chemical Sensors. *J. Am. Chem. Soc.* **2000**, *122* (12), 2763-2772.

39. Allendorf, M. D.; Bauer, C. A.; Bhakta, R. K.; Houk, R. J. T. Luminescent Metal-Organic Frameworks. *Chem. Soc. Rev.* **2000**, *38* (5), 1330-1352.
40. Serre, C.; Millange, F.; Thouvenot, C.; Gardant, N.; Pellé, F.; Férey, G. Synthesis, characterisation and Luminescent Properties of a New Three-Dimensional Lanthanide Trimesate: $((C_6H_3)(CO_2)_3)$ (M = Y, Ln) or MIL-78. *J. Mater. Chem.* **2004**, *14* (10), 1540-1543.
41. Park, Y. K.; Choi, S. B.; Kim, H.; Kim, K.; Won, B. H.; Choi, K.; Choi, J. S.; Ahn, W. S.; Won, N.; Kim, S.; Jung, D. H.; Choi, S. H.; Kim, G. H.; Cha, S. S.; Jhon, Y. H.; Yang, J. K.; Kim, J. Crystal Structure and Guest Uptake of a Mesoporous Metal-Organic Framework Containing Cages of 3.9 aand 4.7 nm in Diameter. *Angew. Chem. Int. Edit.* **2007**, *46* (43), 8230-8233.
42. Horcajada, P.; Serre, C.; Vallet-Regf, M.; Sebban, M.; Taulelle, F.; Férey, G. Metal-Organic Frameworks as Efficient Materials for Drug Delivery. *Angew. Chem. Int. Edit.* **2006**, *45* (36), 5974-5978.
43. Rehder, D. *Bioinorganic Vanadium Chemistry*. Wiley, 2008, 1-20.
44. Wilkenson, G.; Gillard, R. D.; McCleverty, J. A. *Comprehensive Coordination Chemistry: The Synthesis, Reactions, Properties and Applications of Coordination Compounds*. Pergamon Press, 1987, 454-567.
45. Bailar, J. C.; Emeléus, H. J.; Nyholm, R.; Trotman-Dickenson, A. F. *Comprehensive Inorganic Chemistry*. Pergamon Press, 1973, 518-524.
46. Haynes, W. M.; Lide. D.R. *CRC Handbook of Chemistry and Physics*. CRC Press, 2010, 4-40.
47. Misono, M. Catalytic chemistry of solid polyoxometalates and their industrial applications. *Molecular Engineering***, 1993**, *3*, 193-203.
48. Orthovanadate Image: https://en.wikipedia.org/wiki/Vanadate#/media/File:Orthovanadate_anion.svg (Accessed: 10/02/2016)
49. Rossotti, F. J. C.; Rossotti, H. Equilibrium Study of Polyanions: I. Isopolyvanadates in Acidic Media. *Acta. Chem. Scand.* **1956**, *10*, 957-984.
50. Evans, H. T. The Molecular Structure of the Isopoly Complex Ion, Decavanadate($V_{10}O_{28}^{6-}$). *Inorg. Chem.* **1966**, *5* (6), 967-977.
51. Stomberg, R.; Olson, S. The Crystal Structure of Ammonium Fluoro-oxodiperoxovanadate(2-), $(NH_4)_2[VFO(O_2)_2]$. *Acta Chem. Scand. A.* **1984**, *38*, 801-806.
52. Decavanadate Image: http://canmin.geoscienceworld.org/content/49/5/1243/F2.large.jpg (Accessed: 10/02/2016)
53. Ammonium Metavanadate Image: https://en.wikipedia.org/wiki/Ammonium_metavanadate#/media/File:Ammonium-metavanadate-2D.png (Accessed: 10/02/2016)

54. 1, 2, 4, 5 – Benzenetetracarboxylic Acid Image: http://www.sigmaaldrich.com/catalog/product/fluka/83181?lang=en&region=ZA (Accessed: 10/02/2016)
55. Nakamoto, K. *Infrared and Raman Spectra of Inorganic and Co-ordination Compounds Part B*. Sixth edition. John Wiley & sons, Inc. New Jersey, 2009, 64-67.
56. Van Der Voort, P.; Leus, K.; Liu, Y. Y.; Vandichel, M.; Van Speybroek, V.; Waroquier, M.; Biswas, S. Vanadium Metal-Organic Frameworks: Structures and Application. *New. J. Chem.* **2014**, *38*, 1853-1867.
57. Riou, D.; Férey, G.; Marrot, J.; Barthelet, K. A Breathing Hybrid Organic-Inorganic Solid with Very Large Pores and High Magnetic Characteristics. *Angew. Chem. Int. Ed.* **2002**, *42* (2), 281-284.
58. Yaghi, O. M.; Phan, A.; Czaja, A. U.; Gándara, F.; Knobler, C. B. Metal-Organic Frameworks of Vanadium as Catalysts for Conversion of Methane to Acetic Acid. *Inorg. Chem.* **2011**, *5*, 7388-7390.
59. Riou, D.; Férey, G.; Barthelet, K. $[V^{III}(H^2O)^3O(O^2CC^6H^4CO^2)^{3\cdot}(Cl, 9H^2O)$ (MIL-59): A Rare Example of Vanadocarboxylate with a Magnetically Frustrated Three-Dimensional Hybrid Framework. *Chem. Commun.* **2002**, 1492-1493.
60. Riou, D.; Férey, G.; Marrot, J.; Barthelet, K. $V^{III}(OH)\{O_2C\text{-}C_6H_4\text{-}CO_2\}.(HO_2C\text{-}C_6H_4\text{-}CO_2H)x(DMF)y(H_2O)z$ (or MIL-68), A New Vanadocarboxylate with a Large Pore Hybrid Topology: Reticular Synthesis with Infinite Inorganic Building Block. *Chem. Commun.* **2004**, 520-521.
61. Riou, D.; Férey, G.; Nogues, M.; Barthelet, K. Synthesis, Structure, and Magnetic Properties of Two New Vanadocarboxylates with Three-Dimensional Hybrid Frameworks. *Inorg. Chem.* **2003**, *42*, 1739-1743.
62. Férey, G.; Barthelet, K.; Adil, K.; Millange, F.; Serre, C.; Riou, D. Synthesis, Structure Determination and Magnetic Behaviou of the First Porous Hybrid Oxyfluorinated Vanado(III)carboxylate: MIL-71 or $V^{III}_2(OH)_2F_2\{O_2C\text{-}C_6H_4\text{-}CO_2\}$.H2O. *J. Mater. Chem.* **2003**, *13*, 2208-2212.
63. Van Der Voort, P.; Van Speybroek, V.; Waroquier, M.; Denayer, J. F. M.; Leus, K.; Vandichel, M.; Liu, Y.; Gascon, J.; Kapteijn, F.; Volkmer, D.; Grzywa, M.; Biswas, S.; Couck, S. New V^{IV}-Based Metal-Organic Framework Having Framework Flexibility and High CO_2 Adsorption Capacity. *Inorg. Chem.* **2013**, *52*, 113-120.
64. Van Der Voort, P.; Van Sprebroek, V.; Volkmer, D.; Van Deun, R.; Vrielinck, H.; Strubbe, K.; Weinberger, D.; Grzywa, M.; Leus, K.; Liu, Y. Synthesis, Structural Characterisation, and Catalytic Performance of a Vanadium-Based Metal-Organic Framework (COMOC-3). *Eur. J. Inorg. Chem.* **2012**, 2819-2827.
65. Lieb, A.; Leclerc, H.; Devic, T.; Serre, C.; Margiolaki, I.; Mahjoubi, F.; Lee, J. S.; Vimont, A.; Daturi, M.; Chang, J. MIL-100(V) – A Mesoporous vanadium Metal Organic Framework with Accessible Metal Sites. *Micropor. Mesopor. Mater.* **2012**, *157*, 18-23.

66. Van Der Voort, P.; Biswas, S.; Couck, S.; Grzywa, M.; Denayer, J. F. M.; Volkmer, D. Vanadium Analogues of Nonfunctionalized and Amino-Functionalised MOFs with MIL-101 Topology – Synthesis, Characterisation, and Gas Sorption Properties. *Eur. J. Inorg. Chem.* **2012**, 2481-2486.

2. EXPERIMENTAL

2.1 Synthesis

2.1.1 Methods of Synthesis

3 metal salts and 1 ligand were used in the various syntheses; ammonium metavanadate (NH_4VO_3), sodium metavanadate ($NaVO_3 \cdot 4H_2O$) and vanadyl sulphate ($VOSO_4 \cdot 4H_2O$), as the metal salts and 1, 2, 4, 5 – benzenetetracarboxylic acid (H_4B4C), as the ligand. These starting materials were used for every synthesis and the metal to ligand ratio was 2:1, this was kept constant throughout each synthesis, unless otherwise stated. This ratio was chosen from reviewing various synthetic procedures in the literature, which all reported ratios within this range [1-5]. Vanadyl acetylacetonate (VOacac) was included as a metal salt in ambient and reflux syntheses with the ligand.

A number of different synthetic methods were employed in an attempt to form a possible V-MOF, these can be listed as; ambient, solvothermal, gel and reflux.

Ambient syntheses are the most simple of the synthetic methods. The metal salt and ligand are dissolved in an appropriate solvent, combined, stirred for a given time to ensure proper mixing and then stored under ambient conditions with the aim of forming a product. Ambient syntheses are kinetically controlled, where there is little to no activation energy involved, the reaction is driven by mixing of the various components in solution under ambient conditions. These syntheses are generally left for up to a week or more, to allow time for the precipitation of the maximum amount of product from the solution, to ensure that the greatest yields are achieved.

Solvothermal synthesis involves a similar set-up as ambient synthesis, but the reaction mixture is placed into an autoclave, which exposes the mixture to high temperatures and pressures. Solvothermal syntheses are also kinetically controlled, but follow a different reaction pathway, as the reaction mixture is exposed to elevated temperatures (150-200°C) and pressures (autogenous). Under these conditions a new product is formed, which is generally exhibits stronger bonding, with a more ordered structure, when compared to ambient syntheses. Solvothermal syntheses are generally carried out for 3 to 5 days.

Gel synthesis involves use materials which have the ability to undergo gelation. Examples of materials that undergo gelation are; agar, gelatine and sodium metasilicate. For the experiments undertaken, gelatine and sodium metasilicate were used. Sodium metasilicate was chosen, as the material has been well known and well-studied as a medium in which crystals can grow, but can only form a gel at a pH value of ± pH 6.5 [6]. Gelatine was chosen as it is far more robust and can form a gel at a wider pH range [6]. The general procedure for setting up a gel synthesis was to first impregnate the gel with the ligand, this is done by

simply adding the ligand to the gel, by dissolving them both in water and mildly heating the dissolved mixture until the gel hardens and sets. After the gel has set, the metal salt is added over the gel and allowed to slowly diffuse through and react with the ligand over time. The rate of the reaction is determined by the rate of diffusion of the metal salt, which is generally very slow, so these reactions can take months to years to complete. Note that when using gelatine or agar, one needs to heat the powdered material in an autoclave before use. This is to ensure that there are no bacteria associated with the material, as to avoid bacterial growths, which were discovered in the gel syntheses using gelatine and will be discussed in Chapter 3.

Gel syntheses have the advantage of often producing a product with a high purity and can often be in the form of single crystals. Single crystals are very useful in the determination of size and structural factors via X-ray crystal diffraction and are generally difficult to synthesise using other synthetic methods.

Reflux syntheses also involve the same initial steps as ambient syntheses. The reaction mixture is put under reflux at the boiling temperature of the solvent used. The reaction is run at elevated temperatures, but lacks the pressures and temperatures which solvothermal conditions expose the reaction mixture to, so a different kinetic pathway from the ambient and hydrothermal syntheses is expected to be followed.

2.1.2 pH Control

pH control was employed in almost all of the above mentioned methods of synthesis. It is one of the most important factors when using a carboxylic acid based ligand such as H_4B4C in the formation of a MOF or complex. Controlling the pH allows for the manipulation of the ligand, specifically with regards to the number of protons that are attached to the carboxylic acid functional groups, which are substituents of the benzene ring.

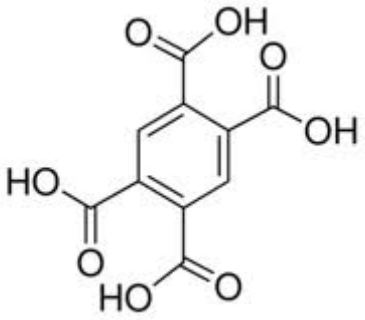

Figure 18: 1, 2, 4, 5 – benzenetetracarboxylic acid with all the carboxylic acid functional groups being protonated [7].

By altering the pH of the solution to be more acidic, it is expected that the majority or all of the carboxylic acid functional groups will be protonated, as the solution will have an excess of H^+ or H_3O^+ ions.

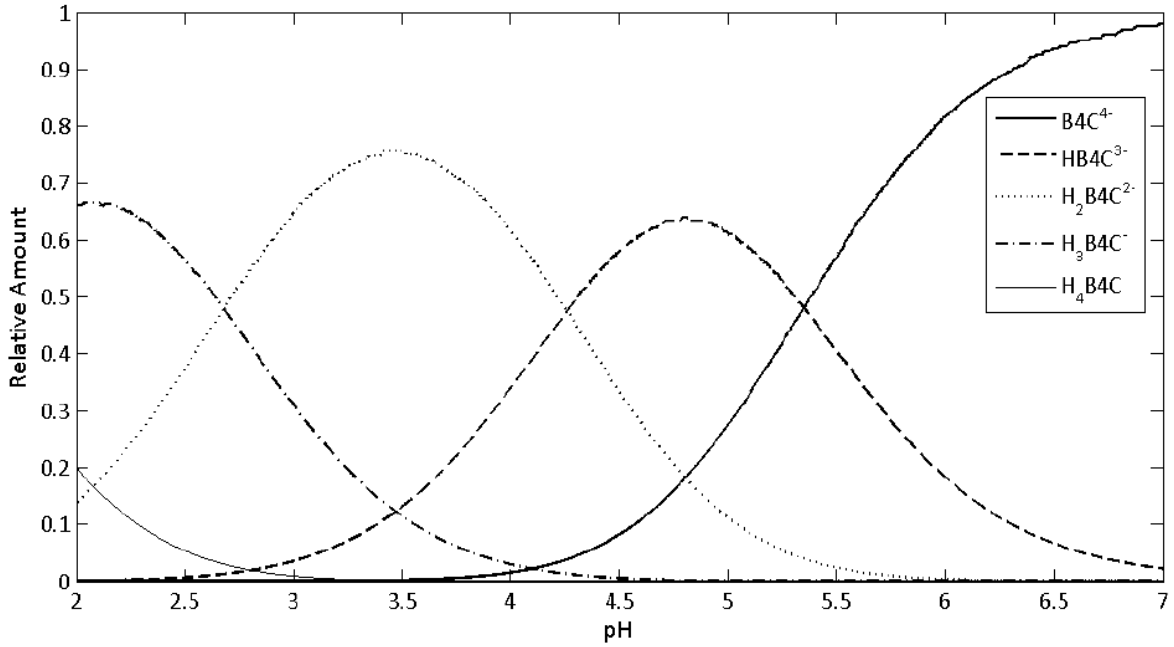

Figure 19: Speciation curves of H_4B4C showing the relative amounts of the various species, over varying pH values.

The distribution curve was modelled by Matthew Coombes [8], using HySS software [9]. The dissociation constants of H_4B4C in the model were [10]: k_1 = 1.20 x 10^{-2}; k_2 = 1.34 x 10^{-3}; k_3 = 3.2 x 10^{-5}; k_4 = 2.35 x 10^{-6}.

The distribution curves in Figure 19 indicate at which pH values, the greatest relative amount of each specific species is observed. The pKa values were determined as the points upon which any two species meet, where their relative amounts are in equilibrium. They were determined to be; 1.92, 2.87, 4.49, 5.63. The equilibrium point between 2 species of H_4B4C was chosen due to it offering two possible pathways for the reaction to proceed through. If an exact point is chosen for just one species, the reaction has only one pathway to proceed through. These pKa values were used for all the different syntheses, as the pH values were altered to match that of the pKa value and thereby controlling the number of protons attached to the ligand.

2.1.3 Attempted and Successful Syntheses

From Table 3 on the following page, one can observe that a number of the attempted syntheses were unsuccessful, by which no apparent complexation was achieved between the metal and ligand.

Table 3: A summary of all the syntheses attempted at the various pKa values of H_4B4C, 'X' denotes a unsuccessful synthesis, whereas 'product' denotes a successful synthesis.

	Ambient			
pH:	**1.92**	**2.87**	**4.49**	**5.63**
$NaVO_3$	X	X	X	X
NH_4VO_3	X	X	X	X
$VOSO_4$	X	Product	Product	X
VOacac	X	X	X	X

	Gel			
pH:	**1.92**	**2.87**	**4.49**	**5.63**
$NaVO_3$	X	X	X	X
NH_4VO_3	X	X	X	X
$VOSO_4$	X	X	X	X

	Reflux	
Atmosphere:	**Air**	**N_2**
$NaVO_3$	X	X
NH_4VO_3	X	X
$VOSO_4$	X	X
VOacac	X	X

	Solvothermal	
pH:	**1.92**	**5.63**
$NaVO_3$	Product	X
NH_4VO_3	Product	X
$VOSO_4$	Product	X
$VOCl_2$	Product	X

Unsuccessful syntheses were most evident for the ambient syntheses involving the metavanadate species. This was due to either the formation of the vanadium oxide (V_2O_5) or decavanadate ($[H_xV_{10}O_{28}]^{X-}$), which both form as the pH of the solution is lowered (see Figure 9; pg. 14). The reason for complexation failure is due to the vanadium metal centres being surrounded by oxygen. When the ligand attempts to bind through either its deprotonated carboxylic acid functional groups at a low pH value (1.92), the oxygen already bound to the vanadium centre will compete with the oxygen from the carboxylic acids. The hope was that binding of metal to ligand may occur from the deprotonated carboxylic acid groups at a higher pH value (5.63), but this was not found to be the case. This was confirmed by the IR spectrum of the mixed solution being identical to that of the

unmetallated ligand at this specific pH value. The results of the ambient syntheses were generally; the formation of a metal salt, with its structure depending on the pH of the solution and a ligand salt, such as Na^+ or NH_4^+ bound to H_4B4C, which was also dependent on the pH of the solution. The unsuccessful syntheses will be addressed in the results section.

In contrast to this, the vanadyl ion of $VOSO_4$ was observed to generally form a complex with the ligand in most syntheses. This is due to the vanadium centre being doubly bound to a single oxygen and still having free coordination sites on the vanadium centre, which allow ligands, such as H_4B4C to bind and form a complex.

2.1.4 The General Synthetic Procedures

2.1.4.1 Ambient Syntheses

Solutions of the metal salt and ligand were added to one another in a molar ratio of 2:1. H_4B4C (1.00 g, 0.0039 mol) was added to H_2O (40ml), to which ±10 drops of absolute ethanol (EtOH) were added to aid in the dissolution of H_4B4C. The mixture was then heated and stirred until all the H_4B4C had been dissolved in a separate flask. $NaVO_3{\cdot}4H_2O$ (1.51 g, 0.0078 mol) or NH_4VO_3 (0.92 g, 0.0078 mol) or $VOSO_4{\cdot}4H_2O$ (1.85 g, 0.0078 mol) was added to H_2O (40 ml), which was also stirred and heated to ensure that the metal salt was completely dissolved. The two solutions were added to one another, stirred and slowly cooled to room temperature. Once at room temperature a pH meter was employed to determine the actual pH of the solution, after which the pH was then adjusted to the required value by adding either 1 M sodium hydroxide (NaOH) or 1 M ammonium hydroxide (NH_4OH) to increase the pH, or 32% hydrochloric acid (HCl) to decrease the pH. The solution was covered with parafilm to prevent impurities from entering and to prevent any appreciable loss of solvent due to evaporation. The solution was stirred, with no heating for one week, to allow for product formation and the potential precipitation of said product. When a product precipitated out of solution, it was filtered, washed with deionised water and allowed to dry under atmospheric conditions. With the above being the general procedure, alterations could and were made to aid in the precipitation of the potential product. These alteration steps were to reduce the initial amount of solvent to which H_4B4C and the metal salt were separately dissolved in. This volume could be reduced to 25 mL for both the ligand and metal salt, which often increased the rate of product formation. If a product had not precipitated out of solution after the length of a week, a vacuum pump was employed to reduce the volume further, until precipitation was observed.

2.1.4.2 Gel-based Syntheses

Two well-known gelling materials were employed in the gel-based syntheses and the methods specific to sodium metasilicate and gelatine will be presented. A straight-tube method was used for all the gel syntheses.

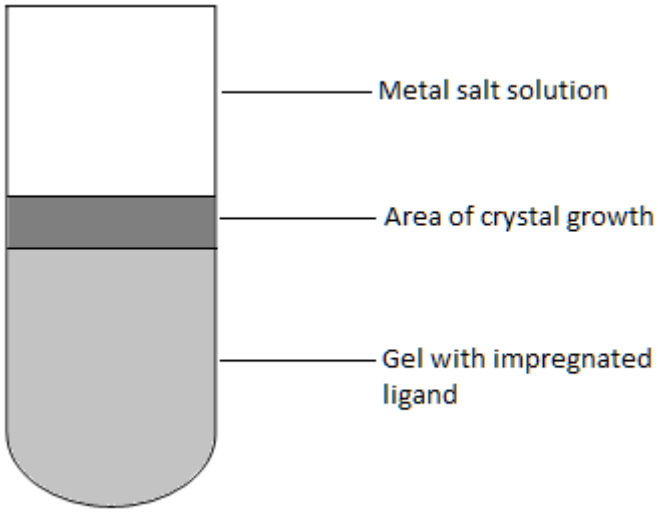

Figure 20: A Typical Straight-tube Synthesis.

Sodium metasilicate as a gelling material:

H_4B4C (1 g, 0.0039 mol) was added to H_2O (25 ml), with ±10 drops of EtOH added to aid with dissolution of H_4B4C. The solution was heated and stirred until all the solid H_4B4C had been dissolved and was then transferred into a boiling tube. A sodium metasilicate stock solution was made up with the concentration of 488 g/L. 5 ml of the stock solution was carefully and immediately added to the dissolved H_4B4C. The pH of the solution was then adjusted to 6.5 through the careful addition of acetic acid. The gel solution, containing H_4B4C, was then heated at a constant temperature of 40°C overnight to allow it to set and harden, with the top of the boiling tube covered with parafilm. $NaVO_3{\cdot}4H_2O$ (1.51 g, 0.0078 mol) or NH_4VO_3 (0.92 g, 0.0078 mol) or $VOSO_4{\cdot}4H_2O$ (1.85 g, 0.0078 mol) was added to H_2O (40 mL) and heated to ensure that the metal salt was completely dissolved. Once cooled to room temperature, this was then carefully layered over the top of the hardened gel in the boiling tube and the top of the boiling tube was re-covered with parafilm. The boiling tube and contents were left for a number of months to allow the metal salt solution to slowly diffuse into the gel that was impregnated with the ligand and possibly form a complex or complexes.

Gelatine as a gelling material:

H_4B4C (1 g, 0.0038 mol) was added to H_2O (25 ml), with ±10 drops of EtOH added to aid in dissolution of H_4B4C. The solution was then heated and stirred to ensure that the H_4B4C had entirely dissolved. Gelatine powder (5.5 g) was added to H_2O (50 ml), then the solution of H_4B4C was added to this and the resultant mixture was transferred to a boiling tube, was heated and occasionally stirred to ensure that the gel dissolved entirely. The pH of the mixture of H_4B4C and the gelatine was naturally 1.80 and from here the pH value was adjusted in the same fashion to that of the previously mentioned ambient syntheses, with 1 M sodium hydroxide (NaOH) or 1 M ammonium hydroxide (NH_4OH) being used to increase the pH value and 32% hydrochloric acid (HCl) being used to decrease the pH value. The gel was allowed to stand overnight to allow it to set and harden, with the top of the boiling tube being covered with parafilm. Once the gelatine mixture had set, the solution containing the metal salt dissolved in H_2O (40 mL) and was carefully layered on top of the gelatine and allowed to stand for a number of months, with the top of the boiling tube again being re-covered with parafilm to ensure no appreciable loss of solvent.

2.1.4.3 Reflux Syntheses

The initial steps for the reflux synthesis are identical to the ambient process, in terms of masses and solvent volumes. After the metal salt and ligand solutions are added together, the resultant solution was transferred into a round bottomed flask. The solution was stirred and put under reflux in an inert atmosphere using nitrogen (N_2) or normal atmospheric conditions. The reflux was set at 100°C for water and 65°C for methanol, which was the solvent when using VOacac as the metal salt, and left for a 12 hour period. The reaction mixture was purged with N_2 for 30 minutes before being exposed to the reflux conditions under an inert atmosphere. Any products formed were washed with deionised water, filtered and dried.

2.1.4.4 Solvothermal Syntheses

Solvothermal syntheses were completed using two different types of autoclave. The first autoclave used was a Berghof BR-300 high pressure reactor, which uses a 230 mL Teflon insert to contain the solution. This autoclave is the more sophisticated of the two, as it has been manufactured with programmable temperature settings. The second autoclave is an older metal-heated oven type autoclave, where the oven temperature has to be set manually if any changes are required. With using two different types of autoclaves, the method for each was slightly different. Care needed to be taken with the volume of solvent used in the solvothermal syntheses, as too little solvent would vapourise, leaving the potential product to char and too much solvent could potentially cause the material housing the sample solution to burst or break, as the vapour pressure would exceed the pressures

limits of the material. This was only necessary for the older oven type autoclave, which lacked pressure controls.

High Pressure Reactor:

The initial steps for the solvothermal synthesis are identical to the ambient process, in terms of masses and solvent volumes. After the metal salt and ligand solutions are added together and after any pH adjustment, the resultant solution was transferred into a 230 mL Teflon insert, which was then placed into the autoclave. The temperature program could be set in a number of different ways, an example of a successful temperature program is described below.

Table 4: An example of a temperature program used for a solvothermal synthesis using the high pressure reactor.

Ramp (mins)	Hold (mins)	Temperature (°C)
300	10	50
300	10	100
300	1440	150
300	10	100
300	10	50
300	10	25

'Ramp' was the time taken to reach the specific temperature and 'Hold' was the length of time at which the autoclave was held at the specific temperature. One can observe that there was slow heating up to 150°C and the temperature was held there for 24 hours and then slow cooling was employed to reach room temperature.

Metal Oven Autoclave:

After the metal salt and ligand solutions are added together and after any pH adjustment, the resultant solution was then transferred to an ± 80 mL thick walled glass tubes, which were sealed with a blowtorch. Particular care needed to be taken with the amount of solvent that was added to the tubes, as the vapour pressure could exceed the pressure limits of the tubes, thereby causing the tube to burst, so the tubes were always filled to halfway (40 mL) with the sample solution. These were entered into the autoclave, which was set at 200°C and were left for between 5 and 7 days, depending on the system under study. The sample tubes were then removed from the autoclave, allowed to cool and finally cut in half, to allow for product removal. The product was then filtered, washed and dried.

2.2 Characterisation Techniques

A detailed description of each technique presented in this section is offered in the Instrumentation Appendix, which is displayed from pg 120 onwards. Only the information that is relevant for the thesis is presented in this section.

2.2.1 Microanalysis

A Vario MICRO V1.6.2 elemental analysis system was used for the determination of the percentages of carbon, hydrogen, nitrogen and sulphur (CHNS analysis).

The vanadium content was determined using a Thermo iCap 600 series ICP-OES spectrometer (V detected at wavelengths 292.4 and 311.0 nm) and the sodium content was determined using a Perkin Elmer AAnalyst 200 Atomic absorption spectrometer (with a sodium lamp).

Both the CHNS and ICP analyses can be used as complementary techniques to determine the empirical formulae of the synthesised complexes. With the empirical formulae known, a number of conclusions can be made about the complex of interest, such as the nature of coordination between the metal and ligand, insights into the structure of the basic unit cell and the identity of counter ions and guest molecules present. When microanalysis techniques are combined with the following techniques of characterisation, it is able to provide a strong foundation, upon which to gain deeper insights into the structure of the complex.

Descriptions of the principles of the techniques may be found in literature [11-12].

2.2.2 Vibrational Spectroscopy

A Perkin-Elmer Spectrum 100 FT-IR with an ATR attachment was used for IR analysis of materials prepared as part of this study. The mid IR region (4000 - 650 cm^{-1}) was analysed using 4 scans at a resolution of 4 cm^{-1}. All the spectra were; baseline corrected and smoothed, using the Spectrum software (version 6.3.5).

The bands of interest in the IR and Raman spectra are those associated with the carboxylic acid groupings of the H_4B4C molecule, as these are the points of coordination to the metal centres. Upon coordination to the metal centres, their modes of vibration become limited, so generally stretches are all that can be seen, as bending vibrations become restricted. The region in which the *v*(C=O) and *v*(C-O) stretches are seen from 1300 cm^{-1} to 1700 cm^{-1} [2][4][13]. Bands associated with the vanadium oxide species are also of interest, as they can be used to identify which vanadium oxide species is present within the complex. The region of interest for *v*(V=O) and *v*(V-O) stretches are around 1000 cm^{-1} for the *v*(V=O) stretch and around 800 to 500 cm^{-1} for the *v*(V-O) stretches and bends [2][4].

Descriptions of the principles of the techniques may be found in literature [13-14].

2.2.3 X-ray Powder Diffraction

The X-ray powder diffraction studies were completed using a Bruker D8 Discovery X-ray powder diffractometer. Copper K_α radiation (λ_1 = 1.54060 Å, λ_2 = 1.54439 Å, ratio = 0.5), with a nickel filter was used. The generator tube was operated at a potential of 40 kV with a current of 40 mA. The divergence slit width was 0.6 mm and the primary Soller slit was 4.0°.

Descriptions of the principles of the techniques may be found in literature [15-16].

2.2.4 Thermogravimetric Analysis

A Perkin-Elmer TGA 4000 with an FTIR attachment was used for the thermogravimetric analysis, using Pyris version 11.0 software. A temperature program of 20°C to 800°C at 10°C/min and held at 800°C for 5 minutes was implemented, with a nitrogen flow rate set at 19.8 mL/min.

The nature of the particle size of the sample is an important factor in TGA, as the heating of the sample should be as uniform as possible. For this reason the sample should be in the form of a powder, as this will have the best thermal conductivity [17-19]. All the samples precipitated out in the form of a powder or small crystallite, so further sample preparation was unnecessary.

Descriptions of the principles of the techniques may be found in literature [17-19].

2.2.5 Differential Scanning Calorimetry

DSC studies were performed using a Perkin-Elmer DSC 6000, using Pyris version 11.0 software. A temperature program of 20°C to 445°C at 10°C/min and held at 445°C for 5 minutes was implemented, with a nitrogen flow rate set at 19.8 mL/min.

TGA and DSC couple well together, as TGA provides the mass losses associated with temperature and DSC is able to provide the change in enthalpy of these specific mass losses. Determining the change in enthalpy for a given process is important for guest inclusion studies, when specifically studying MOFs, as knowing the energy required to release the guest molecules is very important. If the ΔH is too high, then the guest molecules are being held too strongly in the pores and may require too high an energy requirement to remove [18]. If the ΔH is too low, then there is little to no interaction between the guest molecule and the pore and the guest molecules can be removed too easily and the material will not be suitable as a storage material [18-19].

Descriptions of the principles of the techniques may be found in literature [17][19].

2.2.6 Gas Chromatography for Catalysis

An Agilent 7890A GC system connected to an Agilent 7000 GC/MS triple quad detector was used for the study. An Agilent 7693 autosampler was used for sample injections. The software used was MassHunter Workstation Software, version B.05.00 with the NIST mass spectrum database. The column used was a Zebron ZB-WAX plus (100% polyethylene glycol) column, with specifications of; length: 30 m, internal diameter: 0.32 mm, film thickness: 0.25 µm. The method for all the runs was set with the temperature initially being set to 40°C, where it was held for 1 min and increased at 30°C/min to 250°C, where it was held for 3 min.

The inlet was set at a temperature of 250°C and split injection was used at a ratio of 20:1. The carrier gas was helium and the column flow rate was set to 1.2784 mL/min. The temperature of the MS detector was set at 230°C.

Descriptions of the principles of the techniques may be found in literature [20- 23].

2.2.7 Scanning Electron Microscopy – Energy Dispersive X-ray Spectroscopy

SEM imaging was done using a Vega TESCAN and EDX was done using an Inca PentaFET x3 attachment.

Descriptions of the principles of the techniques may be found in literature [24].

References:

1. Riou, D.; Férey, G.; Marrot, J.; Barthelet, K. A Breathing Hybrid Organic-Inorganic Solid with Very Large Pores and High Magnetic Characteristics. *Angew. Chem. Int. Ed.* **2002**, *42* (2), 281-284.
2. Cevik, S.; Poyraz, M.; Sari, M.; Büyükgüngör, O. A Novel Three Dimensional Organic-Inorganic Hybrid Based Porous Phase: Synthesis and Characterization of Reduced Oxovanadium Pyromellitate, $[V^{IV}_2O_2(H_2O)_2(C_6H_2(COO)_4)]$. *J. Chem. Crystallogr.* **2007**, *37*, 497–502.
3. Vasović, D. D.; Stojaković, D. A Polymeric Oxovanadium(IV) Pyromellitate Complex. *J. Serb. Chem. Soc.* **1999**, 64 (9), 513-518.
4. Li, Y.; Yan, C.; Wu, Z.; Zhu, C. Synthesis and Magnetism of μ-Tetracarboxylato-Bridged Dinuclear Oxovanadium(IV) Complexes. *Syn. React. Inorg. Met.* **2005**, *35*, 319–324.
5. Van Der Voort, P.; Van Speybroek, V.; Leus, K.; Vandichel, M.; Liu, Y.; Muylaert, M.; Musschoot, J.; Pyl, S.; Vrielinck, H.; Callens, F.; Marin, G. B.; Detavernier, C.; Wiper, P. V.; Khimyak, Y. Z.; Waroquier, M. The Coordinatively Saturated Vanadium MIL-47 as a Low Leaching Hetergeneous Catalyst in the Oxidation of Cyclohexene. *J. Catal.* **2012**, *258*, 196 - 207.
6. Henisch, H. K. *Crystal Growth in Gels and Liesegang Rings*, Cambridge University Press, 1988.
7. Image of 1, 2, 4, 5 - Benzenetetracarboxylic Acid; http://www.sigmaaldrich.com/catalog/product/aldrich/b4007?lang=en&region=ZA (Accessed: 14/02/16)
8. M. Coombes**.** A Comparative Study of Two Copper(II) Based Metal-Organic Frameworks: $Cu_{2}1_{/4}(OH)_{1/2}B4C{\cdot}8H_2O$ and $Cu_2Na(OH)/B4C{\cdot}8H_2O$. M.Sc. Dissertation, Rhodes University, 2012.
9. Alderighi, L.; Gans, P.; Lenco, A.; Peters, D.; Sabatini, A.; Vacca, A. Hyperquad Simulation and Speciation (HySS): AUtility Program for the Investigation of Equilibria Involving Soluble and Partially Soluble Species. *Coordin. Chem. Rev***. 1999**, *184* (1), 311-318.
10. Maxwell, W.; Partington, J. The Dissociation Constants of Some Polybasic Acids. – Part III. *J. Chem. Soc. Faraday. Trans.* **1937**, *33*, 670-678.
11. Skoog, D. A.; West, D. M.; Holler, F. J.; Crouch, S. R. *Fundamentals of Analytical Chemistry*. Thomson Brooks/Cole, 2004.
12. Christian, G. D. *Analytical Chemistry*. Fifth Edition. John Wiley & Sons, 1994.
13. Nakamoto, K. *Infrared and Raman Spectra of Inorganic and Co-ordination Compounds Part A*. Sixth edition. John Wiley & sons, Inc. New Jersey, 2009.
14. Gardiner, D. J. *Practical Raman Spectroscopy*. Springer-Verlag, 1989.
15. Azároff, L. V.; Buerger, M. J. *The Powder Method in X-ray Crystallography*. McGraw-Hill book company, 1958.

16. Cullity, B. D. *Elements of X-ray Diffraction*. 2nd edition. Addison-Wesley, 1978.
17. Brown, M. E. *Introduction to Thermal Analysis: Techniques and Applications*. Second edition. Kluwer Academic Publishers, 2001.
18. Farrusseng, D. *Metal-Organic Frameworks: Applications from Catalysis to Gas Storage*. Wiley-VCH, 2011.
19. Wunderlich, B. *Thermal Analysis*. Academic Press, Inc, 1990.
20. Hübschmann, H. J. *Handbook of GC/MS: Fundamentals and Applications*. Second Edition. Wiley-VCH, 2009.
21. McNair, H. M.; Miller, J. M. *Basic Gas Chromatography: Techniques in Analytical Chemistry*. John Wiley & Sons, 1998.
22. De Hoffmann, E.; Stroobant, V. *Mass spectrometry: principles and applications*. Second Edition. Wiley & Sons, 2002.
23. Sparkman, D. O. *Mass Spectrometry Desk Reference*. Pittsburgh: Global View Publishers, 2000.
24. Goldstein, J. *Scanning Electron Microscopy and X-ray Microanalysis*. Springer, 2003.
25. McMullan, D. Scanning Electron Microscopy 1928-1965. *SCANNING*. **1995**, *17*, 175-185.

3. CHARACTERISATION RESULTS

3.1 Unsuccessful Syntheses

In the summary tables (Table 3; pg. 34) of Chapter 2, it was noted that a number of the synthetic methods were found to be unsuccessful, due to the fact that no complexation between the metal and ligand took place. The following subsections are a summary of the unsuccessful syntheses, with a discussion and reasons as to why they may have been unsuccessful.

3.1.1 Ambient Syntheses

The majority ambient syntheses attempted were found to be unsuccessful, specifically for those involving the vanadate ions. The reason for the failure was due to the pH sensitivity of the vanadate ion. When the pH was adjusted to the various values stated in Chapter 2 - Table 3, the vanadate ions structure would be transformed to either V_2O_5 or the decavanadate species with varying degrees of deprotonation. Decavanadate species will be anionic in solution, so under ambient conditions the ion will be attracted to cations to form an ionic bond, neutralising the net charge of the species, i.e. the role sodium plays in decavanadate ($Na_6[V_{10}O_{28}]$). H_4B4C can only be neutral (fully protonated) or have a varying degree of deprotonation associated with it, depending on the pH of the synthesis. Full deprotonation of the ligand will not yield a product without the inclusion of a bridging cation. Protonation of the ligand yields the chance to bind to the oxo-vanadium clusters through possible hydrogen bonding, but this was not what was found, due to the ligand already being in a neutral state. Under ambient conditions there is just insufficient energy to initiate the substitution of the oxygen within the vanadium cluster for those of the carboxylic acid groups, allowing for oxo-coordination between the metal and ligand. This has only been observed to occur under solvothermal conditions. Different M:L ratios were attempted for the vanadate syntheses, ranging from 1:1 to 4:1 but this had no effect on the outcome of the reaction.

The vanadyl ion differs from the vanadate ion, as it is coordinatively unsaturated, so has available sites, where binding can occur. The reason for the failure of complexation shown in Table 3 for $VOSO_4$ at pH 1.92, was due to the fact that the ligand was completely protonated at this particular pH value, leading to it being neutral and precipitating out of solution with no coordination to the metal ion occurring. Conversely, at pH 5.63, the ligand is expected to be fully deprotonated and therefore should be able to coordinate to the metal ion. The product however precipitated out as a black sludge, which was identified to be a mixture of a number of products with the inclusion of the sulphate ion, through a number of different separation and recrystallisation steps. The vanadyl ion is only found to

be stable below a pH value of approximately 3.5. When the pH exceeds this value, the formation of various hydroxy-substituted vanadates, deca- and orthovanadates have been known to form, which would inhibit coordination between the metal and ligand for the same reasons as previously discussed [1].

Syntheses were assessed as successful or unsuccessful, by interpreting the IR spectra and the SEM-EDX data of the isolated material. The IR spectra and SEM-EDX data were adequate to conclude if a product of interest had precipitated out of solution. SEM-EDX was a technique used to determine, at a qualitative level, the identity of the elements present in the samples. If either vanadium or carbon was absent, the synthesis was simply noted as being unsuccessful. The IR spectrum was examined for bands which showed coordination between the metal and ligand, these regions are indicated in the Chapter 2. The bands of particular interest were the carbonyl stretches (ν(C=O) and ν(C-O)), which are expected in the region of 1700 cm^{-1} to 1250 cm^{-1} and the vanadyl stretch (ν(V=O)) at approximately 1000 cm^{-1}. If these bands were found to be present in the spectrum, they were then compared to that of the free ligand and free metal ion, to compare the bands position, shape and intensity to determine if any shifts and changes were evident. If the bands were very similar in position, shape and intensity to that of the free ligand or metal salt, the product was identified as a mixture containing the ligand and/or metal salt. If the bands were shifted in terms of position, shape and intensity, the product was noted as a promising potential complex and set aside for further analysis.

A general example of an unsuccessful synthesis is displayed as the addition of $NaVO_3 \cdot 4H_2O$ and H_4B4C at pH 1.92, to which the results will be discussed.

The product of the ambient synthesis of $NaVO_3 \cdot 4H_2O$ and H_4B4C at pH 1.92 precipitated out of solution after a week in the form of a homogenous dark red powder, with no obvious visual evidence of a mixture. SEM-EDX initially found the product of the synthesis to exhibit appreciable amounts of carbon and vanadium, indicating that it may be a product of promise. IR was utilised to further analyse the product. The ligand and metal salt were individually exposed to the same pH value of 1.92. This was able to form the resultant ligand and metal salts at pH 1.92, which could then be used in the interpretation of the IR spectrum as references in the determination of whether a product or mixture had formed. The ligand salt Na-B4C forms at pH 1.92, as one may expect there to be one deprotonated carboxylic acid group to which a sodium atom may ionically bind. The metal salt shifts from the metavanadate species to V_2O_5 at pH 1.92. Na-B4C, V_2O_5 and the product of the reaction were plotted together in Figure 21.

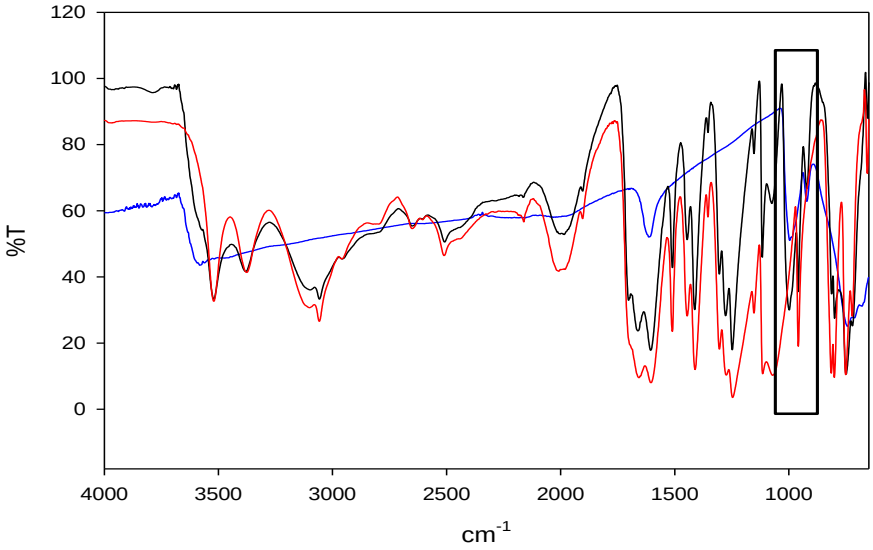

Figure 21: The IR spectra of Na-B4C (red), V_2O_5 (blue) and the product (black).

Table 5: An IR comparison of Na-B4C, V_2O_5 and the reaction product.

	Product(cm^{-1})	**Na-B4C (cm^{-1})**	**V_2O_5(cm^{-1})**
***v*(O-H)**	3522, 3381	3522, 3381	3577
H-bonding and overtone region	2656 -1980	2656 -1980	None
***v*(C-H)**	3057	3057	None
***v*(C=O) and *v*(C-O)**	1700 -1252	1700 -1252	None
***v*(V=O)**	998	None	998

Visually analysing and comparing the three spectra displayed in Figure 21 concludes that the spectra of the product and Na-B4C closely match one another in terms of peak position. This is further proven when the positions of the bands of interest are compared, shown in Table 5, where one can again observe that all the band positions are identical except for the band associated with the vanadyl band, as it is not found to be present in the Na-B4C salt. Upon viewing the vanadyl region, the band for the product at pH 1.92 matches that of the metal species (V_2O_5) at 998 cm^{-1}. With this information it can be confirmed that the ambient product at pH 1.92 is a mixture of the V_2O_5 and Na-B4C, with the vanadyl band originating from the metal salt and the organic functional groupings originating from the ligand salt.

3.1.2 Reflux Syntheses

All the reflux syntheses were determined to be unsuccessful, as they were identified to either be uncoordinated metal or ligand salts from IR spectroscopy and SEM-EDX. The vanadate refluxes produced the dark-red V_2O_5 metal salt, confirmed via IR spectroscopy, and the vanadyl refluxes produced a ligand salt, as no vanadium was found to be present via

SEM-EDX. The reactions were exposed to elevated temperatures, which altered the metal species and the kinetic pathway of the reaction, but no coordination was observed. This was possibly due to insufficient pressure being supplied into the reaction, to initiate the previously mentioned oxo-substitution between the ligand and metal species. Solvothermal syntheses are noted to build up pressure as they are contained in a closed environment, so the vapour pressure of the solvent builds up autogenously throughout the course of the reaction. This is the driving force behind the oxo-substitution of the ligand oxygen groups, being substituted for those of the vanadium cluster. Reflux syntheses lack this build-up of pressure, so the metal and ligand are not forced into close proximity, which leads to the absence of coordination.

3.1.3 Gel Syntheses

The gel syntheses were all found to be unsuccessful, due to the fact that no product formed within any of the attempted syntheses. Sodium metasilicate is known to be successful in the synthesis of MOFs from previous studies using divalent metals, such as Cu and Ni [2-4]. The problem with sodium metasilicate is that it only gels at a pH value of approximately 6.5, which is a problem, as a greater range of pH values were to be tested. Upon impregnating the gel with H_4B4C at pH 6.5, the expectation was that the ligand will be completely deprotonated. The metal salt was entered above the gel at its natural pH value; but as the metal solution slowly diffused through the gel, the pH of the metal salt would be expected to change in accordance to the pH of the resultant gel and this would cause a change to the V-species. The V-species present at pH 6.5 for both the vanadate and vanadyl salts would be the deca or orthovanadate species (see Figure 9; pg. 14). This poses a similar problem to what was observed in the ambient and reflux syntheses, as the ligand is deprotonated and cannot coordinate to the oxo-vanadium clusters under ambient conditions and requires the pressure associated with a solvothermal synthesis to initiate the oxo-substitution of the oxygen in the oxo-vanadium clusters, with those of the ligand. Ultimately, the metal salt slowly diffused through the gel, but no product was observed to form along the way.

Gelatine was used for the majority of the gel syntheses, as it had the ability to gel over a wider range of pH values. The results of the syntheses were varied, but there were certain characteristics common to the majority of the results. Initially the gel was able to for harden at each of the pH values chosen (1.92, 2.87, 4.49, 5.63) without any problems. With time, the materials obtained lower pH values were discovered to be more susceptible to dissolution than those obtained at higher pH values. The dissolution began gradually at the edges of the gel, which was in contact with the boiling tube, as can be observed in Figure 22. Dissolution progressed gradually over time, leaving a central column remaining.

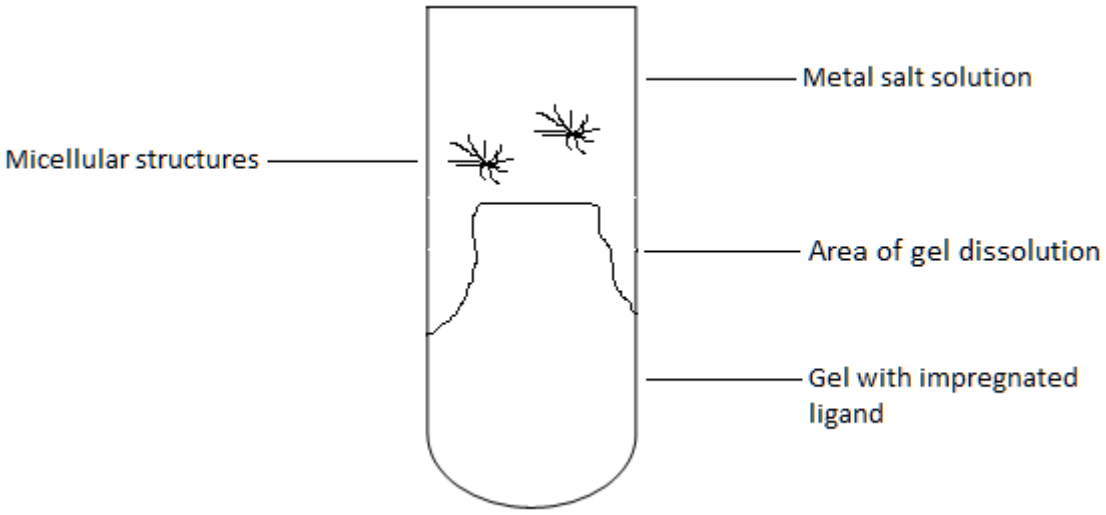

Figure 22: An example of a gelatine synthesis, where the gelatine began to dissolve around the edges of the boiling tube and micellular structures formed within the metal solution.

Syntheses using the vanadate salts were susceptible to dissolution at the lower pH values (1.92 and 2.87), whereas the materials produced at greater pH values (4.50 and 5.93) were not as susceptible, as the gel was still found to be intact, with only the top-most layer observed to have undergone partial dissolution. An interesting observation was the growth of micellular structures in the reactions involving vanadate salts at the lower pH values (1.92 and 2.87), which occurred in the metal salt layer. The micellular structures were thought to be bacterial growths, present due to the increased amount of dissolved gelatine in solution, as this would act as a food source for the bacteria. Added to this, the micelluar structures were only observed to form after significant dissolution had taken place, again indicating that the elevated levels of organic matter in solution was the cause of the bacterial growth.

Syntheses using vanadyl sulfate at low pH values (1.92 and 2.87) were found to be free of micellular structures. At pH 1.92 the entire gel layer had been completely dissolved into a viscous solution and at pH 2.87 the gelatine had also dissolved, but was slightly more viscous. The lack of micellular structures in these reactions were thought to be due to two possible reasons. The first was that the vanadyl ion is present and stable in solution at these pH values [1], which may have an effect in preventing bacterial growth [5-7]. The second reason was that insufficient time had passed to allow for any bacterial growth, but this was a weaker reason, due to the fact that at pH 4.50 and 5.63, bacterial growth was observed and all the syntheses were initially set up at the same time and had all been left for approximately 8 months. At greater pH values the gelatine was noted to show far less dissolution than the syntheses carried out at the lower pH values and it was largely noted to be intact with only partial dissolution. At the greater pH values, the colour of the metal solution was also noted to shift from blue to black.

3.1.4 Solvothermal Syntheses:

The solvothermal method of synthesis was found to yield the greatest number of potential MOFs. A number of solvothermal syntheses were attempted at both low (1.92) and high (5.63) pH values. It was evident that the greater the pH, the more likely the synthesis was to fail, as the products of these syntheses were a black powder, which was found to be vanadium oxide (V_2O_3) via IR studies. The ligand is expected to be deprotonated at high pH values, so was expected to be able to coordinate to the metal to form a MOF, but this is not what was found, instead when the ligand was protonated, coordination between the metal and ligand was observed. The problem may lie with the vanadium species present at the greater pH value, where the vanadate and the vanadyl species shift to become decavanadates, which may not be able to break-down into the VO octahedra, which was observed in the successful syntheses carried out at the lower pH values.

3.2 Successful Syntheses

3.2.1 Ambient Syntheses

Table 3 (pg. 34) showed that the ambient syntheses were most successful when involving the vanadyl ion at pH values of 2.87 and 4.50. A series of syntheses were carried out over this pH range of interest at; pH 2.87, pH 3.10, pH 3.50, pH 4.0 and pH 4.50 to optimise the product. With an increase in pH above 4, the vanadyl ion becomes unstable and begins to form deca or orthovanadate species, which is problematic, as this leads to mixture of products precipitating out of solution. After a series of tests using microanalysis and TGA, it was found that pH 3.5 yielded the purest product, which precipitated out of solution as an olive green powder. The product of the synthesis performed at pH 3.5 will be referred to as RU-V2 for the remainder of the thesis and was chosen to be used in catalysis studies.

3.2.1.1 Elemental Analysis of RU-V2

Figure 23 shows the basic structural unit which was the most logical fit according to IR, elemental analysis and TG data. The vanadyl ion has possibly been bound to two of the carboxylic acid groups via bidentate coordination, as at a pH value of 3.5 the dominant ligand species is expected to be H_2B4C^{2-} (see Figure 19; pg. 33), therefore two of the carboxylic acid groups are expected to be protonated, with the remaining two being deprotonated and able to coordinate to the metal centres. Six water molecules were found to be associated with the structure via TGA, but the exact positioning of the water molecules cannot be confirmed and only assumed. A single water molecule may be weakly bound to each of the vanadyl centres, giving the metal centres a tetrahedral geometry, with the remaining four waters expected to be associated with the Na atoms. Table 6 shows the empirical formula was found to be the best fit to both the elemental and TG data.

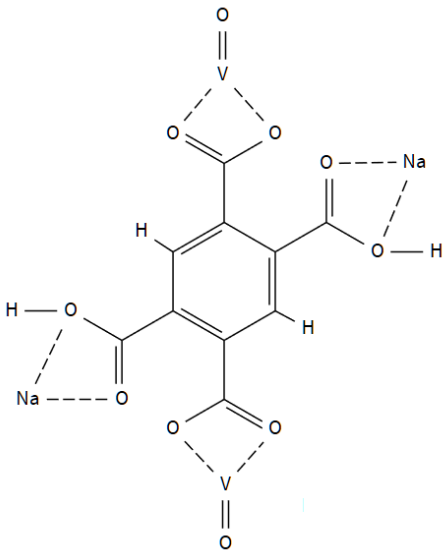

Figure 23: The basic vanadyl structural unit, upon which the microanalysis calculations were based (associated waters are excluded).

Table 6: Elemental Analysis Results for RU-V2.

Formula	**% C**	**% H**	**% Na**	**% V**	**V:B4C**
(Experimental)	22.37	2.58	8.25	17.96	1.89:1
$V_2O_2(Na_2H_2B4C)\cdot 6H_2O$	22.23	2.99	8.51	18.86	2:1

3.2.1.2 Vibrational Analysis of RU-V2

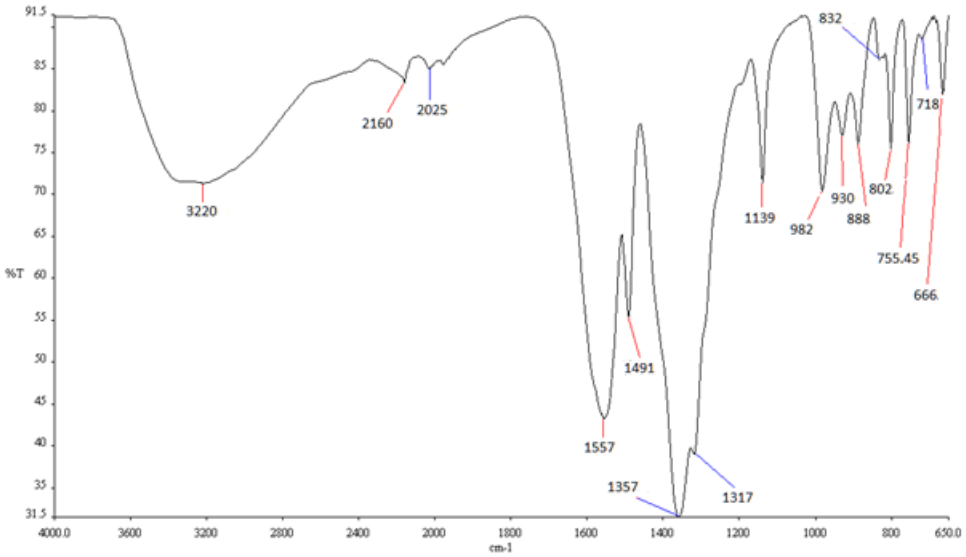

Figure 24: The IR Spectrum of RU-V2.

The analysis of the infrared spectrum of RU-V2 offers a great deal of information on which functional groups are present in the complex, namely the carboxylate and vanadyl groups, and possibilities on how these groups are coordinated to one another. In IR spectroscopy there are three main factors to observe; band shape, intensity and position. The band shape, particularly the broadness of the band, determines whether the functional group is coordinated or uncoordinated, as if a broad band is observed, the group is able to vibrate over a larger area, so can be concluded to be uncoordinated and potentially in a terminal position. If the band is sharp and well defined, the group is more restricted in the extent to which it can vibrate, due to another group being directly coordinated to it. Band intensity is due to the polarisability of the bond, as the more polar the group, the greater the intensity of the corresponding band. Changes in the environment surrounding the bond may act to alter the polarisabilty of said bond. Band position is a measure of the amount of energy required to vibrate a group, e.g. C=O and C-O, where the double bond is stronger than the single bond, so will require more energy in order to vibrate. Different modes of vibration also have different energy requirements, e.g. stretches > bends. These phenomena will be referred to in the following results and discussion sections.

Table 7: The Vibrational Bands of RU-V2.

Vibrational Assignment	**RU-V2 (cm^{-1})**
ν(O-H)	3220
Combination and overtone region	2160; 2025
$\nu_a(CO_2^-)$	1575 (shoulder); 1557; 1491
$\nu_s(CO_2^-)$	1405 (shoulder); 1357; 1317;1285 (shoulder)
ν(V=O)	982

The first band of interest is at 3220 cm^{-1}, which is the O-H asymmetric stretch (ν_a(O-H)), which indicates that there is water associated with the structure. The broadness of the band is indicative of the water being uncoordinated, which can be termed as ‘free water’, which is weakly bound to the vanadium metal or Na ions via hydrogen bonding. The broad band can be observed to contain a number of minor shoulders. A number of bands are to be expected, as the uncoordinated water is in a number of different environments, being weakly bound in different positions, surrounding both the vanadium metal and Na ions.

The second region is the combination and benzene overtone region, however this region does not yield a great deal of information about the possible coordination chemistry of the compound.

The next region of interest and possibly the most important is the carbonyl region, which offers a great deal of information on the coordination between the metal and the carboxylic acid groups of the ligand. Deacon and Phillips have studied a number of different systems involving carbonyl coordination to different metals and have identified several modes of coordination[5]. The carbonyl functional group can bind through three different

modes; unidentate (through a single oxygen), bidentate (through both oxygens) and bridging (each oxygen binds to a different metal). The difference between the asymmetric and symmetric stretches of the carbonyl groups within a compound gives insight into the mode of coordination. The study [8] compared the difference between the stretching vibrations of carbonyls [$\nu_a(CO_2^-)$-$\nu_s(CO_2^-)$] of an ionic salt, in this case Na-B4C, to that of a number of carbonyls exhibiting alternate modes of coordination (unidentate, bidentate or bridging) to a metal. These modes of coordination can be observed in Figure 11 (pg. 15).

The study concluded that if the coordination of the carbonyl was unidentate, the difference was greater than the difference between the carbonyls for the ionic compound [8]. This is due to the uncoordinated carbonyl becoming more double bond in character and the coordinated carbonyl becoming more single bond in character due to the coordination, which would lead to a large difference in terms of band position [8]. The coordination mode was regarded to be bidentate if the difference was less than the difference for the ionic compound. This is due to the double bond character being shared between of the carbonyls, so there is assumed to be less of a difference between the symmetric and asymmetric stretches. Finally the coordination mode was regarded to be bridging if the difference was similar to that of the ionic compounds difference. The ionic bond between the Na and ligand would have a similar effect to that of the metal and the ligand, as Na would remove the double bond from the carbonyl, leading to both of the carbonyls exhibiting more single bond character, which is observed for the bridging coordination mode.

Table 8: Differences between $\nu_a(CO^{2-})$ and $\nu_s(CO^{2-})$ for Na-B4C and RU-V2.

	Na-B4C (cm^{-1})	**RU-V2 (cm^{-1})**
$\nu_a(CO_2^-)$	1623; 1545; 1474	1557; 1491
$\nu_s(CO_2^-)$	1360; 1328; 1292	1363; 1357
Difference	263; 217; 182	194; 134

Table 8 shows the differences between $\nu_a(CO_2^-)$ and $\nu_s(CO_2^-)$, only for the clearly defined bands and not for the shoulders present. The differences for RU-V2 are similar to and less than those of Na-B4C, so an initial conclusion can be drawn that the mode of coordination is either bidentate or bridging. The IR spectrum of Na-B4C at pH 3.5 is provided in the appendix (Appendix 1, pg. 109).

The final band of interest is the vanadyl band, present at 983 cm^{-1}. The vanadyl band serves to show that vanadium is present and coordinated to the ligand. Comparing the vanadyl band position in the metal salt (977 cm^{-1}) to that of RU-V2, where the $\Delta\nu$ = 6 cm^{-1}, which indicates that the V=O has strengthened slightly and become more double bond in character, indicating that it is in a terminal position. Another possibility to describe this change is that there is weaker σ - bonding between the oxo-ligands, which acts to strengthen the π - bonding between the oxygen and vanadium after coordination.

The other bands in the spectrum have been assigned as follows; the band at 1139 cm^{-1} was associated with benzene ring vibration and possibly an in plane stretch (*ν*(C-C)). The 'fingerprint region' can be observed below the vanadyl region, which is particularly difficult to interpret, with a number of possibilities of low energy vibrations for each band.

3.2.1.3 Thermal Analysis of RU-V2

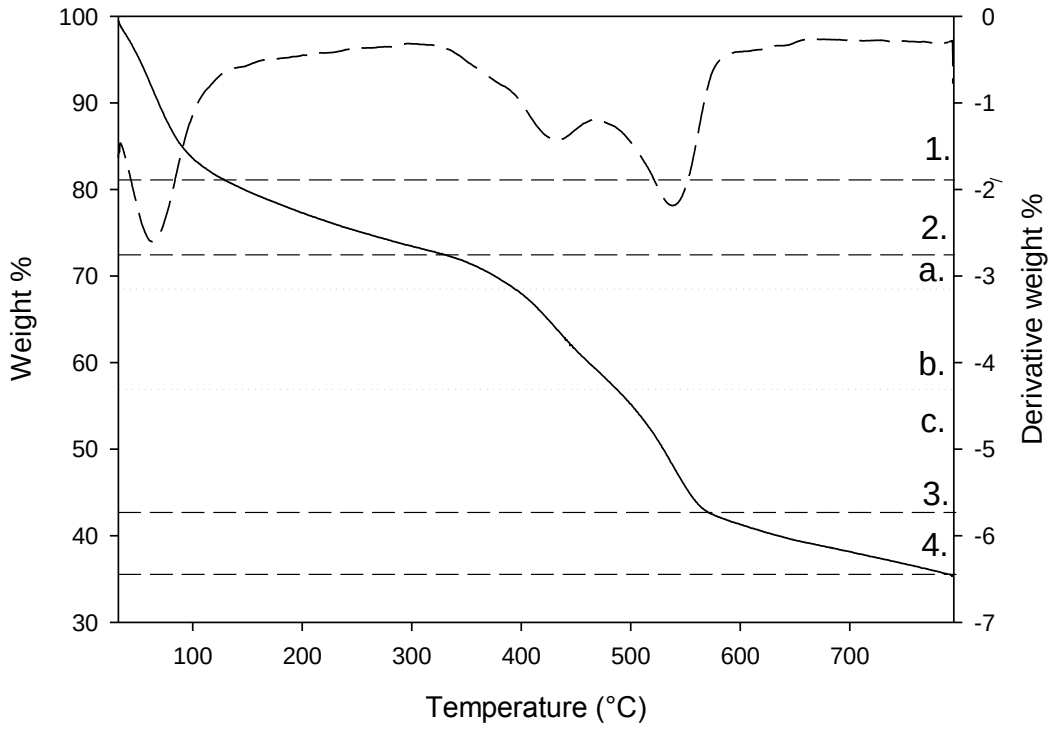

Figure 25: Thermal decomposition profile of RU-V2 with its derivative curve.

The thermal decomposition profile of RU-V2 shows a multi-step decomposition, which has been characterised into 4 stages. Stage 1 shows the loss of 16.58% which indicates the loss of six water molecules (calculated: 16.68%) from 32°C to 103°C. The loss in stage 1 merges into stage 2, which shows a loss of 12.19%, indicating the loss of 1.5 carbon dioxide molecules (calculated: 12.22%) from 103°C and 362°C. Stage 3 is a difficult mass loss step to interpret, as it is not a uniform loss and is made up of 3 parts (a - c). The first loss (a.) is a gradual loss of 4.24% which is indicative of the loss of 0.5 of a CO_2 molecule (calculated: 4.07), which occurs from 362°C to 413°C. A second loss (b.) of 10.76%, which is indicative of the loss of two carbon monoxide molecules (calculated: 10.37%), which occurs from 413°C to 496°C. A third loss (c.) of 12.93%, which is indicative of the loss of a further 2 CO molecules and a CH_2 molecule (calculated: 12.97%) and occurs from 496°C to 570°C. When all these masses losses are added together the overall loss sums up to 27.95%, which can be broadly explained as the loss of another 1.5 carbon dioxide molecules and 4 carbon monoxide molecules (calculated loss: 27.41%). The combined mass loss stages of 2 and 3 show the complete decomposition of the ligand to CO_2, CO and residual carbon.

The loss of the initial 1.5 of a carbon dioxide molecule initiates the decomposition of the ligand. The ligand does not simply break away from the compound, it breaks away from the metal centres under elevated temperatures and proceeds to break down into smaller, more stable decomposition products, such as carbon dioxide (CO_2) and carbon monoxide (CO). Once these molecules are liberated from the structure all that is left is a small amount of residual carbon.

1. $C_6H_2(COO^-)_4 \longrightarrow 2CO_2 + 4CO + C_4H_2$ (Stage 2 + 3)
2. $C_4H_2 \longrightarrow CH_2 + 3C$ (Stage 3)

The final loss in stage 4 is difficult to characterise, as it is an incomplete decomposition step, due to the thermogram failing to level out, indicating that there is more mass gradually being lost, but cannot be observed, due to the upper limits of the instrument (800°C). Stage 4 shows a loss of 7.57% from 570°C to 794°C. This loss may be caused by the residual carbon binding to the oxygen associated with the vanadium oxide species being released as CO, as the loss of 1.5 CO is equivalent to the loss of 7.78%. After stage 4, a residue of 35.72% of the parent material is left remaining and is assumed to be made up of metal oxides, sodium oxides and residual carbon. The residual carbon is often able to react with oxygen associated with the metal oxides, to form carbon monoxide or carbon dioxide, to be liberated from the residue and ultimately leave a residue of only metal oxides. The final TG residue was black in colour, indicating that there is residual carbon still present, as the metal oxides are expected to be grey in colour. The residue was investigated using FTIR, and is shown in the appendix (Appendix 2, pg. 109). One can observe that all the bands associated with the ligand have been lost, but the *v*(V=O) band is still present at 997 cm^{-1}, indicating the presence of vanadyl-based metal oxide species.

All the thermal profiles discussed above are similar to previous studies with metal complexes involving 1,2,4,5 – benzenetetracarboxylates [2][4][9].

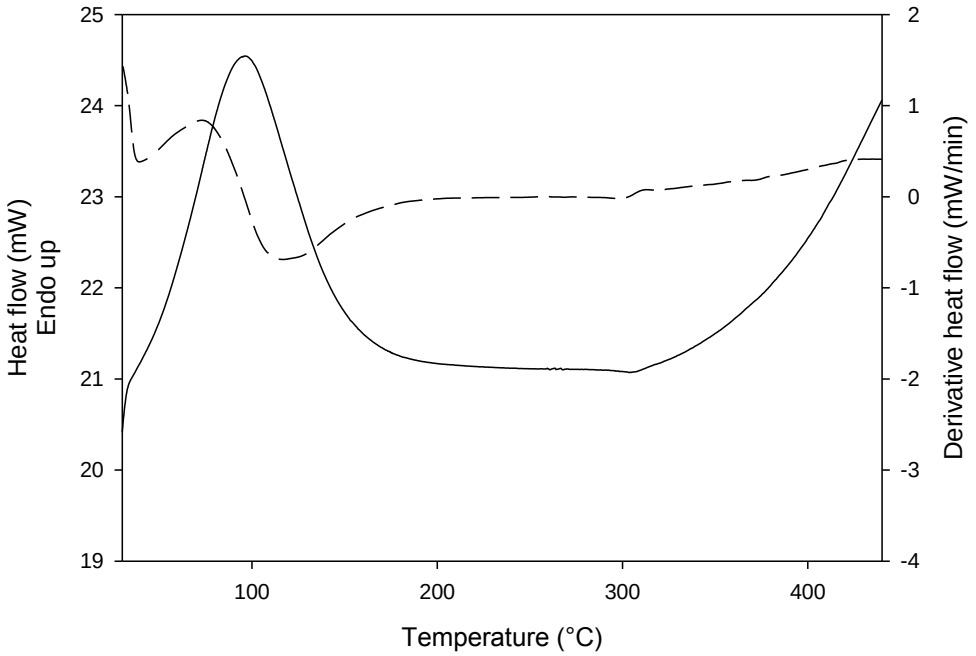

Figure 26: DSC of RU-V2 and its derivative curve (heated at 10°C/min under a nitrogen purge, with a flow rate of 19.8 ml/min).

The DSC confirms the findings observed in the TGA, as there is an initial broad endotherm present at 95.73°C, which has an associated enthalpy change of 418 J/g. The endotherm ranges from 30°C to approximately 160°C and is asymmetric, as the derivative curve seems to have a shoulder before gradually reaching a plateau after the endotherm. This is potentially indicating that there is a dominant endotherm, with a smaller endotherm merged into it to cause the shoulder observed in the derivative curve. This fits the TG data, as the mass losses expected in this region are the loss of the six waters molecules (dominant endotherm) and the initial loss of 0.5 of a CO_2 molecule (minor endotherm). An endotherm corresponding to the entire loss of the 1.5 CO_2 molecules is not observed, as the mass loss is very gradual, spanning from 103°C to 362°C to complete. The change in enthalpy (ΔH) of the entire endotherm (418 J/g) was recorded and was converted into kJ/mol, the value was determined to be 226 kJ/mol of parent material, which is associated with the loss the total of 6 water molecules and 0.5 of a CO_2 molecule (as noted from the TG results).

The determination of the exact energy required to remove a water molecule was not able to be accurately determined due to the merging of the endotherm associated with the loss of 0.5 of a CO_2 molecule. However, an estimate of the energy required to remove a water molecule can be determined, as when dividing the total 226 kJ/mol by 6, one obtains a value of 37.7 kJ/mol, therefore the value per water molecule is expected to be >37.7 kJ/mol. This value is smaller than the enthalpy of vapourisation of water at 100°C (44 kJ/mol), therefore one can deduce that the water associated with the compound requires less energy to be removed than the energy required to vapourise water at 100°C.This indicates that the water

is weakly bound to the complex via hydrogen bonding and is uncoordinated, this correlates to what was observed in the IR spectrum (Figure 24; pg. 50). At 305°C one can observe a minor disturbance in the derivative curve, which may be the initiation of the ligand decomposition which is observed as the growing endotherm from approximately 305°C to 442°C. The endotherm can be observed to be incomplete and this was due to the upper limit of the instrumentation being 450°C. From observing the TG decomposition after 305°C, it can be concluded that the endotherm corresponds to the complete removal of the ligand from the compound, which breaks down as discussed in the TG results.

All the thermal profiles discussed above are similar to previous studies with metal complexes involving 1,2,4,5 – benzenetetracarboxylates [2][4][9].

3.2.1.4 X-ray Crystal Powder Diffraction of RU-V2

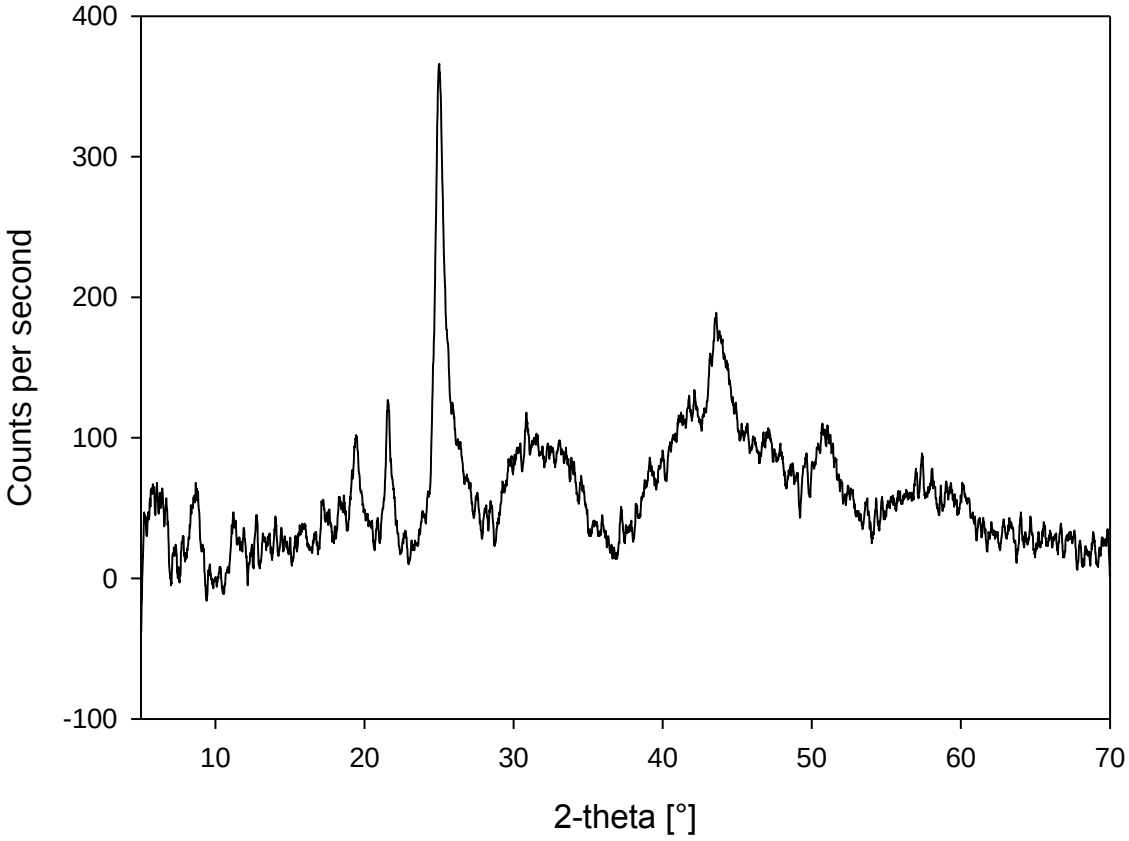

Figure 27: The X-ray Powder Diffraction Pattern of RU-V2.

The XRPD pattern is observed to be largely amorphous, lacking any significant crystallinity. The metal and ligand species bound to each other and do not maintain an ordered overall structure, which lack any planes upon which x-rays can interact and diffract from. This leads to the broad peaks observed in Figure 27. Three peaks can be observed in conjunction with amorphous bands, this is potentially indicating that some of the functional groups of each of the individual complexes may be 'stacking' upon one another in an ordered and crystalline

fashion. These peaks were matched to those of similar compounds, in attempt to identify and gain any structural information, but were unfortunately not found to match any of the compounds.

3.2.1.5 Scanning Electron Microscopy of RU-V2

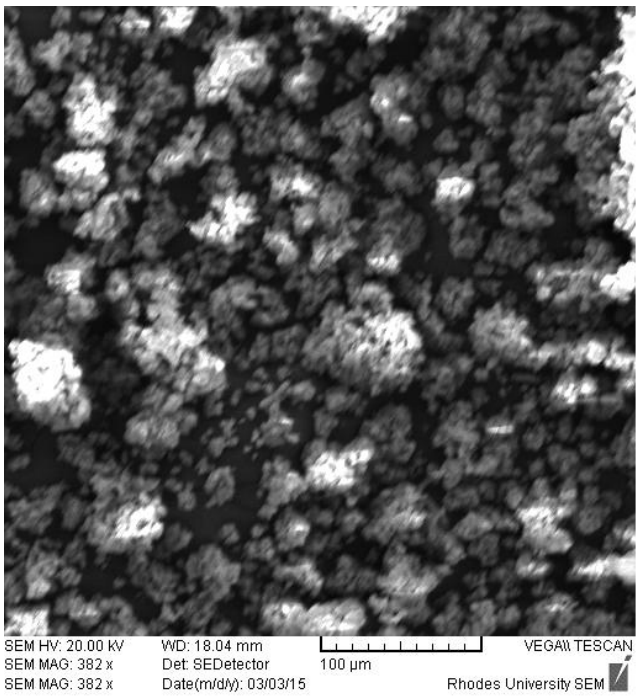

Figure 28: An image of RU-V2 taken using SEM.

Figure 28 shows that RU-V2 is in the form of a fine powder, with very small particle sizes of approximately >10 µm in size. The particles can be observed to aggregate into clumps, with no uniformity or crystallinity being observed from the image.

3.2.2 Solvothermal Syntheses

The solvothermal syntheses were determined to be the most successful method of synthesis to produce a potentially crystalline product. Table 3 of Chapter 2 (pg. 34) shows the solvothermal syntheses to be a great deal more effective than any of the other syntheses, with 5 major products being synthesised using this method.

The names have been shortened to the metal salt used and the pH value of the synthesis. The successful syntheses are displayed in Table 3; with one additional synthesis that uses $VOSO_4$ added to H_4B4C at a pH value of pH 3.5. This was done to directly match the products of the ambient synthesis to those of the solvothermal synthesis.

Table 9: The 5 Solvothermal Products with their Shortened Names.

	Shortened name:
1.	$NaVO_3$ Hydrothermal (pH 1.92)
2.	NH_4VO_3 Hydrothermal (pH 1.92)
3.	$VOSO_4$ Hydrothermal (pH 1.92)
4.	$VOCl_2$ Hydrothermal (pH1.92)
5.	$VOSO_4$ Hydrothermal (pH 3.5)

Each of the hydrothermal syntheses were found to yield the same product, regardless of the different metal salts used or the pH values. The product had been previously synthesised and characterised by Cevik et al, with the formula: $[V^{IV}_2O_2(H_2O)_2(C_6H_2(COO)_4)]$ [10]. The product formed as small dark blue crystals and the IR spectra, XRPD spectra and elemental analysis results all matched those of the material previously developed by Cevik et al indicating that the products were the same. The strong dark blue colour of the product gave an indication that the oxidation state of vanadium was in the V^{IV} oxidation state. Not all of the products formed as small crystals, instead some were found to precipitate out of solution as a light blue powder, but crushing the crystals revealed the light blue powder, indicating that the products were, in fact, the same.

$VOSO_4$ Hydrothermal (pH 3.5), was thought to exhibit a minor impurity, as it precipitated out of solution as an aqua coloured powder, which was different from the others. This did not affect its structure, as it was still identical to the other products in terms of IR, TG and XRPD spectra.

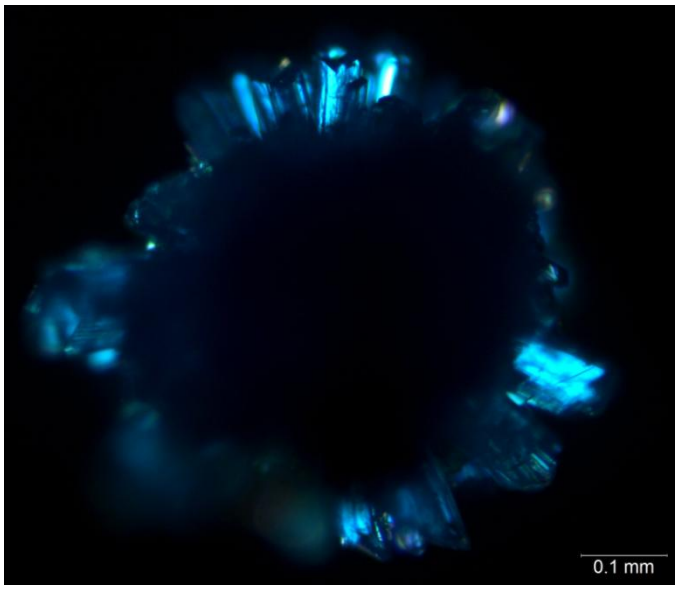

Figure 29: An Image taken by a Polarising Light Microscope.

Figure 29 shows an example of the small crystals, which had formed in a cluster, as the centre is dark, indicating that the sample was too thick to allow the light to penetrate. However, on the edges of the cluster, one can observe the blue single crystals.

In the following sections, all the compounds will be compared, to prove that they are in fact the same in structure. The product which made use of $VOCl_2$ as a starting material will be used as an example when taking a closer look at more specific properties within each of the individual results. $VOCl_2$ hydrothermal will be used for this purpose, as it was the first promising compound synthesised and it was used for the catalytic studies discussed in the Chapter 4. $VOCl_2$ hydrothermal will be referred to as RU-V1 for the remainder of the thesis.

3.2.2.1 Elemental Analysis

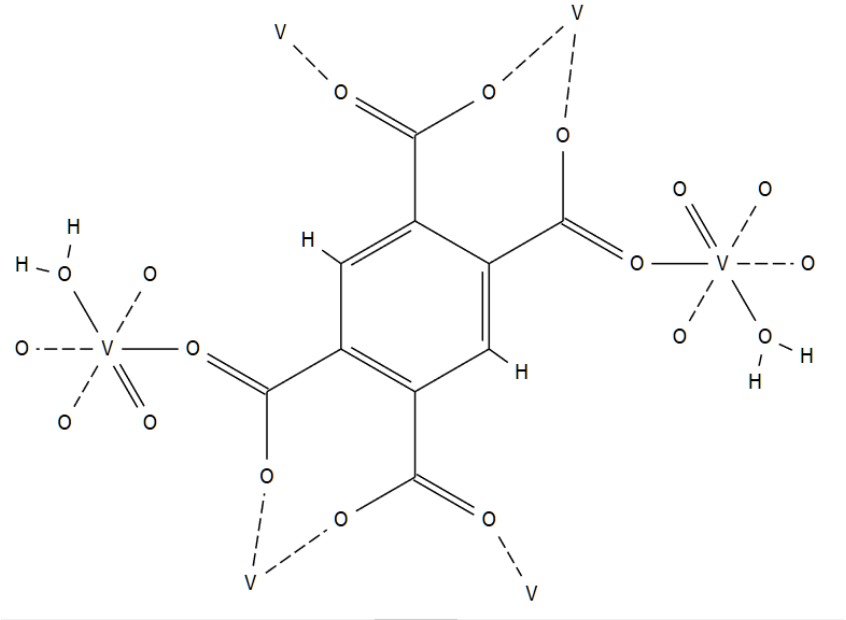

Figure 30: The basic structural unit of RU-V1 [10].

The bonds with solid lines are part of the unit cell used in elemental analysis, the dashed lines are showing where and how the unit cell links to another unit cell.

Table 10: The experimental and calculated values for RU-V1 from this study and from Cevik et al [10].

Formula	% C	% H	% V	V:B4C
Experimental	27.96	0.98	23.18	-
RU-V1	28.59	1.44	24.25	1:2
Experimental [7]	28.57	1.44	24.26	-
$V_2O_2(H_2O)_2(B4C)$ [7]	28.59	1.42	24.02	1:2

The experimentally found values match those of the calculated values within 1% for each element, except for vanadium, but this is due to there being some degree of error when using 2 different techniques (ICP-OES and Microanalysis) together.

3.2.2.2 Vibrational Analysis of the Solvothermal Compounds

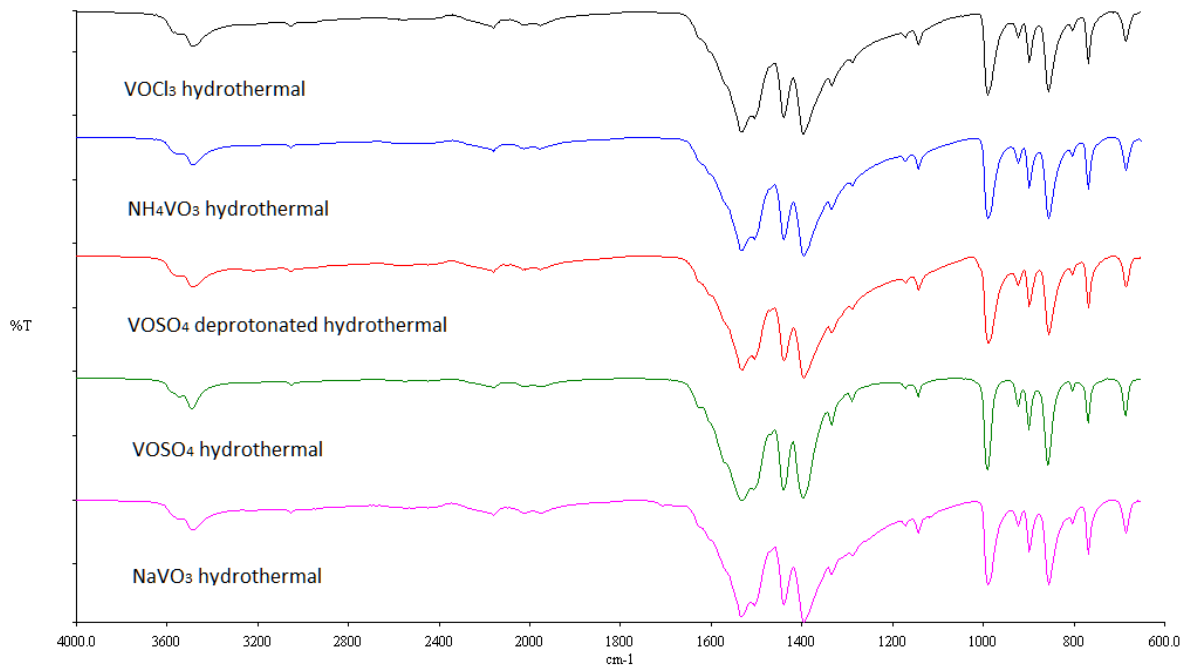

Figure 31: A Comparison of all the IR Spectra of the Hydrothermal Syntheses.

The IR spectra of all the hydrothermal syntheses have identical band positions and intensities. This shows that all the products from the hydrothermal syntheses are the same in their coordination geometry and structure.

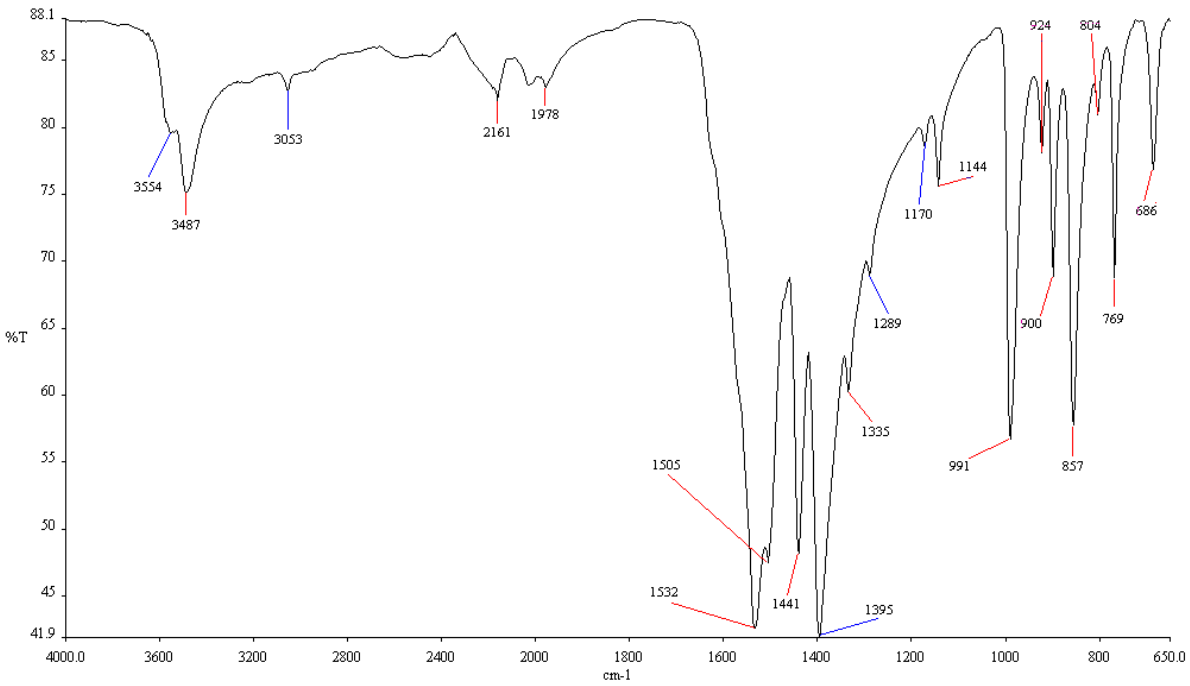

Figure 32: The IR spectrum of RU-V1.

The bands of interest for RU-V1 are the same as those investigated for RU-V2.

The first bands of interest are the stretches (ν(O-H)) associated with water bound to the MOF occurring at 3554 cm^{-1} and 3487 cm^{-1}, which is potentially indicating that coordinated waters are present within the structure, due to the band being narrow and well defined. Two bands are present indicating that the water molecules may be in slightly different environments. When comparing the stretches (ν(O-H)) of the RU-V2 to those of the RU-V1, one can readily observe the difference between coordinated and 'free' water, as the bands associated with RU-V2 are broader and reduced in terms of wavenumbers.

The next area of interest is the carbonyl region from 1532 to 1289 cm^{-1}. Small unresolved shoulders are observed merged into the $\nu_a(CO_2^-)$ at approximately 1650 cm^{-1} and 1570 cm^{-1}.

Table 11: Differences between $\nu_a(CO^{2-})$ and $\nu_s(CO^{2-})$ for Na-B4C and RU-V1.

	Na-B4C (cm^{-1})	**RU-V1 (cm^{-1})**
$\nu_a(CO_2^-)$	1623, 1545,1474	1650 (shoulder); 1570 (shoulder); 1532; 1505
$\nu_s(CO_2^-)$	1360, 1328, 1292	1441; 1395; 1335; 1289
Difference	263, 217, 182	209, 175, 197, 216

The differences between the asymmetric and symmetric stretches are similar to those of the ligand salt, which is indicative of bridging coordination and this was confirmed via XRD analyses [6].

The vanadyl region shows that vanadium is coordinated to the ligand, as one can observe the *v*(V=O) present at 991 cm^{-1}. When comparing the position of the *v*(V=O) to the metal salt; $VOSO_4$ (977 cm^{-1}), the Δv = 14 cm^{-1}. This shows that the vanadyl bond is becoming more double bond in character after coordination and is in a terminal position. Another possibility to describe this change is that, similarly to the ambient, there is weaker σ - bonding between the oxo-ligands, and stronger π – bonding between the oxygen and vanadium after coordination.

The unassigned bands were assigned as follows; the band at 3053 cm^{-1} is assigned as an aromatic C-H stretch (*v*(C-H)), this was not observed in the spectrum of RU-V2, as the broad bands associated with the uncoordinated waters likely masked it from appearing in the spectrum. The bands at 1170 cm^{-1} and 1144 cm^{-1} are assigned as benzene ring vibrations, potentially being in-plane stretches (*v*(C-C)) or out of plane bends (δ(C-H)). Once again, below the vanadyl band one is able to observe the 'fingerprint region', which is particularly difficult to interpret, with a number of possibilities of low energy vibrations for each band. The strong band present at 857 cm^{-1} can be assigned as the H-O-H rocking (p_r(H-O-H)), which originates from the coordinated water.

3.2.2.3 Thermal Analysis of RU-V1.

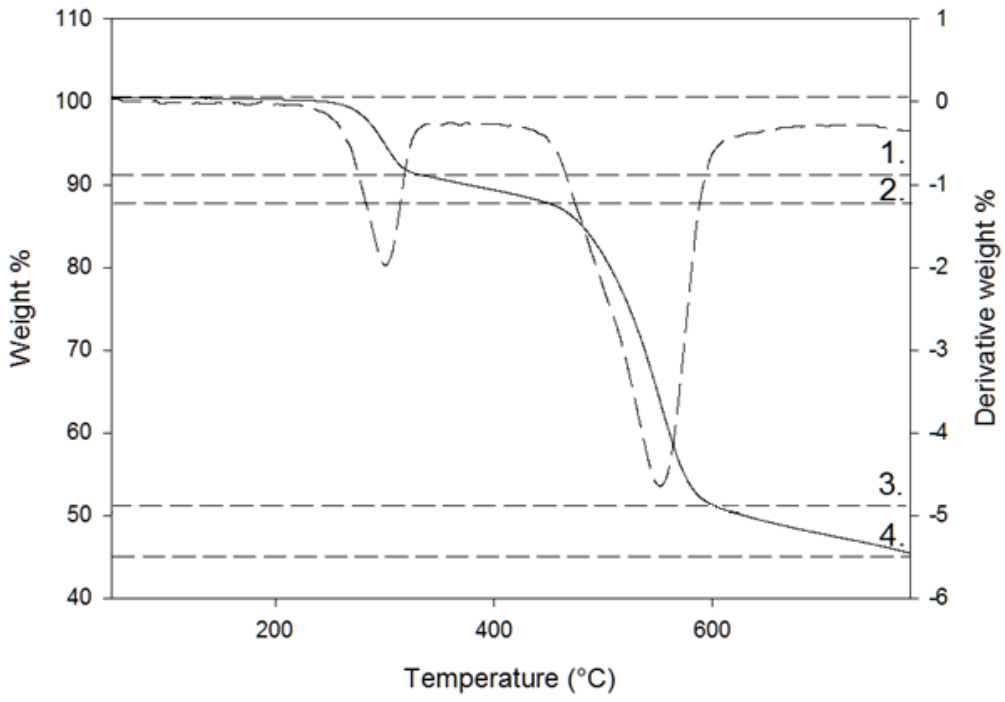

Figure 33: Thermal decomposition profile of RU-V1 with its derivative curve.

The thermal decomposition profile of RU-V1 shows a multi-step decomposition, which has been characterised into 4 stages. The molecule is stable from 23°C to 238°C, as above this temperature one can begin to observe the mass losses associated with the MOF. Stage 1 shows a loss of 8.65% from 238°C to 320°C, which is made up of two water molecules (calculated loss: 8.58%), which are coordinated to two of the vanadium centres, due to the high temperature at which they are released from the structure. Stage 2 shows a gradual loss of 4.47% from 320°C to 458°C, which is the loss of half a carbon dioxide molecule (calculated loss: 5.24%). Stage 3 is initiated by stage 2 and shows a loss of 35.87% from 458°C to 597°C, which is indicative of the liberation of all the carbonyl groups from the vanadium centres and benzene ring as 3.5 carbon dioxide molecules (calculated loss: 36.67%).

1. $C_6H_2 \longrightarrow 4C + C_2H_2$

Stage 4 occurs after the structure of the complex has collapsed and shows a loss of 6.60% from 597°C to 786°C. After stage 3, all of the carboxylic acid groups are expected to have been removed from the structure, so all that would be left over would be various vanadium oxides and the benzene ring of the ligand. The benzene ring structure can break down, as shown above, into C_2H_2 (calculated loss: 6.20%) and four C. With a further increase in temperature the residual carbon has the potential to bind to oxygen from a metal oxide and be liberated as CO.

The break-down of the ligand was noted to be completely different between RU-V1 and RU-V2. The carboxylic acid groups of the ligand in RU-V1 fragment as four CO_2 molecules, whereas with RU-V2 the carboxylic acid groups broke away as two CO_2 and four CO molecules. This difference can be potentially explained when observing the coordination of the complexes, as the carboxylic acid groups of RU-V1 are all bound to VO octahedra, whereas the acid groups of RU-V2 are bound to VO and Na centres. The acid groups of RU-V2 initially cleaves from the structure as the two CO_2 molecules, which are followed by the cleavage of the four CO molecules. This possibly involves the Na ions completely dissociating from the structure, followed by the decomposition of the acid group releasing a CO_2 molecule. The VO centre may exhibit different behaviour and break its bidentate coordination to the acid group, in favour of unidentate coordination at elevated temperatures. This will allow for the removal of a CO molecule and when the unidentate coordination is finally broken, the second CO molecule is able to be released.

All the thermal profiles discussed above are similar to previous studies with metal complexes involving 1,2,4,5 – benzenetetracarboxylates [2][4][9].

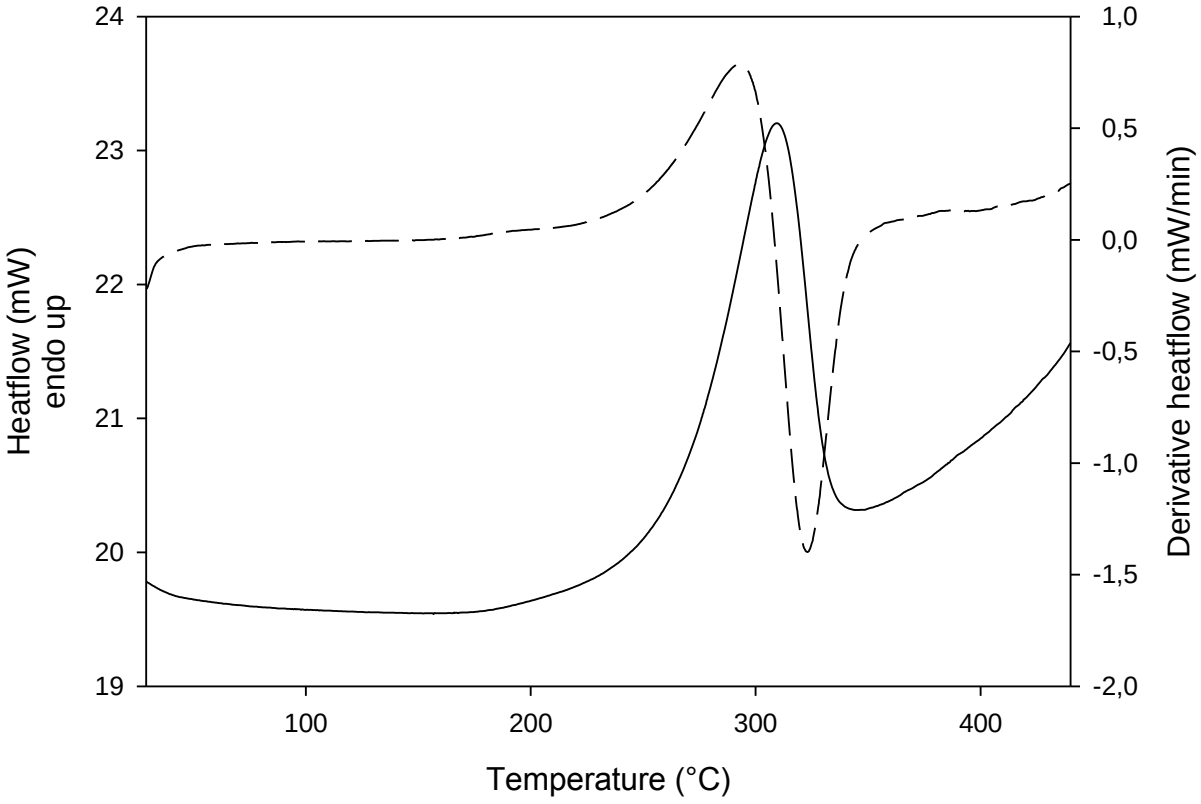

Figure 34: DSC of RU-V1 with Derivative Curve.

The DSC data perfectly matches the TG data, as one can observe a large endotherm, starting from 238°C and ending at 320°C, this is the range where the loss of the two water molecules is observed in the TG data. The endotherm is observed to merge into the following gradual endotherm, associated with the loss of half of a CO_2 molecule, but to a lesser extent than was observed for RU-V2. The ΔH of the endotherm (288 J/g) can be converted to a value of 121 kJ/mol of parent material, to give an idea about the amount of energy required to remove the water molecules from the parent material. Each water molecule was calculated to require 60.5 kJ/mol to be removed from the structure and when this is compared to the enthalpy of vapourisation of water at 100°C (44 kJ/mol) and the energy required to remove a water molecule from RU-V2 (>37.7 kJ/mol), the value is significantly greater, which indicates that the water is held strongly by the structure and is coordinated to the metal.

After the endotherm associated with the water loss, the plot begins to increase, which can be assumed to be moving into the temperature range corresponding to the loss of the carbonyl groups of the ligand, which initiates structural collapse of the MOF.

All the thermal profiles discussed above are similar to previous studies with metal complexes involving 1,2,4,5 – benzenetetracarboxylates [2][4][9].

3.2.2.4 X-ray Crystal Powder Diffraction of RU-V1

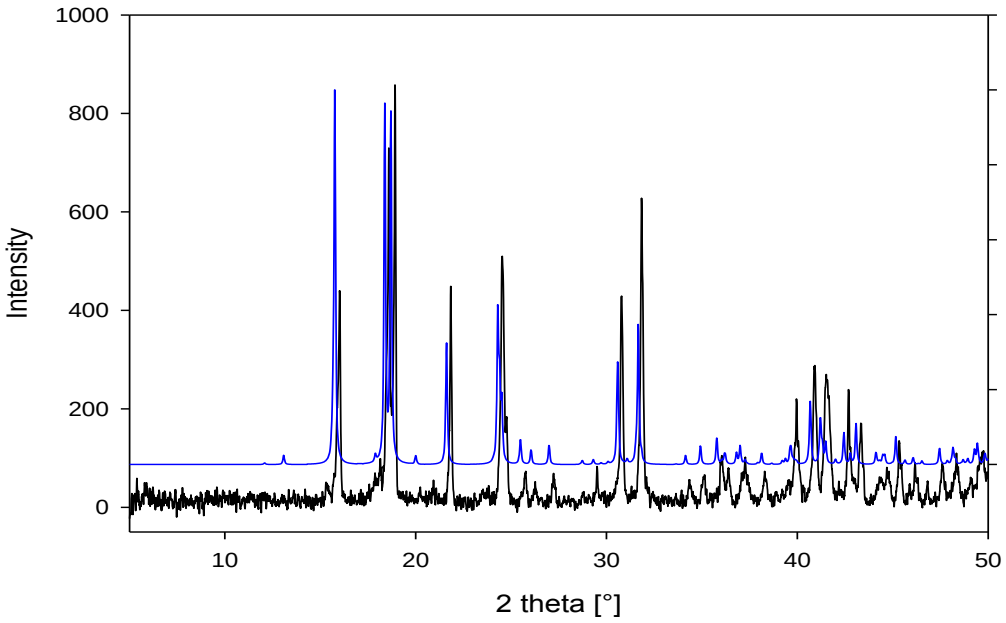

Figure 35: The XRPD spectra of RU-V1 (black) and the spectrum of $[V^{IV}_2O_2(H_2O)_2(C_6H_2(COO)_4)]$ (blue).

The spectrum of $[V^{IV}_2O_2(H_2O)_2(C_6H_2(COO)_4)]$ has been shifted slightly above that of RU-V1, to visibly show that the peaks match up perfectly, indicating that the compounds are structurally identical.

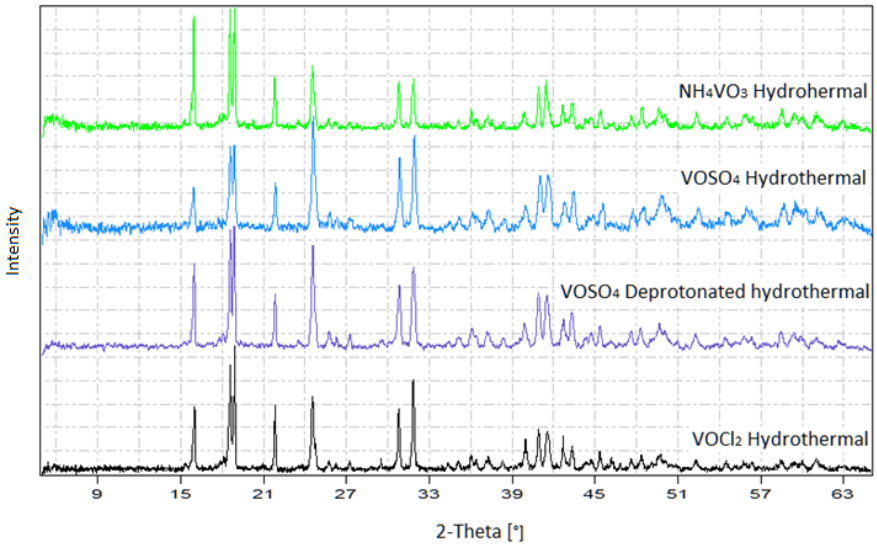

Figure 36: The basic powder diffraction patterns of each of the 4 hydrothermal products, the synthesis with $NaVO_3$ hydrothermal is not present, as the yield was too small for XRPD analysis.

Once superimposed all the XRPD plots of the synthesised hydrothermal products were found to be identical in structure, which indicates that all the synthesised hydrothermal products are structurally the same as $[V^{IV}_2O_2(H_2O)_2(C_6H_2(COO)_4)]$.

Table 12: Structural information of $[V^{IV}_2O_2(H_2O)_2(B4C)]$ [10].

Crystal System	Monoclinic
Space group	C 2/c
A	11.756(5) Å
B	9.645(3) Å
C	11.822(7) Å
A	90.00
B	107.10(4)°
Γ	90.00
Z	8
Cell volume	1281.2(10) $Å^3$

All the structural factors were determined by Cevik et al and have been included for the sake of completeness.

3.2.2.5 Scanning Electron Microscopy of RU-V2

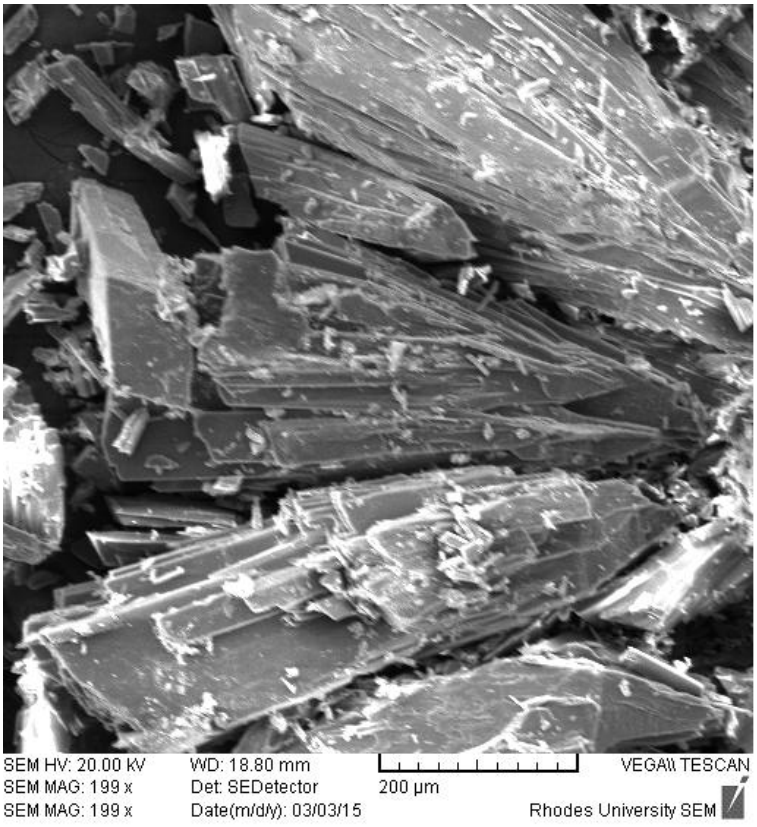

Figure 37: An image of RU-V1 taken using SEM.

Figure 37 clearly indicates that RU-V1 is a crystalline material, with particle sizes reaching up to 0.1 mm in size.

3.2.3 Decavanadate Ion

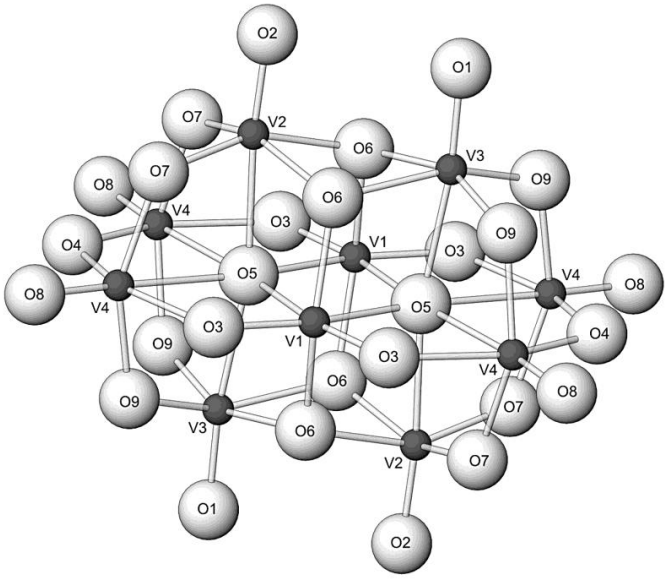

Figure 38: The structure of a decavandate ion $[V_{10}O_{28}]^{6-}$ [11].

The decavanadate ion is a vanadium species which has been well studied [12-15], so will not be analysed to the depth at which RU-V1 and RU-V2 were investigated. The decavanadate ion has a 6- charge associated with it, thus requires counter ions in order to be stabilised. The possible counter ions are ammonium (NH_4^+), sodium (Na^+) and hydrogen (H^+), depending on the metal salt used for the synthesis. There are generally 16 to 18 water molecules associated with the decavanadate structure, depending on the counter ions present.

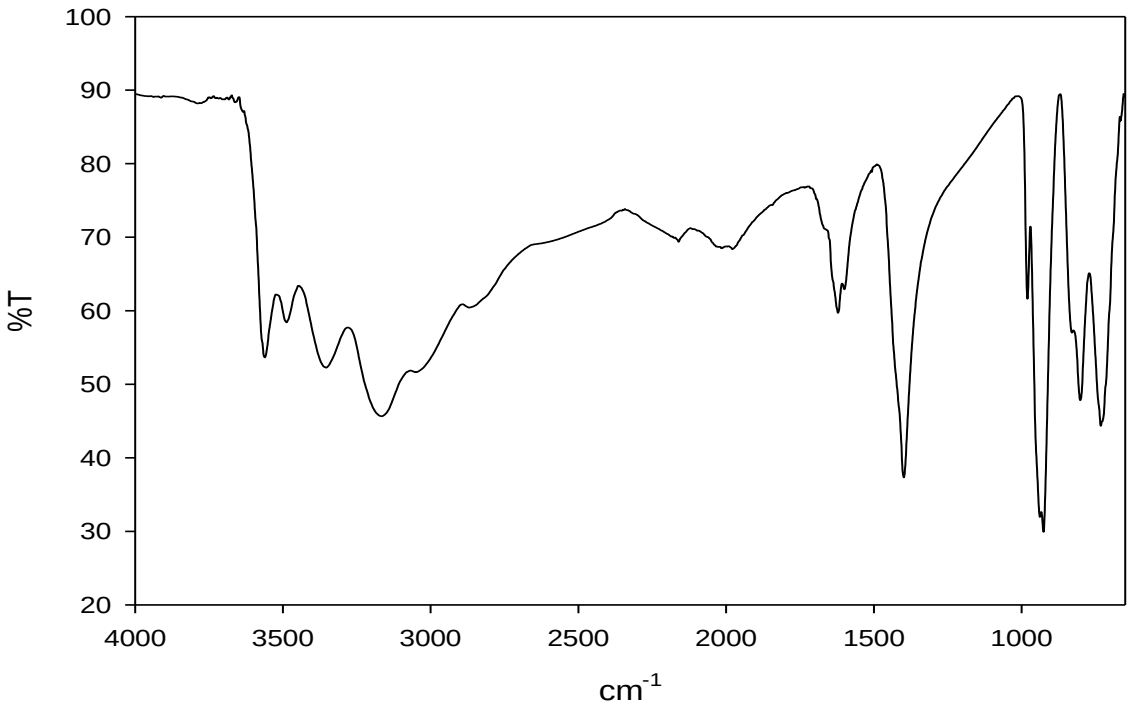

Figure 39: The IR spectrum of the decavanadate ion.

The decavanadate compound was precipitated out of solution in the form of small orange crystals at pH 5.9, but precipitation only occurred after 85% - 90% of the volume of the solvent (H_2O) was removed, due to the high solubility of the ion in water. The decavandate product was analysed via IR spectroscopy, where it was found that ammonium was present, due to ν_a(N-H) and ν_s(N-H) expected from 3500 cm^{-1} to 2800 cm^{-1}. Assigning bands in this area is a challenge as there are a number of bands associated with the 16 – 18 uncoordinated water molecules, leading to difficulty in identifying each individual band conclusively. The combination and overtone bands are present from 2164 cm^{-1} to 1973 cm^{-1}. The bands present at 1621 $cm^{-1}$and 1600 cm^{-1}, which are associated with N-H bending vibrations (δ(N-H)). The band present at 1402 cm^{-1} is assigned as the with the umbrella vibration (δ_d(umbrella))of the tetrahedral NH_4^+ molecule. The vanadyl bands (ν(V=O)) are present and at 984 cm^{-1}, 944 cm^{-1} and 926 cm^{-1}, three bands are present due to the vanadium centres being in slightly different environments within the ion. Finally one can observe 3 bands present at 834 cm^{-1}, 804 cm^{-1} and 732 cm^{-1}, which are assigned as N-H wags (ρ_w(N-H)).

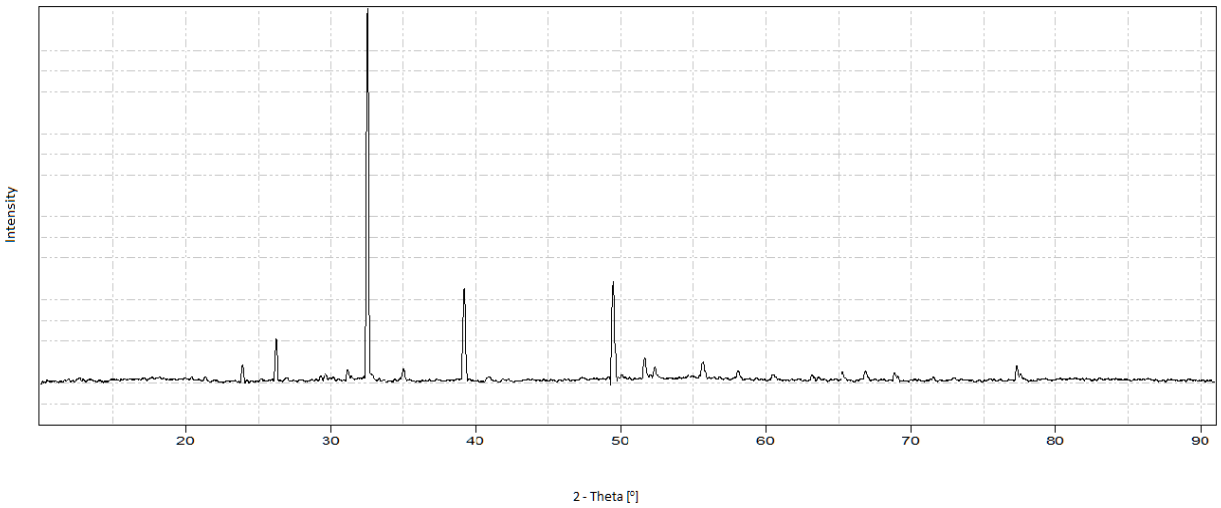

Figure 40: The XRPD spectrum of the decavanadate ion.

The XRPD spectrum of the decavanadate ion shows that the structure is clearly crystalline in nature.

Table 13: Structural information of the decavanandate ion [14].

Crystal System	**Monoclinic**
Space group	$P\bar{1}$
A	10.778(3) Å
B	11.146(3) Å
C	8.774(3) Å
A	104.57°
B	109.32°
Γ	65.00°
Z	1

The structural information is taken from the study completed by Evans and is presented here for the sake of completeness.

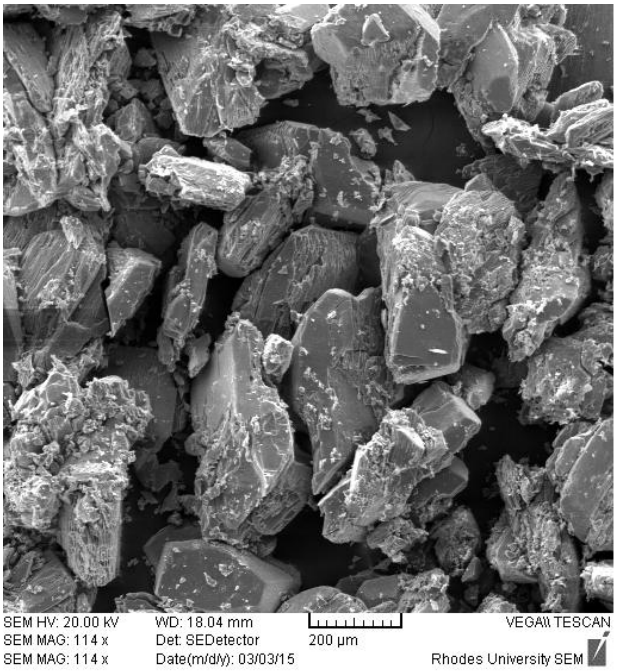

Figure 41: An image of the decavanadate ion taken using SEM.

The SEM image again provides evidence to the product being crystalline, with particle sizes reaching up to 500 µm in length.

References:

1. Rehder, D. *Bioinorganic Vanadium Chemistry*. Wiley, 2008, 1-20.
2. Coombes, M. A Comparative Study of Two Copper(II) Based Metal-Organic Frameworks: $Cu_{2}{}_{1/4}(OH)_{1/2}B4C^{\cdot}8H_2O$ and $Cu_2Na(OH)/B4C^{\cdot}8H_2O$. M.Sc. Dissertation, Rhodes University, 2012.
3. Henisch, H. K. *Crystal Growth in Gels and Liesegang Rings*, Cambridge University Press, 1988.
4. Lamprecht, E. Thermal, Spectroscopic and X-ray Diffraction studies of Copper(II) 1,2,4,5-Benzenetetracarboxylates and Copper(II) Oxalate: A Study of Metal-Organic Frameworks. Ph.D. Dissertation, Rhodes University, 2008.
5. Farzanfar, J.; Ghasemi, K.; Rezvani, A. R.; Delarami, H. S.; Ebrahimi, A.; Hosseinpoor, H.; Eskandari, A.; Rudbari, H. A.; Bruno, G. Synthesis, characterization, X-ray crystal structure, DFT calculation and antibacterial activities of new vanadium(IV, V) complexes containing chelidamic acid and novel thiourea derivatives. *J. Inorg. Biochem.* **2015**, *147*, 54-64.
6. Munawar, K. S.; Tahir, S. A. M. N.; Khalid, N.; Abbas, Q.; Quershi, I. Z.; Shazadi, S. Investigation of derivatized Schiff base ligands of 1,2,3-triazole amine and their oxovanadium(IV) complexes: Synthesis, structure, DNA binding, alkaline phosphatise inhibition, biological screening, and insulin mimetic properties. *Rus. J. Gen. Chem*. **2015**, *85* (9), 2183-2197.
7. Taheri, O.; Behzad, M.; Ghaffari, A.; Kubicki, M.; Dutkiewicz, G.; Bezaatpour, A.; Nazari, H.; Khaleghian, A.; Mohammadi, A.; Salehi, M. Synthesi, crystal structures and antibacterial studies of oxidovanadium(IV) complexes of salen-type Schiff base ligands derived from meso-1,2-diphenyl-1,2-ethylenediamine. *Transit. Metal. Chem*. **2014**, *39* (2) 253-259.
8. Deacon, G. B.; Phillips, R. J. Relationships between the Carbon-Oxygen Stretching Frequencies of Carboxylato Complexes and the Type of Carboxylate Coordination. *Coordin. Chem. Rev.* **1980**, *33*, 227-250.
9. Brown, M. E.; Lamprecht, E.; Watkins, G. M. The Thermal Decomposition of Copper(II) Oxalate Revisited. *Thermochim. Acta.* **2006**, *446*, 91-100.
10. Cevik, S.; Poyraz, M.; Sari, M. A Novel Three Dimensional Organic-Inorganic Hybrid Based Porous Phase: Synthesis and Characterization of Reduced Oxovanadium Pyromellitate, $[V^{iv}{}_2O_2(H_2O)_2(C_6H_2(COO)_4)]$. *J. Chem. Crystallogr.* **2007**, *37*, 497-502.
11. Kampf, A. R.; Hughes, J. M.; Marty, J.; Gunter, M. E.; Nash, B. Rakovanite, $Na_3\{H_3[V_{10}O_{28}]\}.15H_2O$, A New Member of the Pascoite Family with a Protonated Decavanadate Polyanion. *Can. Mineral.* **2011**, *49*, 595-604.
12. Das, S. K.; Tripuramallu, B. K.; Yerra, S. Decavanadate-Based Discrete Compound and Coordination Polymer: Synthesis, Crystal Structures, Spectroscopy and Nano-Materials. *Polyhedron.* **2014**, *81*, 147-153.

13. Pessoa, J. C.; Marcâo, S.; Avecilla, F.; Correia, I. Structural Studies of Decavandate Compounds with Organic Molecules and Inorganic Ions in Their Crystal Packing. *Inorg. Chim. Acta.* **2004**, *357*, 4476-4487.
14. Evans, H. T. The Molecular Structure of the Isopoly Complex Ion, Decavanadate ($V_{10}O_{28}^{6-}$). *Inorg. Chem.* **1966**, *5* (6), 967-977.
15. Rossotti, F. J. C.; Rossotti, H. Equilibrium Study of Polyanions: I. Isopolyvanadates in Acidic Media. *Acta. Chem. Scand.* **1956**, *10*, 957-984.

4. CATALYSIS RESULTS

4.1 Epoxidation Reaction and Catalytic Materials

The three products characterised in Chapter 3 were the subject of a preliminary study, which was conducted on the catalytic epoxidation of cyclohexene to cyclohexene oxide. This specific epoxidation reaction was chosen due to a study having been completed by Van der Voort et al [1], which showed that a V-MOF (MIL-47) had the ability to successfully catalyse the reaction. The study with MIL-47 provided a good model system upon which to base this catalytic study. By carrying out the study in this way, the results from each catalytic material, could be readily compared to the published results. Having synthesised a vanadium complex (RU-V2) and a MOF (RU-V1), a preliminary study was done to determine if both or either of them exhibited any catalytic activity for the desired reaction.

The purpose of the reaction is to employ possible catalytic materials to find a highly selective method to produce cyclohexene oxide, which is a useful precursor in a number of organic syntheses, especially polymerisation reactions [2-4]. The problem with cyclohexene oxide is that it is unstable and it is able to form one of a number of different oxidation products (e.g. b, c and d in Figure 42), depending on the environment in which it finds itself in. This is why studies such as Van der Voort et al's have been conducted, as having a selective catalyst could be highly advantageous in reducing the costs and time, otherwise involved in these syntheses.

From the characterisation of the vanadium-based materials discussed in the results section, RU-V2 was determined to be a vanadium-based complex and not a MOF, however many vanadium-based compounds are catalytically active for the epoxidation of olefins. RU-V1 was found to be a MOF that has been previously synthesised and characterised by Cevik et al [5], but has not been used in any application as of yet, so the opportunity was taken to test and observe whether the vanadium-based complex or V-MOF exhibited any catalytic activity in the reaction as a heterogeneous catalyst. Both materials were tested and their results compared to those of MIL-47. MIL-47 differs from RU-V1 in that 1, 4 - benzenedicarboxylic acid (H_2B2C) was used as the ligand in the synthesis of the MIL-47, instead of 1, 2, 4, 5 – benzenetetracarboxylic acid (H_4B4C). This is the most important difference, as H_2B2C only has four potential coordination sites available, whereas H_4B4C has eight.

The decavanadate ion has received attention as a homogeneous and phase-transfer catalyst for the oxidation of hydrocarbons and olefins [6-7]. The decavanadate ion is completely soluble in water, but when paired with a quaternary onium salt, e.g. Hex_4NCl, forms a micellular structure which has been applied to the oxidation of various hydrocarbons [7]. In this study the possibility of using the decavanadate ion as a heterogeneous catalyst in an organic medium was investigated. There were two goals of the investigation, the first was to

determine the effectiveness of the catalytic activity of the decavanadate ion in the solid state, in an organic medium and the second, depending on the results of the first, was to inquire into the possibility of using the decavanadate ion as a basis from which to design a MOF in a future study. If synthesised, a decavanadate-based MOF may exhibit interesting properties, which may be useful for catalysis and possibly a number of different applications.

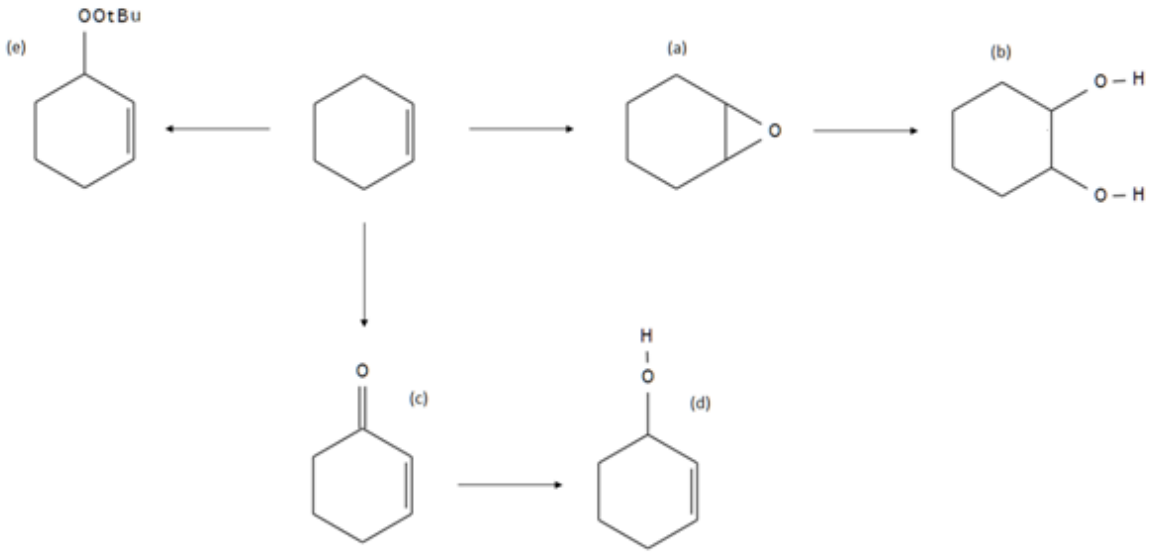

Figure 42: The pathways for the conversion of cyclohexene to the various oxidation products [1].

Figure 42 shows the formation of the epoxide; cyclohexene oxide, however this is not the only product that can form in this reaction, as the epoxide is unstable and may follow an additional reaction mechanism to one of the oxidation products presented, especially in the presence of water.

4.2 Preliminary Testing

Preliminary reactions were run using RU-V1 to test the reaction system and to determine if it functioned to give the desired result. These initial reactions were run over a period of 72 hours, to ensure that the reaction was given an adequate amount of time to reach completion or near completion. These reactions were monitored periodically with no set interval, as their sole purpose was to determine whether cyclohexene was being converted into any products of interest. Aliquots of 10 µL were only taken at the start of reaction and once again at the end of the reaction, these were diluted with 40 µL deuterated chloroform ($CDCl_3$) and were analysed using ^{1}H and ^{13}C NMR, in an attempt to determine whether there

was any conversion of cyclohexene to any possible products shown in Figure 42. All ^{1}H and ^{13}C studies were completed using a BRUKER 600 MHz NMR spectrometer.

A blank reaction mixture was initially run, which simply lacked any catalytic material, and was confirmed to show no catalytic activity as the NMR spectra for both ^{1}H and ^{13}C were identical before and after the reaction. The reaction was performed with the oxidant (TBHP) either being in water or decane. This was important, as using TBHP in decane ensured that there was no significant amount of water present in the reaction, as the solvent ($CHCl_3$) had thoroughly dried. When using TBHP in water, a small portion of water was present into the reaction mixture and this could have a possible effect on the outcome of the reaction.

A reaction with RU-V1 as the catalyst was done initially using TBHP in decane and was run for 72 hours. The ^{1}H and ^{13}C NMR spectra of the reaction mixture from before and after the reaction were found to be identical (Appendix 3 and 4, pg 110 - 111), indicating that no reaction had taken place. When the ^{1}H and ^{13}C spectra of cyclohexene are added to this, it is evident that cyclohexene was still present in a high concentration. This was confirmed when observing the catalytic material after the reaction, as it had not undergone any change and was still dark blue in colour. Further analysis carried out via IR spectroscopy indicated that the material had not been altered during the course of the reaction and was still in its original state.

The reaction was repeated, but TBHP in water was used as the oxidant. This had a dramatic effect on the catalyst, as it was observed to break down and gradually dissolve into solution as the reaction progressed. From visually monitoring the reaction over time, it was observed that the initially clear and colourless solution changed to a light green colour over time, which coincided with a colour change in the catalytic material, from dark blue to dark green. After this, the catalytic material was observed to change from green to a light orange colour and gradually breakdown and dissolve into solution. After the reaction had been run for 72 hours there was still a residual amount of catalyst left over, which was kept for further analyses. These colours match the oxidation states of vanadium, as V^{III} is green and V^{V} is orange, potentially indicating that the vanadium centres of RU-V1 are undergoing changes to their original oxidation states (V^{IV}), which is indicating that the V-centres are most likely responsible for the catalytic activity.^{1}H and ^{13}C NMR analyses of the reaction mixture were done and showed results that were difficult to interpret due to the number of signals present in the mixture, but allowed for some useful insights into what may be occurring nonetheless. When comparing the ^{1}H and ^{13}C spectra in Appendix 5 and 6 (pg. 112 - 113), with those of cyclohexene, one can observe that cyclohexene is clearly being consumed during the reaction and converted into another product/s.

NMR was purely used as a qualitative method to determine if any catalytic conversion of the cyclohexene was occurring. Identifying which product had been formed conclusively through ^{1}H and ^{13}C NMR alone is a challenge due to the number of overlapping signals, especially in the region of between 10 and 40 ppm in the ^{13}C spectra and the 1 to 3 ppm

region in the ^{1}H spectra. Observing the signals downfield from this region, generally associated with an electronegative centre, such as oxygen, or a double bond, simplifies the identification process. A number of signals can be seen from 120 to 200 ppm in the ^{13}C spectra, which are indicative of oxidation products, being situated so far downfield, however with the break-down of the catalyst may introduce peaks associated with the ligand; 1, 2, 4, 5-benzenetetracarboxylic acid, but these are expected to have a low intensity, as the amount of catalyst used was relatively small compared to that of the initial starting materials, therefore can be expected to have an extremely low concentration.

The method used to potentially identify these possible products was to focus specifically on the ^{13}C NMR spectrum of the reaction mixture (Appendix 5, pg. 112), identify all the signal values and note them down, this was completed using the software; MestReNova Version: 6.0.2-5475 and is displayed in Appendix 7 (pg. 113-114). The ^{1}H spectrum had all of its signals clustered in the region between 1 and 4 ppm, which made the identification of individual products exceedingly difficult. A number of the previously mentioned oxidation products were readily available in the laboratory, namely; cyclohexene oxide, cyclohexane-1,2-diol and 2-cyclohexen-1-one, which were easily analysed via NMR. The spectra of 2-cyclohexen-1-ol and *tert* butylperoxy-1-cyclohexene were found via literature search [8] and by using the 'Spectral Database for Organic Compounds' [9]. A list of all the chemical shifts for each of the potential products is also displayed in Appendix 7, where one is able to compare the chemical shifts of potential oxidation products, to that of the reaction mixture, post reaction. Upon comparing the values together, it becomes apparent that cyclohexene and cyclohexane-1,2-diol have the greatest probability of being present in solution, as all of their chemical shifts are able to be closely matched to those present in the reaction mixture, within a range of approximately 0,2 ppm from chemical shifts in the reaction mixture. The appearance of cyclohexene in the reaction mixture, post reaction indicates that there is either an excess of cyclohexene initially or the reaction has not yet reached completion. The NMR spectra were compared with primary standards and also against literature. It should be noted that care was taken to only choose literature values which had used $CDCl_3$ as a solvent. NMR analysis was an initial tool which was used to identify whether a reaction was indeed occurring and offer insight into which of the potential products may be forming. Studies using GC-MS were used to conclusively identify the products of the reaction.

4.3 Reaction Procedure

After identifying that the cyclohexene was undergoing conversion to a potential oxidation product/s, the reaction was setup to be closely monitored over time to identify exactly what was taking place and which product/s were being produced. The reaction procedure was taken directly from the previously referred to study [1] and replicated for comparative purposes, with the only differences being that RU-V1, RU-V2 and the solid decavanadate ion

were substituted as catalysts and the entire reaction was scaled down by a factor of 4 in order to conserve reagents.

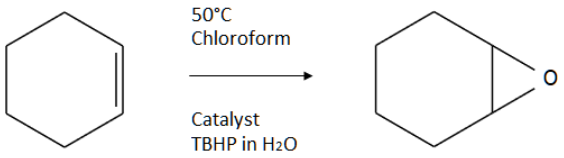

Figure 43: The epoxidation of cyclohexene to cyclohexene oxide [1].

The typical catalytic procedure was to charge a 50 mL two-necked round bottom flask with anhydrous chloroform ($CHCl_3$) (7.5 mL), as the solvent. Cyclohexene (1.25 ml) and of 1,2,4-trichlorobenzene (1.55 mL), which was used as an internal standard for GC analysis, were added to the flask. Tertiary butyl hydroperoxide (TBHP) was used as the oxidant for the reaction; it was commercially available in two solvents, either 70% TBHP in water or 5.5 M in decane. Both were made use of, either; 70% TBHP in water (3.39 mL) or of 5.5 M TBHP in decane (4.47 mL) were added to the reaction flask. The molar ratio of cyclohexene to oxidant was 1:2. The reaction were run at a temperature of 50°C with constant stirring, under an N_2 atmosphere, which was achieved by initially purging the system followed by placing an N_2 containing balloon above the condenser. The vanadium loading for each catalyst was 0.42 mmol.

The reactions for each of the 3 materials were performed in duplicate and were carried out over a 24 hour period, with constant monitoring. The 24 hour period was chosen due to the results from the preliminary studies, which showed the catalyst gradually decomposes in the reaction mixture after the 72 hour period. Restricting the reaction to a shorter time frame of 24 hours, which was thought to be sufficient to observe potential catalytic activity , while keeping the catalyst intact for post-reaction analysis. Aliquots of 10 µL were taken each hour and diluted in 500 µL of HPLC grade methanol (Purchased from Sigma Aldrich), which were then entered into a GC MS system. Blank reactions were completed and were found to exhibit no catalytic conversion to cyclohexene oxide, which indicated that a catalyst is required for the reaction.

Before and after each injection the GC syringe was flushed with solvent (MeOH) 3 times, to ensure that there was no contamination during the injection process. Once the sample had been injected into the GC column, the run would last for 11 minutes and detection would start after 1.5 minutes due to a solvent delay, as the solvent peak will have the greatest intensity, so allowing it to enter the MS detector may have a damaging effect and cause the detector to output inaccurate readings. After each run the column was cleaned by injecting the solvent and elevating the column temperature to 250°C (the maximum temperature reached during runs) and maintained for a 5 minute period.

4.4 GC-MS Results

The GC-MS system (specifications and instrumentation provided in the Chapter 2; pg. 41) was optimised with a number of trial runs to condition the column and ensure that the system was functioning correctly in order to be able to monitor the reaction over a 24 hour period. Once the GC-MS system functioned as required, all the catalytic materials were tested to determine their effectiveness at converting cyclohexene to potential product/s. The reaction was closely monitored each hour, for 24 hours, with small aliquots of the reaction mixture being taken for GC-MS analysis every hour to determine what was taking place within the reaction over time. All of the GC-MS studies were performed using TBHP in water as the oxidant, as NMR studies had proven that catalytic activity was absent when using TBHP in decane over the 72 hour period, so shortening the time frame of the reaction to 24 hours would also result in no catalytic activity. Using TBHP in water had shown to exhibit catalytic conversion of cyclohexene in the NMR studies, so was the ideal choice as oxidant over a shorter reaction time frame.

GC-MS simplifies the process of identifying exactly what was forming within the reaction mixture over the 24 hour period, as the GC column was able to separate the components of the reaction mixture based on their polarities and the MS detector output can then be used to determine fragmentation pattern of each of these components. The fragmentation pattern could then be compared to those in a database of known molecules for easy identification of the components. The spectra were analysed using the software mentioned in the experimental section, MassHunter Workstation Software version B.05.00, where the peaks of the species were matched to the database of mass spectra, NIST mass spectrum database, to accurately identify the products of the reaction [11]. During the course of the reaction, it was found that the cyclohexene and TBHP were steadily decreasing over the course of the reaction, to form cyclohexene oxide, 2-cyclohexen-1-one, 2-cyclohexen-1-ol and cyclohexane-1,2-diol. The GS-MS was able to confirm exactly what had formed in the reaction mixture, but how these products formed over time will be discussed in detail in the following sections. The only product which was expected to be found was tert-butylperoxy-1-cyclohexene, as this was found to be a major product in the previously mentioned study [1]. However, it was absent for from the reaction and potential reasons for this absence will be discussed in a later section. An in-depth explanation on how the GC-MS data was interpreted and how the speciation curves were plotted can be found in Appendix 8 (pg: 114 – 115)

4.5.1 Speciation Curves

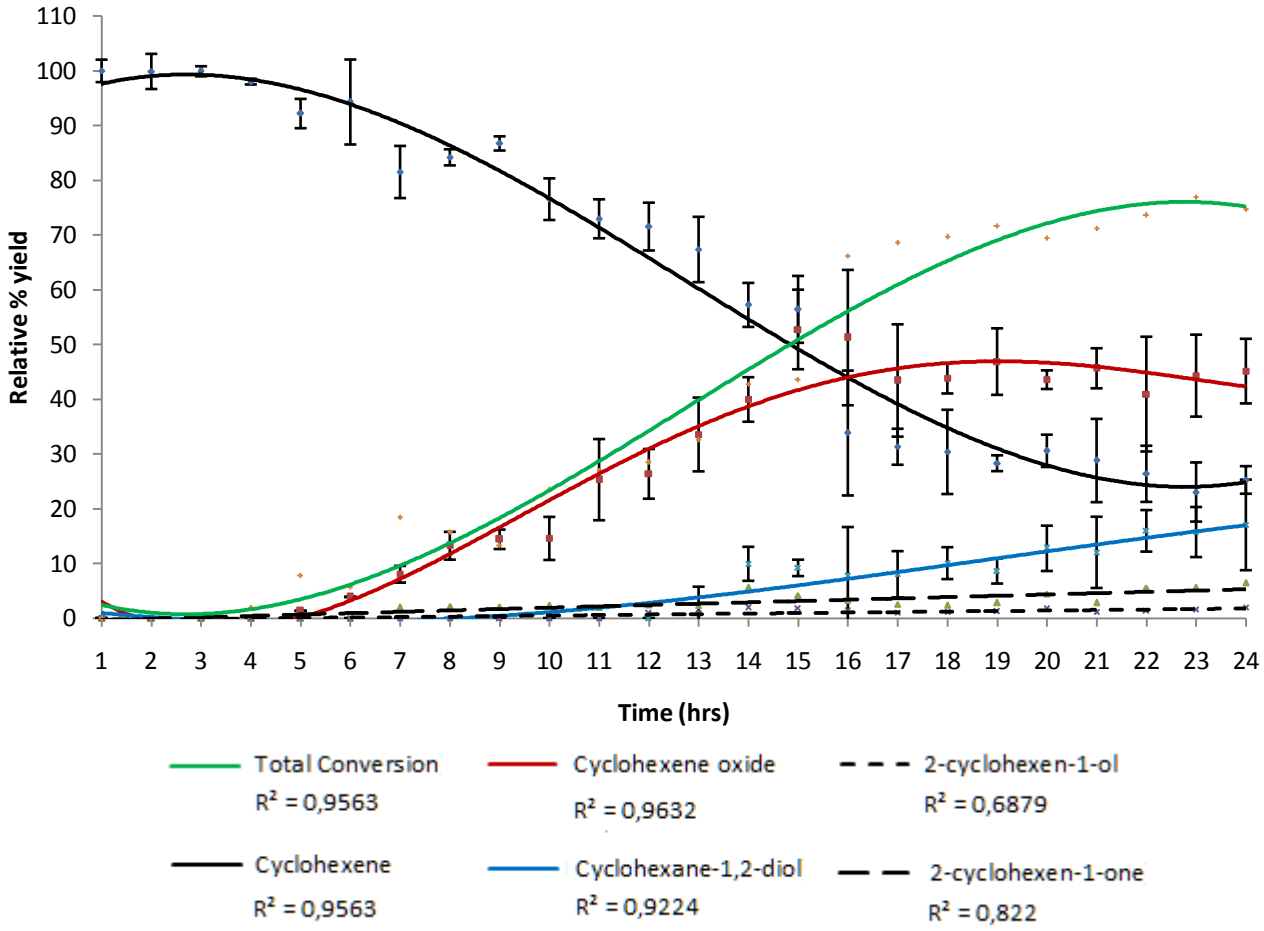

Figure 44: The Speciation curves of the relative % yields of the cyclohexene and its oxidation products over a 24 hr period, using RU-V1 as a catalyst.

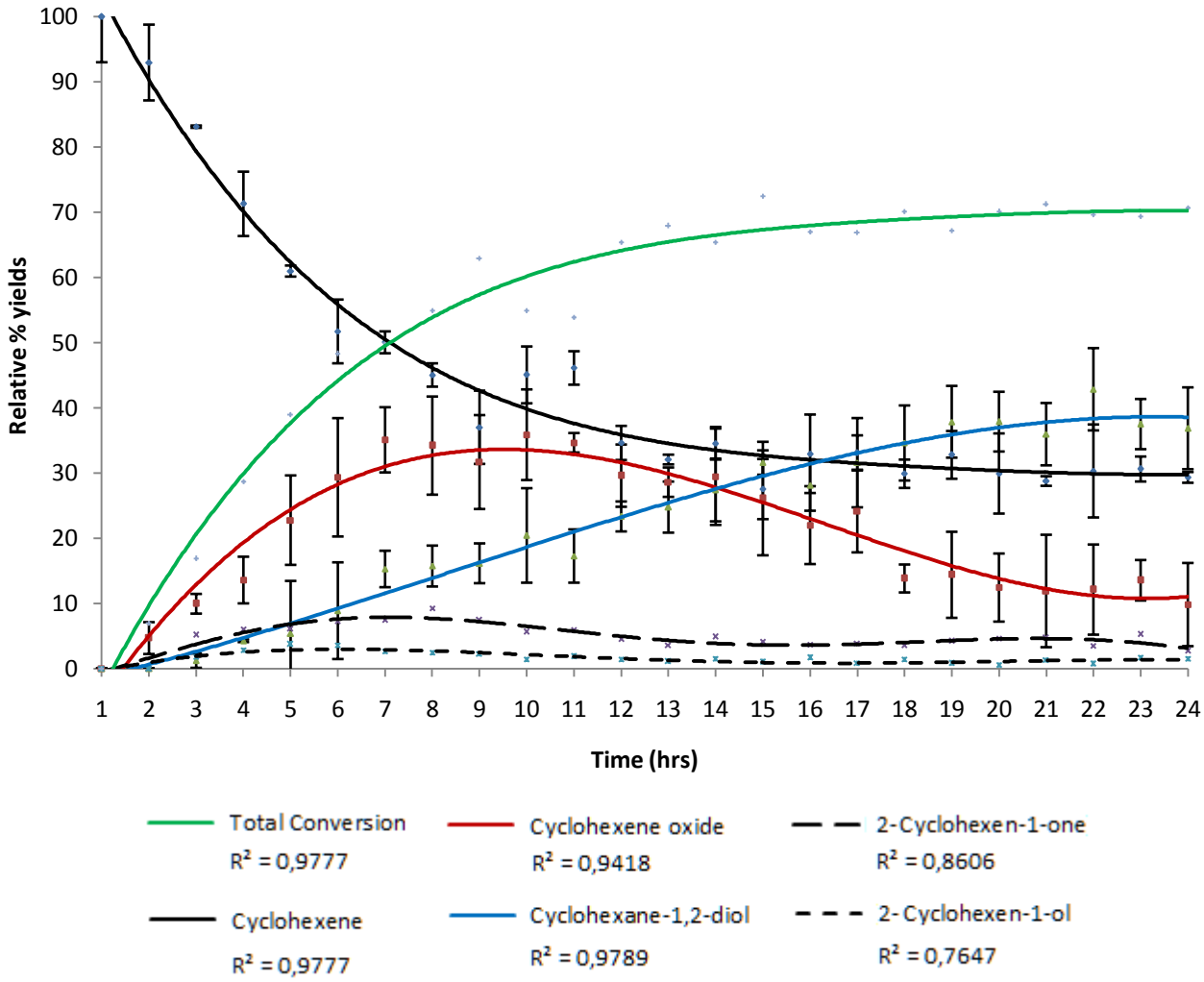

Figure 45: The Speciation curves of the relative % yields of the cyclohexene and its oxidation products over a 24 hr period, using RU-V2 as a catalyst.

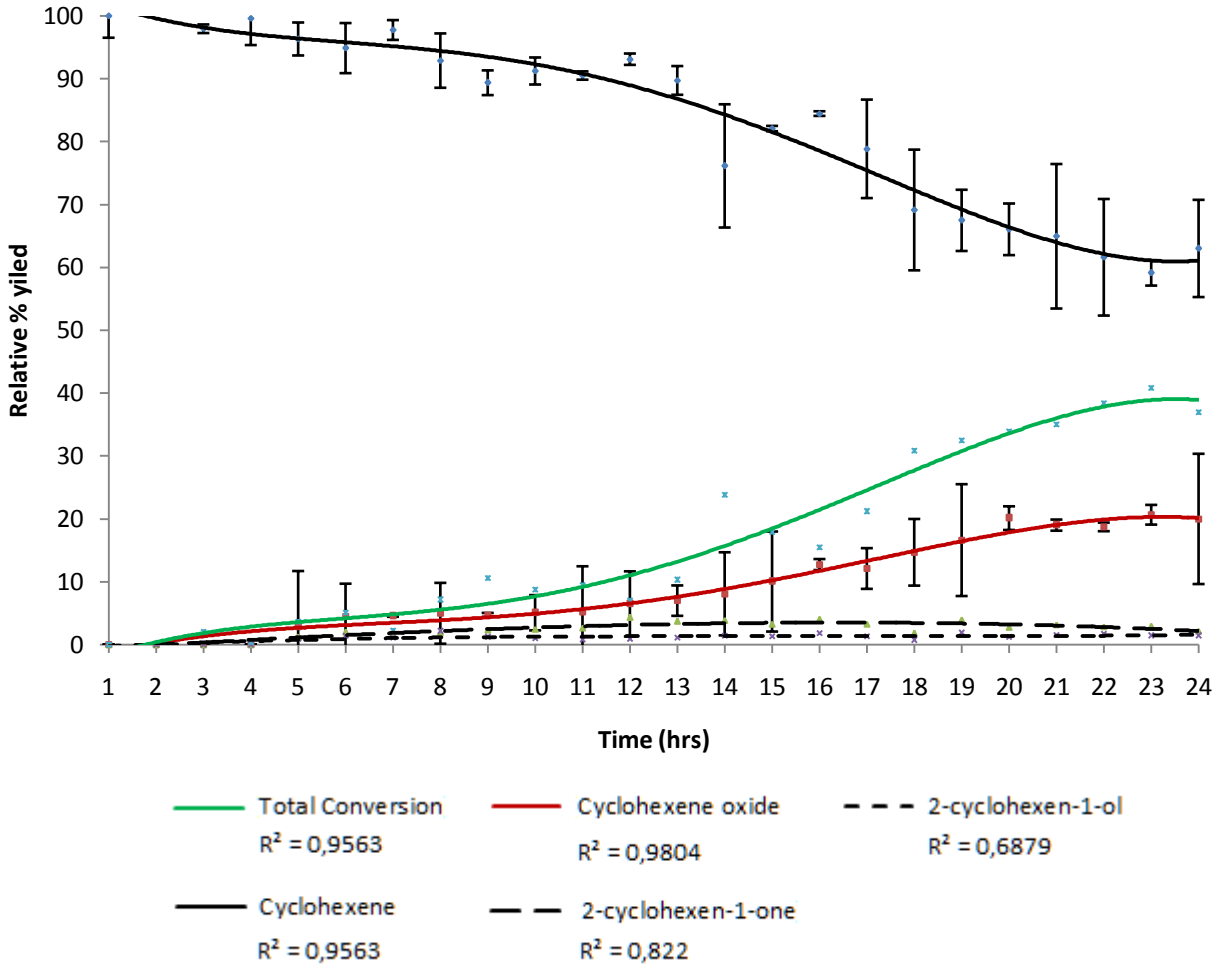

Figure 46: The speciation curves of the relative % yields of cyclohexene and its oxidation products over a 24 hr period, using the solid decavanadate ion as a catalyst.

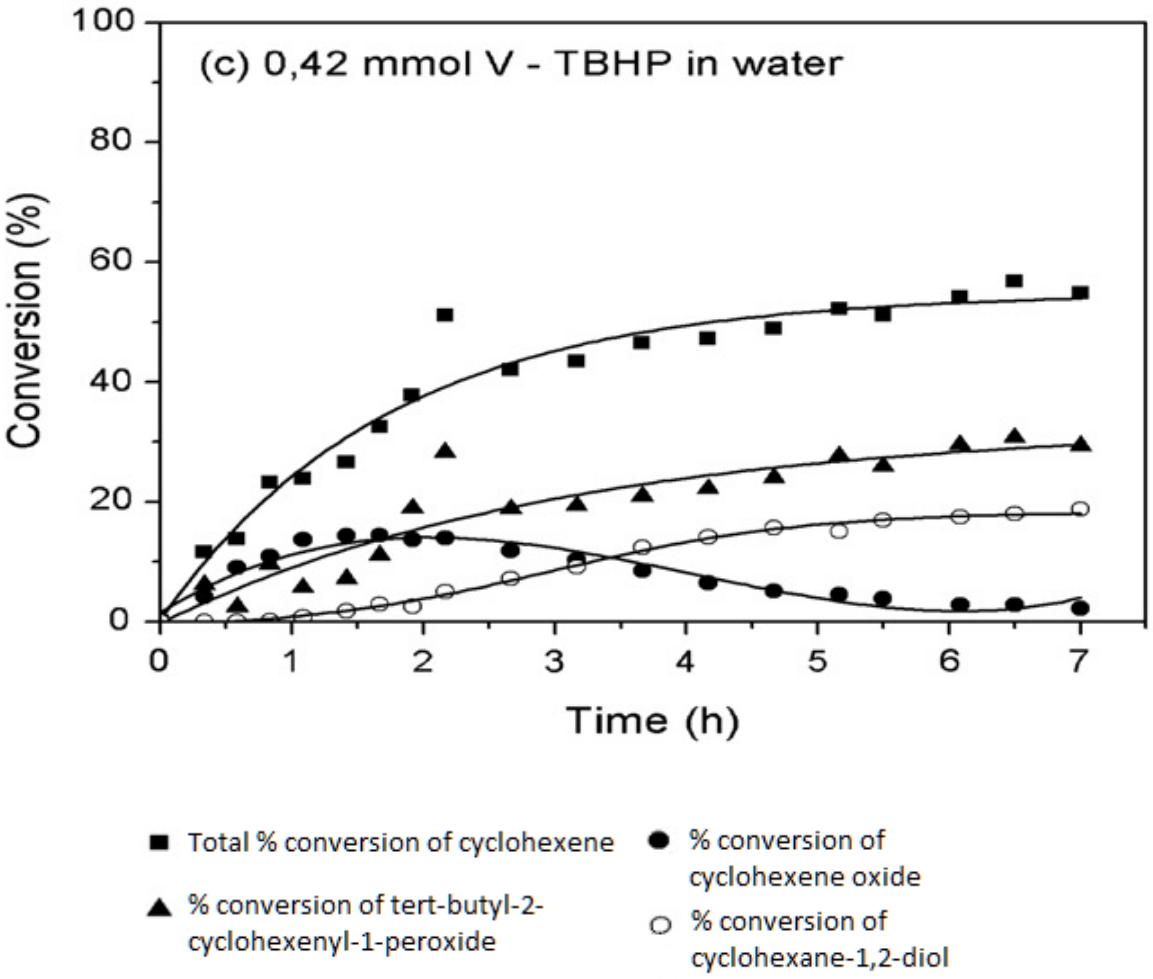

Figure 47: The speciation curves of the relative % yields of cyclohexene and its oxidation products over a 7 hr period, using the MIL-47 as a catalyst and TBHP in water [1]. (Figure taken directly from referenced study)

Table 14: A comparison of the catalytic properties of each of the 3 materials tested and MIL-47.

Catalyst:	TON:[a]	TOF:[b]	Selectivity:[c]
RU-V1	14	0	82
RU-V2	56	9	64
Solid Decavanadate	6	0	25[d]
MIL-47 (H_2O)	67	29	43
MIL-47 (Decane)	28	8	83

a - TON was calculated after 7 hours

b - TOF was calculated after 30 minutes

c - Selectivity was calculated for cyclohexene oxide at 40% conversion of cyclohexene

d - Selectivity was calculated for cyclohexene oxide at 20% conversion of cyclohexene, when using the solid decavanadate (see section 4.5.4)

- TON and TOF were times, in this work, follow that of Van der Voort *et al*, for comparative purposes [1].

4.5.2 The Catalytic Activity of RU-V1

Figure 44 is the graphical representation of how the reaction proceeds over time, which identifies and shows the relative % yield of cyclohexene diminishing and the oxidation products forming over a 24 hour period.

From Figure 44, a number of interesting trends can be observed; the first being that it took a period of approximately 4 hrs before any catalytic conversion was observed, this shows that the catalyst is not immediately active (pre-catalyst) and requires an activation step before it is able to convert cyclohexene. The reason for this is due to the highly coordinated structure of RU-V1, where the vanadium centres are coordinatively saturated with bonds to the ligand. For cyclohexene and TBHP to be able to interact with the metal centre, the most labile bond between the metal and ligand will need to detach from the metal, to allow the reactants an active site to the metal centre. Due to the 4 hour period before any conversion is observed, it is suggested that there may be no particularly labile bonds to dissociate from the metal centre under the specific reaction conditions. The coordinated water molecule is the most likely candidate to be released from the structure after the 4 hour period, opening a free coordination site to the metal centre. TG and DSC data showed that the water is strongly bound to the structure, so would require significant energy to remove and is potentially the reason for the 4 hour delay. After ±6 hours, the initiation of a gradual colour change to the catalyst was observed, shifting from dark blue to dark green, which indicates that the oxidation state of vanadium is being altered and that as the reaction proceeds from 4 hours to the end of the reaction (24 hours), there may be a gradual break down the bonds

between the metal and ligand within the catalyst creating a greater number of coordination sites to the metal and allowing for conversion of cyclohexene with the aid of TBHP (discussed in detail in a further section). In this proposed mechanism the loss of the coordinated water molecule may be important in initiating the entire catalytic process. Having water present in the reaction mixture must also be crucial to initiate catalytic activity, as when the preliminary testing was done over a 3 day period, using TBHP in decane, no catalytic conversion was observed via NMR and the catalyst was found to be unchanged. Future work would include a detailed modelling study of the dehydration of RU-V1.

The use of water may be a 'double-edged sword', due to the fact that it is required to initiate catalytic activity by removing the coordinated water within such a highly coordinated material, but as the reaction proceeds forward, there is no control in place to prevent more of the bonds between the metal and ligand from breaking. This was visually observed as the solution began to change from being initially colourless to having a hint of transparent light green after the 10^{th} to the 12^{th} hour. The catalytic material was found to gradually change from the dark blue to a dark green colour from the around the 6^{th} hour. With the solution gradually progressing to a green colour, one can potentially assume that V-centres are being leached out of the catalyst and into solution, with the continued breakdown of the catalyst as the reaction progresses. To confirm if there is significant leaching taking place, one would need to analyse the reaction solution using ICP-OES or ICP-MS.

After 4 hours, one can observe that cyclohexene is beginning to be converted into cyclohexene oxide, which reaches a maximum of ±47%, at approximately 19 hours. Only once cyclohexene oxide had formed and its % yield had increased to ±20% did cyclohexane-1,2-diol begin to form, which was after 10 to 11 hours. The formation of other minor oxidation products were also observed, namely; 2-cyclohexene-1-one and 2-cyclohexene-1-ol, which were present from the stage when cyclohexene oxide formed, indicating that they are not as a result of the formation of the epoxide, but rather follow a different mechanism. Their % yields are very low, reaching a maximum of ±5% for 2-cyclohexen-1-one and ±1.5% for 2-cyclohexen-1-ol. The total % conversion of cyclohexene was ±77% and the total conversion of all the products together is ±54%, leaving a discrepancy of ±23%. This is indicating that more cyclohexene is being used than what has been accounted for.

When referring back to the study using MIL-47 [1], one can observe that in all of the tests completed, tert-butylperoxy-1-cyclohexene formed in a significant amount, which varied depending on the solvent used. Due to tert-butylperoxy-1-cyclohexene being present for MIL-47, it is very possible that it is the missing product which could account for the extra cyclohexene conversion.

A possible reason as to why tert-butylperoxy-1-cyclohexene was not detected by the GC-MS is possibly due to the nature of the column used for our GC analyses, as this was the only

major difference between our study and that of Van der Voort et al [1]. The stationary phase of the GC column used was polyethylene glycol (PEG), which has a high polarity, whereas the study with MIL-47 used 5% diphenyl/95% poly-dimethylsiloxane, which has a relatively low polarity. The PEG stationary phase may have the potential to weakly bind to the oxygen atoms associated with the peroxide species, as Figure 48 shows that the carbons located next to the oxygen atoms are electron deficient, leading to them having a minor positive charge. This may be enough to bind to the oxygen molecules of the tert-butylperoxy-1-cyclohexene.

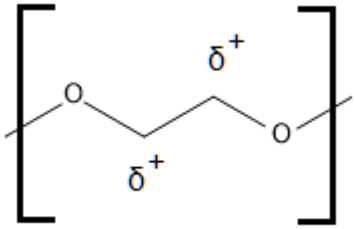

Figure 48: Polyethylene Glycol.

A literature search was completed to determine if the oxygen – oxygen bond of the tert-butyl hydroperoxide had been cleaved before and under what conditions was this likely to occur. Three studies [9-11] were identified which dealt with the tert-butyl hydroperoxy groups and peroxy groups in general. A common factor was found in the studies was that a Lewis acid is required to cleave the O-O bond of the peroxide group, so when referring back to Figure 48 one can observe that the δ^+ carbon atoms may be able to act as a Lewis acid in character and bind to the oxygen of the tert-butylperoxy-1-cyclohexene.

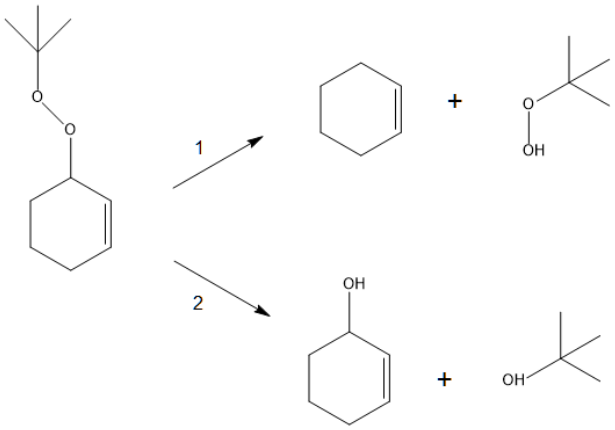

Figure 49: The possible routes and products for the cleaving of the O-O bond in tert-butylperoxy-1-cyclohexene.

There are 2 possibilities for the break-down of tert-butylperoxy-1-cyclohexene, where either the O-O bond is being cleaved or the C-O bond from position 1 on the cyclohexene ring is undergoing cleavage. Evidence for these potential products of the breakdown should be able to be observed on the GC chromatograms and can be observed, as can be seen when referring to Appendix 9 (pg. 116), tert-butanol, 2-cyclohexen-1-ol, cyclohexene and TBHP, can all be observed to be present at the end of the reaction. All the peaks associated with the products of the break-up of tert-butylperoxy-1-cyclohexene already exist in the chromatograms as they are products of the overall conversion of cyclohexene, e.g. TBHP donates an oxygen to the cyclohexene ring to form the epoxide when bound to the V centre (the mechanisms will be discussed in the following section), resulting in tert-butanol, so if the tert-butylperoxy-1-cyclohexene is breaking down via route 2, that peak will have a slightly higher intensity in the chromatogram, but determining exactly how much is being received from the overall reaction or the decomposition of tert-butylperoxy-1-cyclohexene is difficult to determine.

Regardless of whether tert-butylperoxy-1-cyclohexene is decomposing or not, RU-V1 was able to convert cyclohexene into the epoxide. Comparing RU-V1 to MIL-47 together yields a number of interesting results, as can be seen in Table 15, which displays the catalytic properties of all the materials tested and that of MIL-47. Comparing the selectivities to the epoxide shows that RU-V1 = 82 and MIL-47 = 43 (relative % ratios), which is a significant difference.

A potential reason for the difference is the time at which 40% conversion of cyclohexene occurred (the point from which the selectivity was measured, based on the referenced study [1]). 40% Conversion occurs at roughly 2.5 hours into the reaction for MIL-47, whereas for RU-V1, 40% conversion occurs between 12 and 13 hours, as RU-V1 is not initially active and requires an activation period to remove the coordinated water and/or break a bond between the metal and ligand, as previously mentioned. From Figure 47, which shows the catalytic conversion of cyclohexene using MIL-47 [1], one can observe that the catalyst is immediately active and that the two products which are forming from the conversion of cyclohexene are cyclohexene oxide and tert-butylperoxy-1-cyclohexene, cyclohexane-1,2-diol forms from the interaction of cyclohexene oxide with water, so is not being directly converted from cyclohexene. The reaction using MIL-47 was only run for 7 hours and at this point, 50% vanadium leaching was found to be present in the solution, indicating that the MOF was beginning to be broken down due to the open nature of its framework and the relatively low level of coordination, when being compared to RU-V1. With V-species present in solution and the MOF being 'opened-up' by the dissociation the ligand from metal, to expose an active site to the metal, one may assume that the major difference between the selectivities of MIL-47 and RU-V1 for cyclohexene oxide is due to steric hindrance. The difference in selectivities between the two MOFs is due to MIL-47 converting cyclohexene into tert-butylperoxy-1-cyclohexene with a higher % yield than RU-V1 (±29% after 7 hours to ±23% after 24 hours). RU-V1 has a more highly coordinated structure than MIL-47, so as the

reaction with cyclohexene and TBHP proceeds, the active sites on the metal are gradually observed to become available to be used in the conversion of cyclohexene. With this gradual progression, one may expect the bonds between the metal and ligand to slowly break away from each other over time, leading to a gradual increase in the number of coordination sites which initially should be sterically confined as only one bond may have detached to allow cyclohexene and TBHP access to the metal centre. The confined size of the coordination site may be the factor which prevents tert-butylperoxy-1-cyclohexene from forming in large amounts, as the molecule has large bulky groups on either end of the peroxide bridge, with one side occupied by a tert-butyl group and the other occupied with a cyclohexene ring. As the reaction with RU-V1 progresses to the 24th hour, the % yield of cyclohexene oxide begins to plateau and reduce, whereas the total conversion is somewhat more ambiguous, as the % yield may be reaching a plateau or may continue to subsequently decrease slowly as the structure of RU-V1 begins to be progressively broken down and V-centres are leached into the solution. This may lead to a greater number of coordination sites that are free from steric hinderance, leading to an increased % yield of tert-butylperoxy-1-cyclohexene. The reaction will need to be extended for a longer time period, before any of these mentioned assumptions can be confirmed or dismissed.

Table 15 has more properties upon which direct comparisons between MIL-47 in water and RU-V1 can be made. Turnover number (TON) and turnover frequency (TOF) can provide interesting assessments as to the characteristics of each catalyst. TON is calculated as the number of moles of product formed per moles of catalyst or the number of active sites, which in this case would be the loading of vanadium. TON gives an idea as to how effective the catalyst is at converting the reactant into a product. The TON was calculated at 7 hours and was found to be 67 for MIL-47, whereas RU-V1 = 14. This is a major difference which reinforces what was previously mentioned, in that MIL-47 is converting cyclohexene without the delay that was present for RU-V1.

MIL-47 was only run for 7 hours in a reaction mixture which contained water, so when TON was calculated, it was calculated for maximum conversion of cyclohexene. RU-V1 needs a period of 4 hours before activating and at 7 hours, it is only observed to be gradually converting any cyclohexene, leading to a low TON. If the calculation for TON is completed at the midpoint of the reaction, at 12 hours, TON = 35, indicating that a larger quantity of cyclohexene is being converted by the catalyst. Turnover frequency (TOF) is simply the turnover number per hour of the reaction, which gives an idea as to how effective the catalyst is at converting the reactant to a product over a certain time period. TOF in Table 15 was calculated after 30 minutes, which as previously mentioned, will not work particularly well for RU-V1, as the TOF will be 0. The TOF of MIL-47 after 30 minutes was found to be 29 and if one looks at a similar stage on the plot for RU-V1, one can see that after 7 hours, there starts to be a considerable amount of conversion of cyclohexene, but is still in the early stages of the reaction. At 7 hours the TOF was calculated to be 2, which again indicates

that the reaction progresses over a longer time frame, with a far more gradual conversion of cyclohexene.

MIL-47 does not require an initial period of 4 hours to activate the catalyst, it is able to begin conversion from the first hour. This is due to the structure of MIL-47 being far more open than RU-V1, as 1,4-benzenedicarboxylic acid was used as the ligand instead of 1, 2, 4, 5-benzenetetracarboxylic acid. Due to the open nature of the structure when using 1,4-benzenedicarboxylic acid, MIL-47 was catalytically active in decane at a loading of 0,42 mmol, with a selectivity of 83 for the epoxide, which was far greater than when water was present, which only had a selectivity of 43 for the epoxide. The disadvantage to using decane was that the reaction was far slower with an average conversion of 7% per hour and a TOF of 8, whereas when using water, the conversion was seen to be 20% per hour, with a TOF of 29. The time scales for the reactions done on MIL-47, when using TBHP in both water and decane vary greatly, as when using TBHP in water, the time frame for the reaction was only 7 hours, whereas when using TBHP in decane, the timeframe was 55 hours, indicating that when decane is present the reaction progresses at a slower rate, but reaches a greater relative yield and has a far higher selectivity for cyclohexene oxide. It is possible that RU-V1 may also be active in decane, but only after an extremely long period of time (longer than 72 hours) under these specific reaction conditions, which would make for an extremely inefficient catalyst.

TBHP in water caused a number of problems to MIL-47, as the structure of the MOF is not as highly coordinated as RU-V1, so this is why the reaction time was reduced to only 7 hours, as at this point the catalyst was seen to partially decompose and leach ± 50% vanadium into solution. From this information, one can potentially assume that a similar occurrence is taking place with RU-V1, as over time the reaction mixture began to become lime green in colour, which may indicate that V^{III} metal ions are being leached into solution. The structure of MIL-47 was compared before and after the reaction, using XRPD, shown in Appendix 12 (pg. 119) and was found to be the same when using TBHP in decane and significantly different when using TBHP in water. This indicates that the bonding within MIL-47 is labile enough to allow for the catalytic conversion of cyclohexene in decane, which by-passes the damaging effects of having to allow water into the reaction mixture and is a great advantage. RU-V1 was also examined before and after the reaction by using IR spectroscopy, which will be discussed in a later section.

Interestingly MIL-47 (with TBHP in water) was able to be regenerated after the 7 hour period, by exposing it to a tubular furnace at 150°C, under a nitrogen flow [1]. This was able to remove the detached organic compounds within the pores of the MOF and reforming its structure, shown in Appendix 12 (pg. 119). The possibility of regenerating RU-V1 after the 24 hour period was not investigated and may be the subject of future work. This would not be a simple investigation as the reaction will need to be run for various lengths of time and the V-leaching would need to be monitored and tested to determine a stage where the catalyst

has the V-sites coordinatively unsaturated, but still maintains its overall structure, to be able to be regenerated. If the reaction is run for too long a time (72+ hours), the catalyst is known to gradually breakdown completely, leaching elevated levels of vanadium into solution, which was proven from the preliminary testing completed using NMR.

4.5.3 The Catalytic Activity of RU-V2

RU-V2 is the unique product developed via an ambient synthesis. The bonding between the metal and the ligand can be expected to be different than that of the solvothermal product (RU-V1), as solvothermal reactions follow a different kinetic pathway, which is only reached under conditions involving elevated temperatures and pressures. This allows the ligand to undergo oxo-substitution with the metal oxide cluster to create a strong and stable product. In this section RU-V2 will be analysed in detail and compared to that of RU-V1, as this is a direct comparison between the products of the ambient and solvothermal syntheses.

When visually observing the catalyst in solution, the solution was observed to undergo a colour change from the 1st to 2nd hour, indicating that the catalyst was being altered and potentially leaching metal centres into the solution, which progressed until the reaction was completed after 24 hours. Progressing from the 1st to the 12th hour the catalyst was noted undergo a colour change from its khaki-green to red-brown colour and ultimately, after 24 hours, was orange-brown in colour. At the end of the reaction, small amounts of residual material was found stuck to the sides of the reaction flask, this was analysed via IR spectroscopy to be able to gain an idea of what change was occurring within the catalyst as the reaction progressed.

Exhibiting weaker bonding will mean that the bonding between the metal and ligand should detach far quicker and more easily than that of RU-V1. This is observed when analysing Figure 45 (pg. 80), which shows how RU-V2 acts as a catalyst for the reaction over a 24 hour period. The first important occurrence is that the catalyst is immediately active from the first hour of the reaction, which was not the case for RU-V1. As a catalytic material, RU-V2 can be observed to bring about a far more rapid conversion to the oxidation products. A potential issue that may arise is the fact that in MIL-47 vanadium leaching was found to occur when water was present in the mixture and V-leaching was presumed to occur with RU-V1. Both of these species were MOFs synthesised under solvothermal conditions, leading to far stronger bonding than what can be expected for an ambient vanadium based complex. One may assume that when RU-V2 was entered into the solution, vanadium leaching could possibly occur at a greater rate than RU-V1 and MIL-47, with the break-away of the ligand occurring more rapidly. MIL-47 made use of 1,4-benzenedicarboxylic acid under solvothermal conditions and RU-V2 made use of 1,2,4,5-benzenetetracarboxylic acid under ambient conditions, which sets up an interesting comparison to observe whether the solvothermal product using a lowly coordinating ligand is stronger than an ambient product using a highly coordinating ligand. An insight could be obtained when observing the major

difference between the speciation curves of the MIL-47 and RU-V2, which is the time period before maximum conversion is reached; the conversion is observed to plateau before 7 hours when using MIL-47, but only after approximately 14 hours when using RU-V2. A potential reason for this may again be due to the coordination difference between the ligands, as 1, 2, 4, 5-benzenetetracarboxylic acid is multidentate, leading to a much more highly coordinated structure, which may need slightly more time for a bond to completely detach from the metal, for catalysis to occur.

The total conversion of cyclohexene was 67%, which was lower than the 77% cyclohexene conversion of RU-V1. The minor reaction products of 2-cyclohexen-1-one and 2-cyclohexen-1-ol formed at a maximum (7% and 3%) at 7 hours, then reduced and reached a plateau (3% and 0.5%) until the 24th hour. Cyclohexane-1,2-diol was observed to be far more prominent when using RU-V2, as the initial and rapid conversion of cyclohexene to the epoxide, resulted in the conversion of the epoxide to the diol, with water present in the reaction mixture. The diol reaches a maximum conversion of 37% to 39% before reaching a plateau, which closely mirrors that of cyclohexene oxide, as it is converted from the epoxide in the presence of water.

When comparing RU-V2 to RU-V1, one can observe that the latter has a much higher selectivity for the epoxide, with 82 compared to 64 (relative % ratios), but the former is much more rapid in its conversion, as it is able to convert as soon as the reaction is initiated. TON calculated after 7 hours shows a similar result as RU-V1 is far greater at 56 than 14 for RU-V2. TOF calculated after 30 min is not comparable between RU-V1 and RU-V2, due to RU-V1 requiring an activation period, but MIL-47 (water) and RU-V2 can be compared and one can observe that MIL-47 is faster at converting cyclohexene than RU-V2, with a TOF of 29 compared to 9, again possibly owing to the less highly coordinated structure of MIL-47.

Tert-butylperoxy-1-cyclohexene has been discussed in detail in section 4.5.2, but will be touched upon again, as it is forming in a greater quantity when using RU-V2 as a catalyst. The discrepancy between the total conversion of cyclohexene and the total conversion of all the known products combined was approximately 24% after 24 hours, which maybe assumed to be from the formation of tert-butylperoxy-1-cyclohexene.

4.5.4 The Catalytic Activity of Solid Decavanadate Ion

The decavandate ion was originally incorporated into this study, as it has not received any attention in the field of MOFs and could possibly be used as a starting material upon which a MOF may be built around, leading to a MOF or coordination complex which could exhibit interesting catalytic properties. The first step was to test the ion itself for catalytic activity, but in the solid state as a heterogeneous catalyst. This step proved problematic as the solid decavanadate ion was found to completely catalytically inactive in an organic medium, containing mostly $CHCl_3$. The reason for this complete lack of activity was thought to be due to the counter ions and water molecules associated with the molecule which would remain

coordinated to the active sites, blocking any possible activity. However when observing Figure 46 (pg. 81), conversion of cyclohexene is observed to occur and the reason being is that a small portion of water is present in the over-all reaction mixture. These small droplets were observed to become more orange in colour over time, indicating that the solid decavanadate, which is highly soluble in water, is undergoing dissolution into these droplets and is acting as a homogenous catalyst from the aqueous phase. The activity seen is due to interaction between the V – centres of the decavanadate ion at the borders of the aqueous and organic phases, where the cyclohexene and TBHP would be able to interact with the catalyst.

When analysing Figure 46 in detail, one can immediately notice that the conversion of cyclohexene is much lower, relative to RU-V1 and RU-V2, with the reason being, that only a small portion of the solid decavanadate came into contact with the aqueous phase due to the mechanical stirring and limited reaction time. The cyclohexene conversion started very gradually for the first 10+ hours, after this point the conversion began to increase slightly, as more of the solid decavanadate dissolved into the aqueous layer, finally reaching a maximum conversion of ±39%.

Comparing the activity of the decavanadate to the other materials, in terms of TON, TOF and selectivity is not necessary, as the reaction system in which the decavanadate was introduced to test its heterogenous activity and it was found to not exhibit any activity. Regardless of this fact, the TON, TOF and selectivity have been determined and are displayed in Table 15. TON after 7 hours is relatively low, as the conversion was gradual due to the slow dissolution of the decavanadate into the aqueous phase and similarly the TOF = 0 due to there being no catalytic activity after 30 minutes. Selectivity can be used to gain more of an insight into what is forming, as once again there is a discrepancy between the total cyclohexene conversion and the conversion of the products, which is approximately 17%. This indicated that tert-butylperoxy-1-cyclohexene was once again forming as a product, as previously discussed and was forming in a relatively high quantity, when compared to that of cyclohexene oxide, which had a maximum conversion of approximately 20%. These % conversions are relatively close, indicating that the decavanadate ion is not able to select for a specific product, which was expected, as there are no supplementary groups or ligands which are able to sterically hinder the active sites, as observed with RU-V1. Cyclohexane-1,2-diol was not observed to be present in the reaction solution, the reason for this was presumed to be that the reaction had not been run for long enough, with the % yield of cyclohexene oxide being relatively low. If the reaction was completed with an extended time period, more of the solid decavanadate would have dissolved into the aqueous phase, leading to an increased % yield of cyclohexene oxide, which would have slowly began to lead to the conversion of the diol species.

The solid decavanadate ion has a number of potential active sites which are proven to be homogeneously active for the oxidation of olefins, but the challenge arises when trying to

move away from homogenous catalysis and into the region of heterogeneous catalysis. Designing a coordination compound or MOF will be a challenge as the choice of ligand will be very important, in both the steric hinderance of the active sites and to act as a stabilizer to the overall decavanadate structure, as once the associated water molecules are removed the stability of the ion will be in question and once the counter ions are removed, the chosen ligand will be responsible to maintain a charge balance.

4.6 The Proposed Mechanisms for the Reaction

An in depth enquiry towards the mechanism of the reaction for MIL-47 was completed by Van der Voort et al [1], where they proposed 2 major mechanisms. The structure and reaction were comprehensively studied using molecular modelling techniques to elucidate exactly what was occurring and which possibilities were most likely to occur. Two mechanisms will be discussed, the first being the direct method of epoxidation and the second being the radical method of epoxidation.

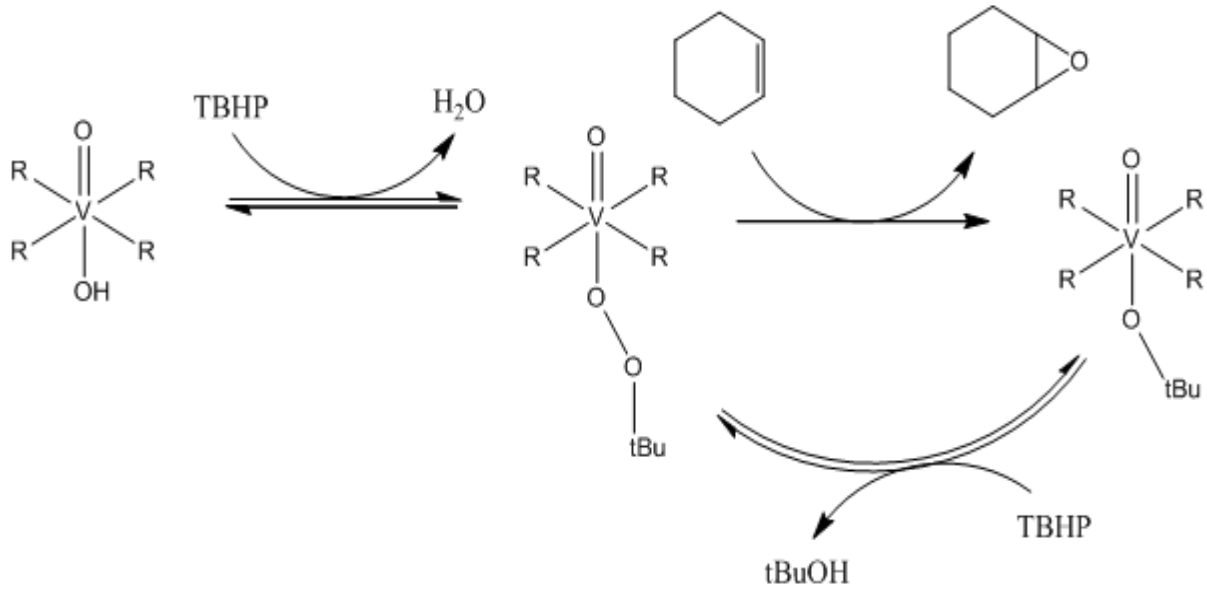

Figure 50: The Direct Method for the Epoxidation of Cyclohexene [1].

Figure 50 displays the direct method of epoxidation of cyclohexene. This is the most basic mechanism for the epoxidation, as once a free coordination site is available to the metal centre, TBHP coordinates and cyclohexene is able to interact with the O-chain of TBHP, thereby removing an O to form cyclohexene oxide.

The radical mechanism displayed in Figure 51 is a more complex method, which was analysed through the use of computational methods [1]. This mechanism requires the attachment of the TBHP group to the metal centre, but the O-O bond undergoes homolytic

cleavage. This cleavage forms a radical ($tBuO^{\cdot}$) and a vanadium centre bound to the ligand and two O's (L-V=O_2). This undergoes a further reaction with an additional TBHP, which coordinates to the metal centre and from here the cyclohexene is able to interact with the O-O chain of the TBHP, forming the epoxide. Once epoxidation has occurred, the tBuO can be replaced with another TBHP group, regenerating the reaction and allowing for the epoxidation to take place once more.

The major difference between the direct and radical mechanisms is that the direct method only requires one free coordination site, whereas the radical requires two or more bonds to be detached from the metal centre, as can be seen throughout the mechanism in Figure 51. This is important as the direct method is assumed to be the initial method which is able to form the vanadium species coordinated to TBHP. Over time, as more of the bonds between the metal and ligand are detached and more open coordination sites to the metal centre become present, one can assume that the radical method may take preference. The direct and radical methods are not mutually exclusive from one another and can occur simultaneously.

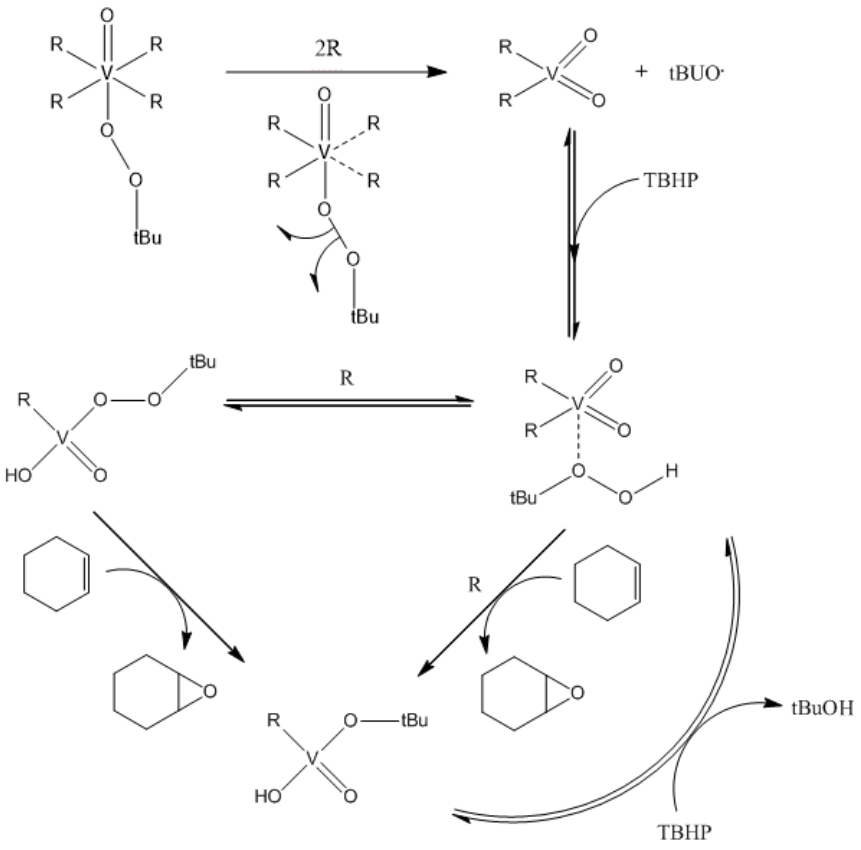

Figure 51: The Radical Method for the Epoxidation of Cyclohexene [1].

RU-V1 can be assumed to initially be following a mechanism similar to that of the direct method, but possibly in a sterically hindered environment, due to the closed nature of the MOF. There needs to be an active coordination site to the metal centre and from consulting

the structure of RU-V1 (Figure 30, pg: 59), the coordinated water molecule is expected to be the released before any of the ligands would become detached. This was proven, as the TG data showed that the coordinated waters associated with the structure were released before the ligand, so is expected to be detached from the structure to allow cyclohexene and TBHP an active coordination site to the metal centre. The water is still strongly bound to the structure, as the MOF required a period of 4 hours before any conversion was initiated and there was a high initial selectivity for the epoxide over the other potential oxidation products. This is suggesting that only a few bonds are breaking at a time, so the direct method may be prevalent. After a period of approximately 12 hours there is a shift from the selectivity for the epoxide and one can observe an appreciable amount of tert-butylperoxy-1-cyclohexene forming, which may be suggesting that enough of the bonds have detached from the metal centre, allowing for the radical method to become more prevalent. With a greater detachment of the bonds between the metal and ligand, a more open environment is assumed, which would lead to an increase in the formation of tert-butylperoxy-1-cyclohexene.

RU-V2 can be assumed to follow a slightly different reaction profile to that of RU-V1, as RU-V2 was found to be immediately active for the epoxidation of cyclohexene. This possibly suggests that the direct method is followed in the earliest stages of the reaction and shortly afterwards the radical method may become more prevalent. Evidence for this suggestion is given in terms of selectivity, as the selectivity for the epoxide is a great deal lower than RU-V1. In conjunction with the selectivity, the structure was noted to decompose more rapidly, which suggests that bonds between the metal and ligand are dissociating, thus increasing the number of free coordination sites to the metal. The lower coordination of the metal centre may favour the radical mechanism.

The decavanadate ion was only found to be homogeneously active when dissolved in the aqueous phase. The direct method is thought to be the prevalent method of catalytic activity since when referring to the IR spectra of the decavanadate before and after the reaction, it was found that the structure remains completely intact. This suggests that the catalytic activity is potentially due to vanadyl groups on the surface of the decavanadate structure, as the bulk material was unchanged.

4.7 Possible Decomposition Path-ways for the Catalytic Materials

From observing the reactions before, during and after the reactions, it has been previously noted that the catalyst was breaking down and partially leaching into the reaction mixture. The possible decomposition path-ways of the catalytic materials were investigated to try and elucidate what was taking place for each of the catalytic materials over the course of the reaction. Proposed decomposition path-ways and a comparison of the IR spectra before and after the reaction are displayed and discussed in the following sections.

4.7.1 RU-V1

From what was mentioned in the previous sections, complexes which are coordinatively saturated require a bond between the metal to be labile enough to be able to detach from the metal centre. This dissociation opens up a potential site for coordination, causing the complex to become catalytically active.

When analysing the dissociation one needs to be careful, as there is a small energy difference between dissociation and complete cleavage of the bond. Possible ways in which the bond may dissociate, but still be able to reattach onto the metal after the catalytic conversion has taken place is by folding away of the ligand from the metal or by the removal of the bridging oxygen between the vanadium centres [1]. MIL-47 in decane was noted to exhibit this form of detachment, as decane is a non-polar solvent, which does not exhibit any attractive forces towards the bonds between the metal and ligand. The opposite is true when a highly polar molecule, such as water, is present is solution, which competes with the labile ligand for coordination to the metal centre. This competitive effect gradually causes a decomposition of the overall structure.

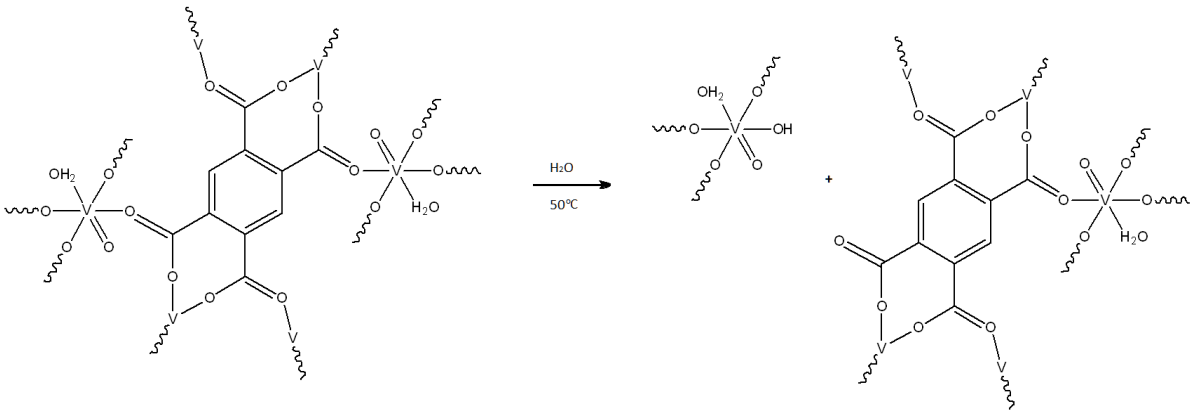

Figure 52: A proposed decomposition path-way for RU-V1.

This is exactly what was observed for RU-V1, because as the reaction progressed, slowly the solution began to gradually change colour, potentially indicating a leaching of metal centres and a gradual structural break down. The structures before and after were compared using IR spectroscopy. The catalyst had notably changed to be green in colour, but this was only found to be the case for the outer most layers of the catalyst, when a small sample was crushed into a homogeneous sample the overall spectrum was identical to the IR spectrum of the catalyst before the reaction. This was interesting as it potentially showed that the catalyst was only reacting on the surface and gradually layers of the surface material were being removed, via the disrupture of the structure in the presence of water and leaching vanadium into the reaction mixture. The green surface material was collected and the IR

spectra thereof are compared to that of the original material, which gave a number of useful insights into what type of structural changes may be taking place overtime, these changes can be observed in Figure 53.

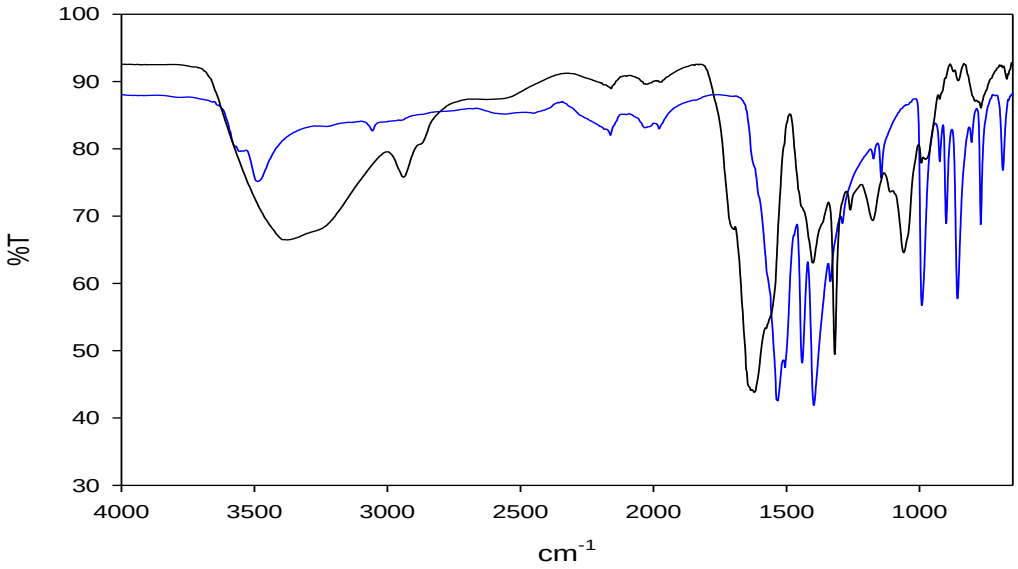

Figure 53: A comparison of RU-V1 before (blue) and after (black) the reaction.

The first region to analyse is the carbonyl region at ±1300 – 1600 cm^{-1}. Bands in this region give a great deal of information as to whether the carbonyl groups are coordinated or terminal/uncoordinated groups. As mentioned in Chapter 3, coordinated carbonyl bands will be and sharp and narrow in nature, as the group will have restrictions to its modes of vibration, whereas a terminal carbonyl band will have no such restrictions, and thus will be observed as a far broader band and will have a greater wavenumber due to having more double bond in character.

Table 15: A comparison of the asymmetric and symmetric stretches of the carbonyl groups before and after the reaction.

	$\nu_a(CO_2^-)$ (cm^{-1})	$\nu_s(CO_2^-)$ (cm^{-1})
RU-V1 (Original)	1532; 1505	1441; 1395; 1335;1289
RU-V1 (Post Rxn)	1621; 1568	1447; 1402; 1320; 1263
$\Delta\nu$ (cm^{-1})	89; 63	6; 7; 15; 26

$\nu_a(CO_2^-)$ in the original catalytic material show 2 major bands at 1532 cm^{-1} and 1505 cm^{-1}, with a minor shoulder from ±1570 cm^{-1} to 1650 cm^{-1}. In the recovered material, the two major bands associated with the $\nu_a(CO_2^-)$ have shifted to 1621 cm^{-1} ($\Delta\nu$ = 89 cm^{-1}) and 1568 cm^{-1} ($\Delta\nu$ = 63 cm^{-1}), the latter is less defined in the spectrum of the residue, as it was in the original, indicating a change to the environment, causing a change to that specific mode of

vibration. These shifts are indicating that the carbonyl group has been altered into a terminal position, evidence for this is due to the nature of the band, as the broadness of the band found in the residue is significantly broader than the original band, indicating that the functional group is now uncoordinated and added to this, terminal carbonyls are more double bond in character, increasing the force constant of the group, thus having a higher wavenumber.

The $\nu_s(CO_2^-)$ band in the spectrum of the recovered material was observed to be drastically altered when compared with that of the original material, with a number of shifts and changes to the intensity of the individual bands. A reduction in intensity can be observed to occur with a number of the bands and this is commonly due to changes in the polarizability of the bonds, indicating that the close environment surrounding the carbonyl group has changed. Possible changes to the environment can include; some of the carbonyl groups being stripped away, leaving a larger area in which those left behind can vibrate, some carbonyls may have been dissociated from the metal, resulting in a terminal group as previously discussed. When specifically observing the individual bands, one can identify 4 bands associated with the $\nu_s(CO_2^-)$ in the original material, at; 1441 cm^{-1}, 1395 cm^{-1}, 1335 cm^{-1} and 1289 cm^{-1}. One should note that the $\nu_s(CO_2^-)$ with the lowest wavenumber (1289 cm^{-1}) may not be associated with the carbonyl, but could possibly be associated with a benzene ring vibration. These bands are significantly altered in terms of intensity and relatively minor shifts can be observed in terms of band position. In the spectrum of the residue, the bands can be observed to shift to; 1447 cm^{-1} ($\Delta\nu$ = 6 cm^{-1}), 1402 cm^{-1} ($\Delta\nu$ = 7 cm^{-1}), 1320 cm^{-1} ($\Delta\nu$ = 15 cm^{-1}) and 1263 cm^{-1} ($\Delta\nu$ = 26 cm^{-1}). The shift of 26 cm^{-1} is considerably larger than the other shifts described, so again may be indicating that the band could be associated with a benzene ring vibration.

The second region of interest is the region where the vanadyl band occurs, which is generally between 980 cm^{-1} and 1000 cm^{-1}. This region is more challenging to analyse, as there are also a number of other bands which occur in this region, known as the fingerprint region, which can be assigned to several organic species.

Table 16: A comparison of the stretches of the vanadyl groups before and after the reaction.

	ν(V=O) (cm^{-1})
RU-V1 (Original)	991
RU-V1 (Post Rxn)	994; 975
$\Delta\nu$ (cm^{-1})	3; 16

The vanadyl band is present in the spectrum of the original material at 991 cm^{-1}, but when observing the spectrum of the residue after the reaction, one may notice that the band has had its intensity significantly reduced and has been split into 2 bands (994 $cm^{-1}$and 975 cm^{-1}).The splitting of a band may be suggesting that multiple vanadyl centres have formed from the as a result of the decomposition of the ligand. This is shown in Figure 52, which

proposes a decomposition path-way of RU-V1 over time. Initially the VO octahedra are bound on either side of the benzene ring, but after a period of 24 hours, one may assume that a greater number of bonds would be broken. With the decomposition of RU-V1 in such a manner, one can suggest that dissociation of the bonds would not be a uniform process, resulting in the ligand and metal dissociating at different times. Such a scenario would result in the vanadium octahedra existing in different environments. Another reason for the splitting of the band could be due to the lifting of degeneracy through the loss of a centre of inversion, proposed in Figure 52. An alternative option is that the vanadyl band has shifted to a new position entirely. A band is present at 1061 cm^{-1}, which is not present in the original IR spectrum of the material. This is option is similar to what was observed in the carbonyl, as the vanadyl has been shifted to a higher wavenumber and is broader than it the original, indicating that it may be more double bond in character and is now a terminal group, due to the loss of coordination. The problem with this option is that a shift from 994 cm^{-1} to 1061 cm^{-1} is a change of 70 cm^{-1}, which is a large shift and from completing a literature search of vanadyl complexes, the vanadyl band is not likely to occur above ±1040 cm^{-1}[13,14].

Table 17: The band positions of v(C-H) for cyclohexene, cyclohexane-1,2-diol and RU-V1 (post rxn).

	v(C-H) (cm^{-1})
Cyclohexane-1,2-diol	2945, 2881
Cyclohexene	3040, 2935, 2873
RU-V1 (Post Rxn)	2941, 2878

The other region which differs in the spectrum of the residue is that of *v*(C-H) region. There a band is present at 2941 cm^{-1} and a shoulder at 2878 cm-1. These bands may be present due to the presence of cyclohexene (substrate) or cyclohexane-1,2-diol. These are possibly trapped within or associated on the structure, possibly weakly bound via van der Waals forces to an exposed vanadium centre. The absence of the cyclohexene alkene *v*(=C-H) suggests that the substrate is absent. Additional comparisons with the IR spectra of cyclohexane-1,2-diol and cyclohexene, which are taken directly from the Bio-Rad/Sadtler IR Data Collection [15] as given in Appendix 13 and 14 (pg. 120) tentatively supports this interpretation. More compelling is the identification of the coupled *v*(C-O)/δ(COH). As previously noted, the benzene ring vibration region yields an interesting possibility, as discussed above, the vanadyl stretch may be shifting to a higher wavenumber of 1062 cm^{-1}, but this was proven to be unlikely. This band rather provides further evidence for cyclohexane-1,2-diol being present, due to the *v*(C-O)/δ(COH) being present at 1068 cm^{-1} in the cyclohexane-1,2-diol and a similar band can be observed in the spectrum of RU-V1 (post rxn) at 1062 cm^{-1}. The only major band which has not been assigned is present at 1178 cm^{-1}, which has been tentatively assigned as a benzene ring vibration associated with the ligand, 1, 2, 4, 5 – benzenetetracarboxylic acid , or a ring vibration from the cyclohexane ring, as

there is a band at 1156 cm^{-1}, but this is a relatively large shift of 22 cm^{-1}. Finally the bands present in the fingerprint region below 950 cm^{-1} are particularly difficult to interpret, with a number of possibilities of low energy vibrations for each band.

4.7.2 RU-V2

RU-V2 was found to be immediately active for the conversion of cyclohexene, but the solution was also observed to change colour far more rapidly. The RU-V2 was analysed before and after the reaction using IR spectroscopy to attempt to gain an understanding of what type of structural alterations may be occurring in the catalyst over time. The structure of RU-V2 was not directly determined by XRD or XRPD as the compound was found to be amorphous, the IR spectra discussed previously in the characterisation results section gave a number of insights into the structural properties of the compound.

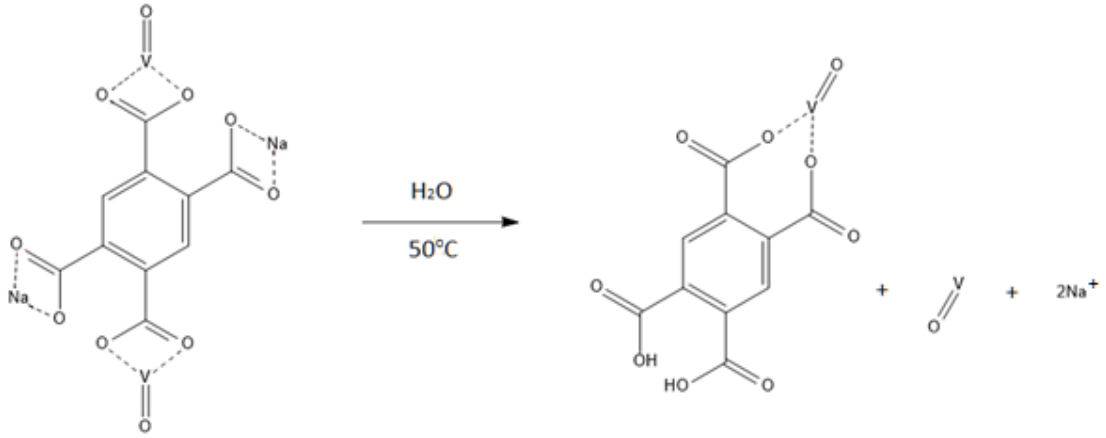

Figure 54: A proposed decomposition path-way for RU-V2.

Figure 54 is a potential decomposition path-way for RU-V2, deduced from observing the IR spectra before and after the reaction. The Na^+ ions are expected to be removed from the complex and leached into the aqueous phase associated with the reaction. This frees two of the carboxylates to the terminal position which is clearly observed and discussed in the IR comparison below.

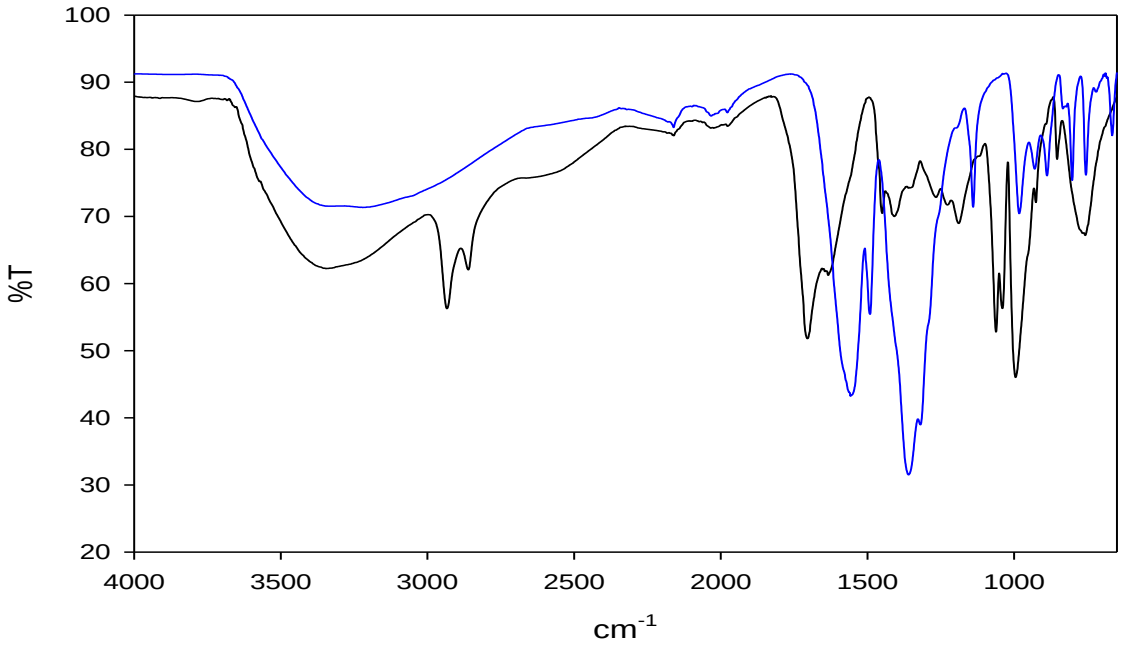

Figure 55: A comparison of the IR Spectra of RU-V2 before (blue) and after (black) the Reaction.

Table 18: A comparison of the asymmetric and symmetric stretches of the carbonyl groups before and after the reaction.

	$\nu_a(CO_2^-)$ (cm^{-1})	$\nu_s(CO_2^-)$ (cm^{-1})
RU-V2 (Original)	1557; 1494	1363; 1320; 1288 (shoulder); 1256 (shoulder)
RU-V2 (Post Rxn)	1707; 1636	1443; 1412; 1353
$\Delta\nu$ (cm^{-1})	150; 142	80; 92; 65

The carbonyl and vanadyl regions will be discussed again, alongside any other major bands. The asymmetric stretch of the carbonyl (ν_a(C-O)) in the original spectrum, has 2 bands associated with it at 1557 cm^{-1} and 1494 cm^{-1}, with a poorly resolved shoulder present at 1575 cm^{-1}. These bands have been shifted to higher wavenumbers of 1707 cm^{-1} and 1636 cm^{-1} which is a change of 150 cm^{-1} and 142 cm^{-1}. These are large shifts, which are strongly indicating that the carbonyl is becoming more double bond in character and in a terminal position. There are two possibilities as to what may be occurring; firstly the Na ions are expected to be removed from the complex and released into the aqueous phase and secondly the coordinating vanadium has been removed and possibly leached into solution, leaving the carbonyls in terminal positions. Figure 54 shows that one of the vanadium centres has been removed and the other has changed from being a bidentate donor with a single carboxylic acid group, to bridging between two carboxylic acid groups. This proposal

of the dissociation frees up two of the carboxylic acid groups which results in two of the carbonyls remaining in terminal positions, which may account for the large $\nu_a(CO_2^-)$ shift observed in the spectrum after the reaction.

The bands associated with the $\nu_s(CO_2^-)$ have also been drastically altered in terms of intensity and in terms of wavenumber. The reasons for the changes are similar to what was discussed for RU-V1, with some having possibly been stripped away, leaving those that remain in different environments. Referring to Table 19 shows shifts of; 80 cm^{-1}, 92 cm^{-1} and 65 cm^{-1}, which are all relatively large shifts, again indicating that the carbonyls which remain are more double bond in character.

Table 19: A comparison of the stretches of the vanadyl groups before and after the reaction.

	ν(V=O) (cm^{-1})
RU-V2 (Original)	982
RU-V2 (Post Rxn)	997
$\Delta\nu$ (cm^{-1})	15

The vanadyl band is present at 997 cm^{-1}, which is a shift of 15 cm^{-1} from the original band at 982 cm^{-1}, which indicates a strengthening of the double bond character and can be seen to be broader than the band in the original spectrum, both of these factors are evidence that the remaining vanadyl group has possibly become a terminal group. The intensity of the band has greatly increased and this can be potentially explained by referring to Figure 54 once more, where one can observe that the proposed product after the reaction lacks a centre of inversion, but the original product exhibits a centre of inversion. Losing a centre of inversion causes the molecule, as a whole, to become more polar and this is able to affect the intensity of the IR band/s. The movement of the vanadium centre from a single carboxylic acid group, to be in a position to be bridging between two of the groups may also have an effect on the polarisability of the bond, as it is in a new chemical environment.

Table 20: The band positions of v(C-H) for cyclohexene, cyclohexane-1,2-diol and RU-V2 (post rxn).

	ν(C-H) (cm^{-1})
Cyclohexane-1,2-diol	2945, 2881
Cyclohexene	3040, 2935, 2873
RU-V2 (Post Rxn)	2934, 2862

The other unassigned bands are again similar to what was observed for RU-V1, where one can observe an appreciable amount of cyclohexane-1,2-diol present. Table 21 shows the C-H stretches present at 2934 cm^{-1} and 2862 cm^{-1} and similarly to the discussion of the bands in this region for RU-V1, cyclohexene exhibits a higher frequency band associated with the alkene, which is not present and provides evidence for the diol over the substrate. The

cyclohexane-1,2-diol ν(C-O)/δ(C-O-H) is present at 1068 cm^{-1} and one can find 2 bands present in this area in the RU-V2 (post rxn) spectrum at; 1065 cm^{-1} and 1040 cm^{-1}. A single band was expected, but has been split into 2 bands indicating that the C-O-H bonds of the diol may be in 2 different environments, causing a difference in the polarisability C-O-H bonds, splitting the band. The only other major bands which have yet to be assigned are present at 1270 cm^{-1} 1228 cm^{-1} 1193 cm^{-1} 1125 cm^{-1} (minor shoulder). These are a challenge to assign as this region had undergone a drastic change after the reaction was completed and has been tentatively assigned as ring vibrations, as this is what is generally expected to be found in this region of the IR spectrum. The specific bands can potentially be described as in-plane stretches: ν_a(C-C) at 1270 cm^{-1} and ν_s(C-C) at 1125 cm^{-1}, out of plane bends: δ(C-H) at 1228 cm^{-1} and 1193 cm^{-1}.

4.7.3 Decavandate Ion

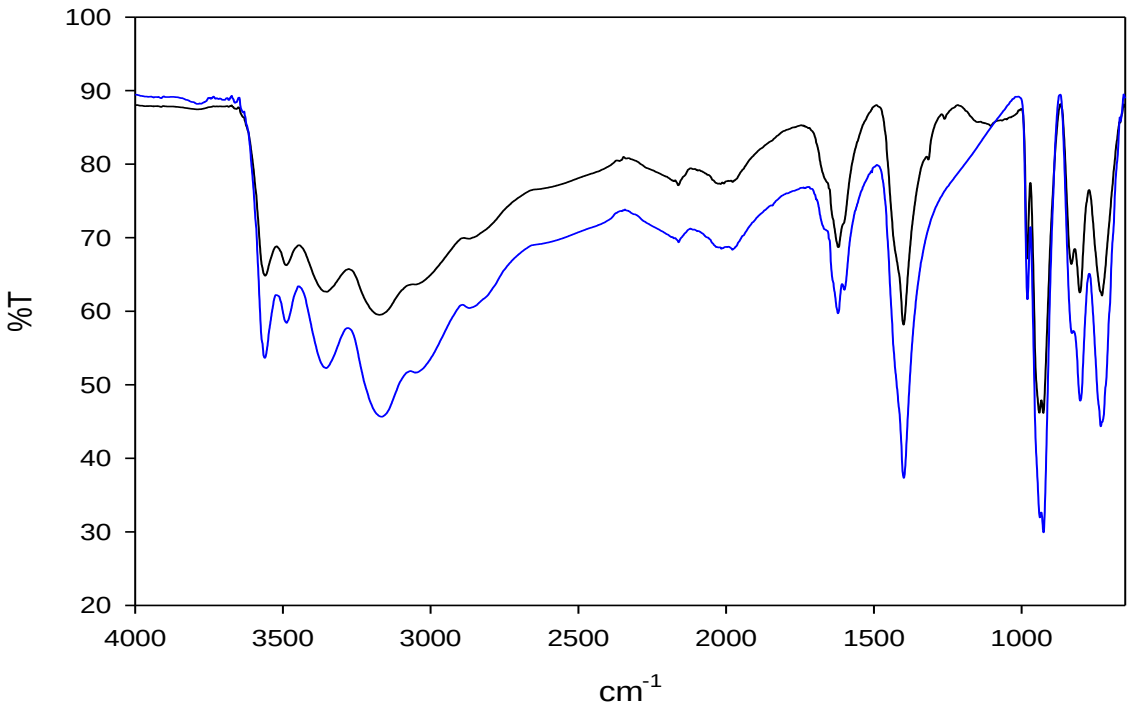

Figure 56: A comparison of the IR Spectra of solid decavanadate ion before (blue) and after (black) the Reaction.

The post reaction analysis for the solid decavanadate ion indicates that it does not undergo any sort of decomposition, as one can observe that the spectra before and after the reaction are almost identical, which indicates that the structure of the decavanadate ion is still intact.

A close inspection of the IR comparison in Figure 56 reveals only a small difference between the spectra and this can be observed in the region of 1315 cm^{-1} to 1015 cm^{-1}. These small

bands are tentatively suggesting that a very small percentage of the NH_4^+ counter ions are becoming deprotonated to NH_3 and possibly coordinating to the metal centres. The minor bands present at 1317 cm^{-1} and 1260 cm^{-1} are possibly indicative of a NH_3 stretch (δ_s(H-N-H)(coordinated)). The band at 1402 cm^{-1} is associated with the tetrahedral NH_4^+ and is described as a δ_d(umbrella) [16].

The rest of the spectrum before and after the reaction matched up identically. The region from 3561 cm^{-1} to 2852 cm^{-1} shows a number of different bands and these can be assigned as the O-H (*v*(O-H)) and the N-H stretches (*v*(N-H)). Identifying exactly which band belongs to which stretch is a challenge, but most of the bands are expected to be associated with free waters in different environments surrounding the decavanadate ion, as there are generally 16-18 uncoordinated waters associated with the ion. The region from 2164 cm^{-1} to 1977 cm^{-1} is assigned as the overtone region. The next band is present at 1625 cm^{-1}, with a shoulder at 1600 cm^{-1}, this has been assigned as the N-H bend (δ_d(N-H)). The vanadyl bands (*v*(V=O)) are present and at 984 cm^{-1}, 944 cm^{-1} and 926 cm^{-1}, three bands are present due to the vanadium centres being in slightly different environments within the ion. Finally one can observe 3 bands present at 834 cm^{-1}, 804 $cm^{-1}$and 732 cm^{-1}, which are assigned as N-H wags (ρ_w(N-H)) [16].

References:

1. Van Der Voort, P.; Van Speybroek, V.; Leus, K.; Vandichel, M.; Liu, Y.; Muylaert, I.; Musschoot, J.; Pyl, S.; Vrielinck, H.; Callens, F.; Marin, G. B.; Detavernier, C.; Wiper, P. V.; Khimyak, Y. Z.; Waroquier, M. The coordinatively saturated vanadium MIL-47 as a low leaching hetergeneous catalyst in the oxidation of cyclohexene. *J. Catal.* **2012**, *258*, 196 - 207.
2. Yahiaoui, A.; Belbachir, M.; Soutif, J. C.; Fontaine, L. Synthesis and structural analyses of poly (1, 2-cyclohexene oxide) over solid acid catalyst. *Mater. Lett.* **2005**, *59*, 759 – 767.
3. Ray, B. C.; Mukherjee, S.; Samanta, S.; Bhaumik, A. Mechanistic study of cyclohexene oxidation and its use in modification of industrial waste organics. *Appl. Catal. B-Environ.* **2006**, *68*, 12 – 20.
4. Sridhar, S. T.; Mahajani, S. M.; Sharma, M. M. Uncatalysed oxidation of cyclohexene. *Chem. Eng. Sci.* **1999**, *54*, 3967 – 3976.
5. Cevik, S.; Poyraz, M.; Sari, M. A novel three dimensional organic-inorganic Hybrid based porous phase: synthesis and characterisation of reduced oxovanadium pyromellitate, $[V^{IV}_2O_2(H_2O)_2(C_6H_2(COO)_4)]$. *J. Chem. Crystallogr.* **2007**, *37*, 497 - 502.
6. Csányi, L. J.; Jáky, K.; Kiss, J. T.; Ilisz, I.; Forgó, P.; Dombi, G. Liquid-phase oxidation of cyclohexene and of tetralin by N_2O in the presence of onium salts under mild experimental conditions. *J. Mol. Catal.* **2007**, *263*, 48 – 54.
7. Csányi, L. J.; Jáky, K.; Dombi, G.; Evanics, F.; Dezsö, G.;. Kóta, Z. Onium-decavanadate ion-pair complexes as catalysts in the oxidation of hydrocarbons by O_2. *J. Mol. Catal.* **2003**, *195*, 101 – 111.
8. Gade, L. H.; Meder, M. B. Co-ordination chemistry of 1, 3-Bis(2-pyridylimino)- and 1,3-Bis-(2-thiazolylimino)isoindole copper complexes: Investigation of their catalytic behaviour in oxidation reactions. *Eur. J. Inorg. Chem.* **2004**, 2716 – 2722.
9. Gan, L.; Chen, B.; Hu, X.; Zhang, X.; Von Ragué Schleyer, P.; Thiel, W.; Chen, Z.; Zhang, S.; Yuan, G.; Zhou, J.; Wang, F.; Xiao, Z.; Huang, S. Preparation of [5,6]- and [6,6]-Oxahomofullerene derivatives and their interconversion by lewis acid assisted reactions of fullerene mixed peroxides. *Chem. Eur. J*. **2005**, *11*, 5449 – 5456.
10. Doyle, M .P.; Chiou, G.; Wang, K.; Choi, H.; McLaughlin, E. C. Allylic oxidations catalysed by Dirhodium Caprolactamate via aqueous tert-butyl hydroperoxide: The role of the tert-butylperoxy radical. *J. Org. Chem.* **2009**, *74*, 730 – 738.
11. Sharpless, K. B.; Chabaud, B.; Warpehoski, M. A. Selenium dioxide oxidation of endolic olefins. Evidence for dissociation – recombination pathway. *J. Org. Chem*. **1982**, *47*, 2897 – 2900
12. The NIST database website - http://www.nist.gov/srd/nist1a.cfm (accessed: 14/02/16)
13. Frederickson, D.; Hausen, M. Infrared Spectra-Structure Correlation study of Vanadium-Oxygen Compound. *Anal. Chem.* **1963**, *35*, 818 – 827.

14. Evans. J. C. The Vibrational Spectra and Structure of the Vanadyl Ion in Aqueous Solution. *Inorg. Chem.* **1963**, *2*, 372 – 375.
15. The Bio-Rad/Sadtler IR collections - http://www.bio-rad.com/en-za/product/ir-spectral-databases. (The spectrum for Cyclohexane-1,2-diol was accessed via Scifinder). (Accessed: 14/02/16)
16. Nakamoto, K. *Infrared and Raman Spectra of Inorganic and Co-ordination Compounds Part B*. Sixth edition. John Wiley & sons, Inc. New Jersey, 2009.

5. CONCLUSIONS AND FUTURE WORK

A number of interesting conclusions can be drawn from the study in terms of the results of the syntheses and the catalytic studies completed.

The syntheses attempted with 2 species of oxo-vanadium ions; the vanadate and vanadyl ions, and 1,2,4,5 – benzenetetracarboxylic acid were strongly dependent on pH, as the ligands degree of protonation and the speciation of vanadium both vary greatly with pH. Various types of syntheses were attempted, which included; ambient, hydrothermal, gel and reflux. Gel syntheses were completed using sodium metasilicate and gelatine, both of these gelling media were found to be unsuitable for the formation of a product. Sodium metasilicate only gelled over a narrow pH range, which was found to be unsuitable for both vanadate and vanadyl ions, as they would form decavanadate ions or hydroxy-species which would not coordinate to the ligand under ambient conditions. Gelatine was found to be unsuitable due to a number of reasons; micellular structures formed which were thought to be bacterial growths and therefore contaminated the synthesis, the metal salt solution moved through the gelatine solution without any product formation and often caused the gelatine medium to break-down into a viscous liquid. Reflux syntheses were found to form various metal salts, with no coordination to the ligand. Ambient and solvothermal syntheses yielded the best results, and produced two products, one product from an ambient synthesis (RU-V2) and another from a solvothermal synthesis (RU-V1).

Extensive characterisation of the two products found the solvothermal product to be the same as the V-MOF found by Cevik et al, whereas the ambient product was found to be novel according to a comprehensive literature review.

RU-V1 and RU-V2 were tested for their catalytic activity in the epoxidation of cyclohexene to cyclohexene oxide. This specific reaction was chosen due to a well-known V-MOF (MIL-47) having been shown to exhibit catalytic conversion for the epoxide in a comprehensive study completed by van der Voort et al. The solid decavanadate ion was included to the study as a potential catalyst, as the ion has never been used in the construction of a MOF and may exhibit interesting catalytic activity, so testing the ion alone was be the first step in this regard.

RU-V1 was found to exhibit a highly coordinated structure, as the use of a multidentate ligand, such as 1,2,4,5-benzenetetracarboxylic acid tends to yield a highly coordinated/closed structure. This property of the material was initially thought to be ill-suited for the application of catalysis, as the catalyst requires a free metal coordination site, with a more open structure. This was shown when the reaction was completed with TBHP in decane, since no catalytic conversion of cyclohexene was observed and was thought to be due to the highly coordinated structure of the V-MOF, not being able to detach a bond to

the metal to free a coordination site for catalytic conversion to occur. When the reaction was completed with TBHP in water a major difference was observed, due to the fact that after a 4 hour delay, one was able to observe a gradual conversion of cyclohexene to the epoxide, with a relatively high selectivity when compared to the study completed by van der Voort et al. The high selectivity was thought to be due to the gradual detachment of the bonds between the metal and ligand, allowing for an open coordination site to the metal centre. Initially only a small number of bonds would be detached, only allowing for a confined space in which cyclohexene could react with the metal centre and TBHP to be converted into the epoxide. This confined space may have had a hindering effect, preventing the formation of other possible oxidation products, such as tert-butylperoxy-1-cyclohexene, which has a bulky tert-butyl group, which may have trouble coordinating to the cyclohexene molecule. The disadvantages of using water were that over time, more of the bonds between the metal and ligand were broken down leading to vanadium being leached into solution and the gradual structural collapse of the catalyst. With water present, the epoxide was also susceptible to the formation of the cyclohexane-1,2-diol, which is not a desired product.

RU-V2 was found to be catalytically active immediately as the reaction was initiated and brought about rapid conversion of cyclohexene to the epoxide. This was not entirely advantageous, as the epoxide reached a maximum % yield (47%) and was then greatly reduced due to the conversion of the epoxide to the diol. The selectivity was reduced due to the increased formation of the oxidation product; tert-butylperoxy-1-cyclohexene, as the structure was not as highly coordinated as that of RU-V1, so the high selectivity was not observed. The structural integrity of RU-V2 was not maintained for very long, as it was observed to significantly decompose over the 24 hour period from general observation of the reaction medium and from an IR comparison of the catalyst before and after the reaction. An interesting fact to note was that the reaction had reached completion after 24 hours and what is meant by completion is that the % yield of cyclohexene oxide had reached a maximum and had begun to be converted to the diol. RU-V1 had only begun to plateau after a 24 hour period, possibly indicating that the reaction had not yet reached completion.

The idea behind using the decavanadate ion, was to test its catalytic activity for this specific reaction, to determine if the ion could possibly be used in the synthesis of a metal organic framework. The findings were not encouraging, due to the fact that the solid decavanadate ion exhibited no catalytic conversion in the organic phase. Only once dissolved in the aqueous phase, did the ion exhibit any catalytic activity, which is termed as homogeneous activity. This is not a desirable property when deciding if the ion could be a potential building block for a MOF. Throughout the ambient syntheses with the vanadate species it was noted that the ligand and metal salts precipitated out of solution with no coordination between the two. At the pH values at which the syntheses were carried out at it was previously identified that the vanadates would be in the decavanadate form with varying degrees of protonation. When the same reactions were put under solvothermal conditions,

the decavanadate species were found to be broken-down into VO octahedra, which were then able to coordinate to the ligand to give the structure of RU-V1. The conclusion of the decavanadate ion is that it is too large to be functionally incorporated into a MOF, without being broken down into smaller vanadium species first and is highly soluble in water, making it more useful in the application of homogenous catalysis, rather than heterogeneous catalysis.

Future work for RU-V1 would be to monitor the reaction closely with an ICP technique to determine the level of vanadium leaching over time and use XRPD to determine the structural integrity of the MOF over time. This will allow for a determination of exactly when the catalytic activity was greatest and the structural integrity of the MOF remained largely intact. At this point it has been proven that the MOF can be treated and regenerated to its original state, leading to it largely functioning as a renewable heterogeneous catalyst.

Future work for RU-V2 would be to test the V-complex in a reaction system in which water is completely absent, as water was observed to have a particularly harmful effect in terms of the break-down of the structural integrity of the catalyst.

Future work for the decavandate ion in the application of the synthesis of a MOF does not seem promising, but potentially using a ligand which is better suited to coordination with the large ion may yield promising results. MOFs find application in a number of different fields, so if the application of catalysis fails, the MOF or complex can potentially find application in gas storage, sensory applications, etc.

In general, highly coordinated MOFs have not been found to show a great deal of activity when applied in catalysis. This is due to a greater number of bonds which need to be broken or the ligand needs to be folded away [1], to provide a free coordination site to the metal centre. Though depending on the conditions of the reaction, highly coordinated MOFs may be able to yield a desired product with a high selectivity, due to the restricted environment and steric hinderance reducing the chances of other undesired products from forming. Only certain reactions would be suitable for this type of catalyst, i.e. reactions which have a number of competing products. Another factor to take into account would be an activating agent, i.e. water for RU-V1, as the MOFs would need to be activated before any activity could be observed. Modelling of the mechanism of the catalytic reaction would need to be completed, using the proposed single vanadium octahedra centre by Van der Voort *et al* [1]. This will give an in depth understanding of exactly what is occurring.

APPENDIX:

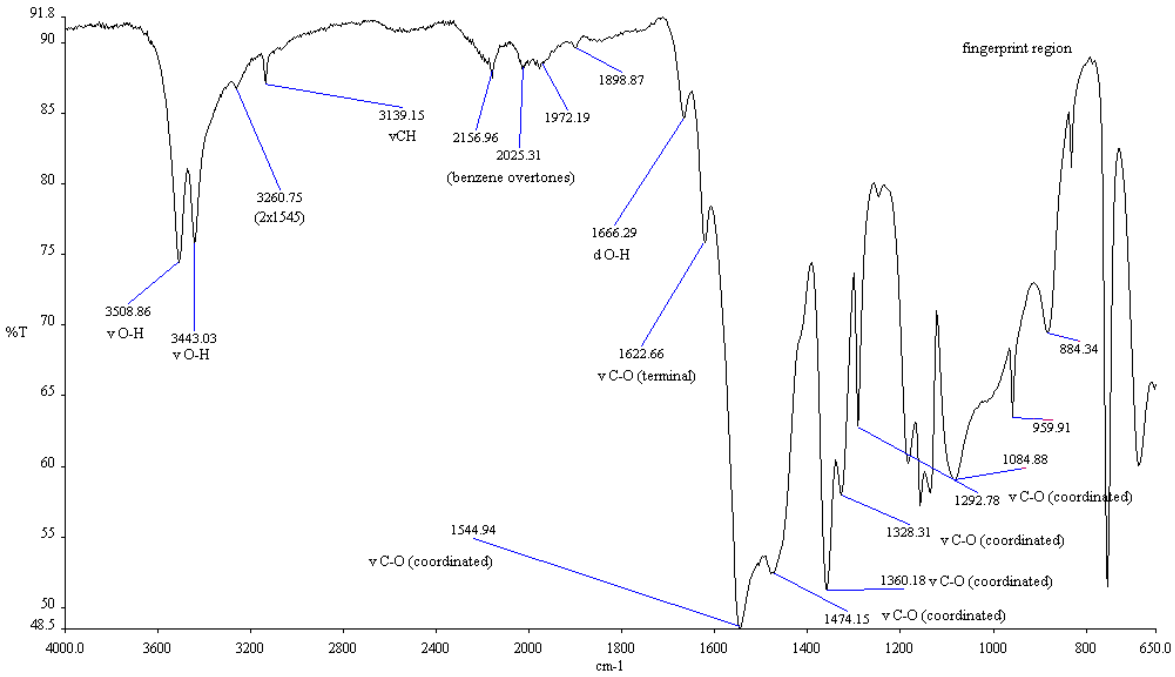

Appendix 1: The IR spectrum of Na-B4C at pH 3.5.

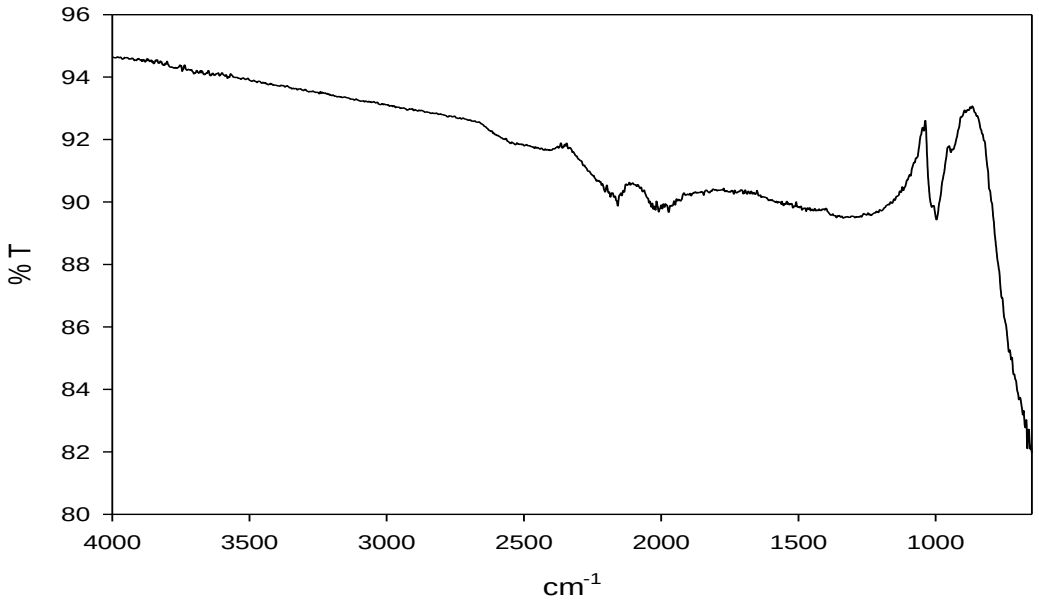

Appendix 2: The IR spectrum of the residue of RU-V2, after TGA.

All ^{1}H and ^{13}C studies were completed using a BRUKER 600 MHz NMR spectrometer.

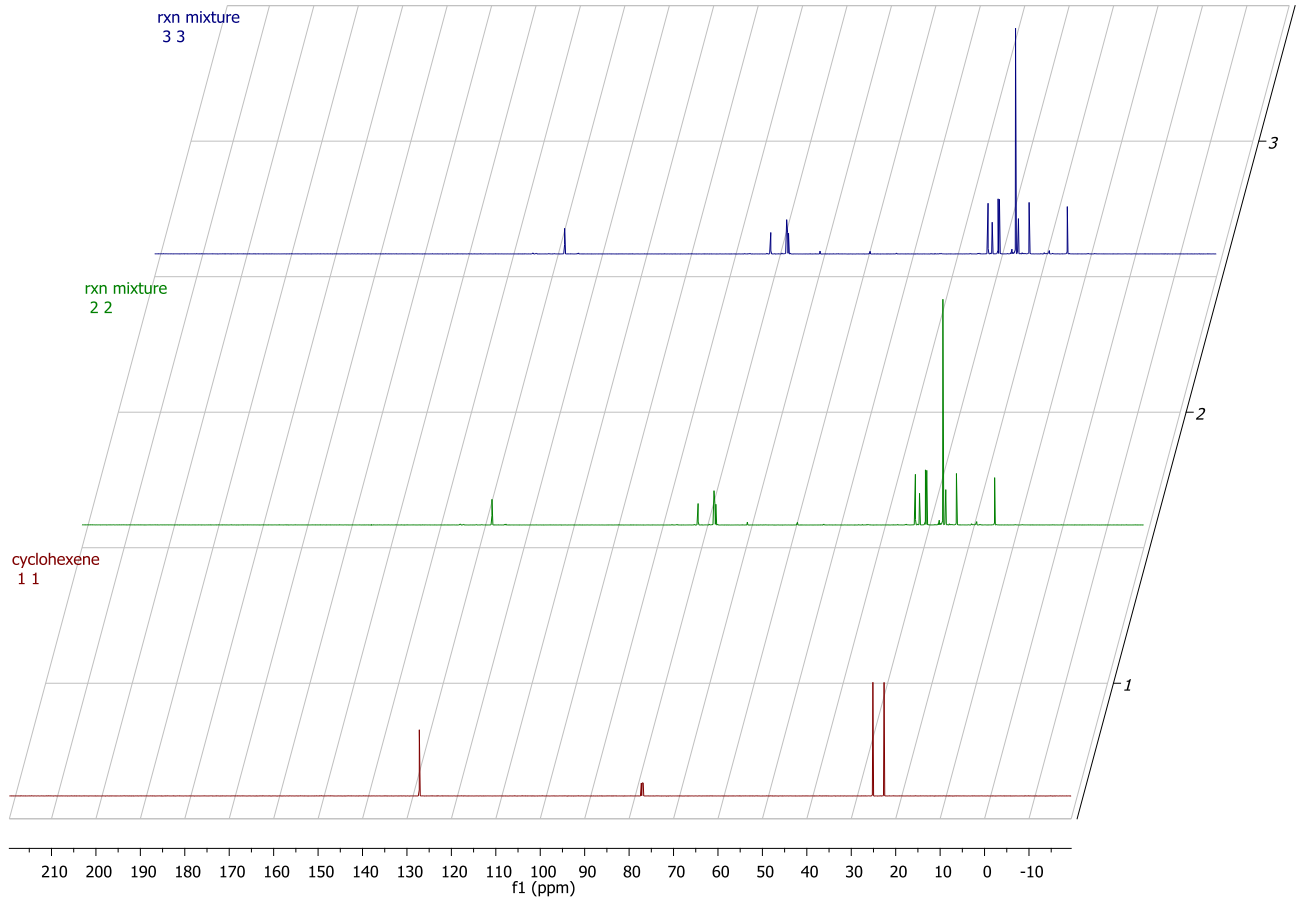

Appendix 3: The ^{13}C NMR spectrum of cyclohexene (spectrum 1) and the reaction mixture with TBHP in decane (spectrum 2), before and after the 72 hours over which the reaction was run.

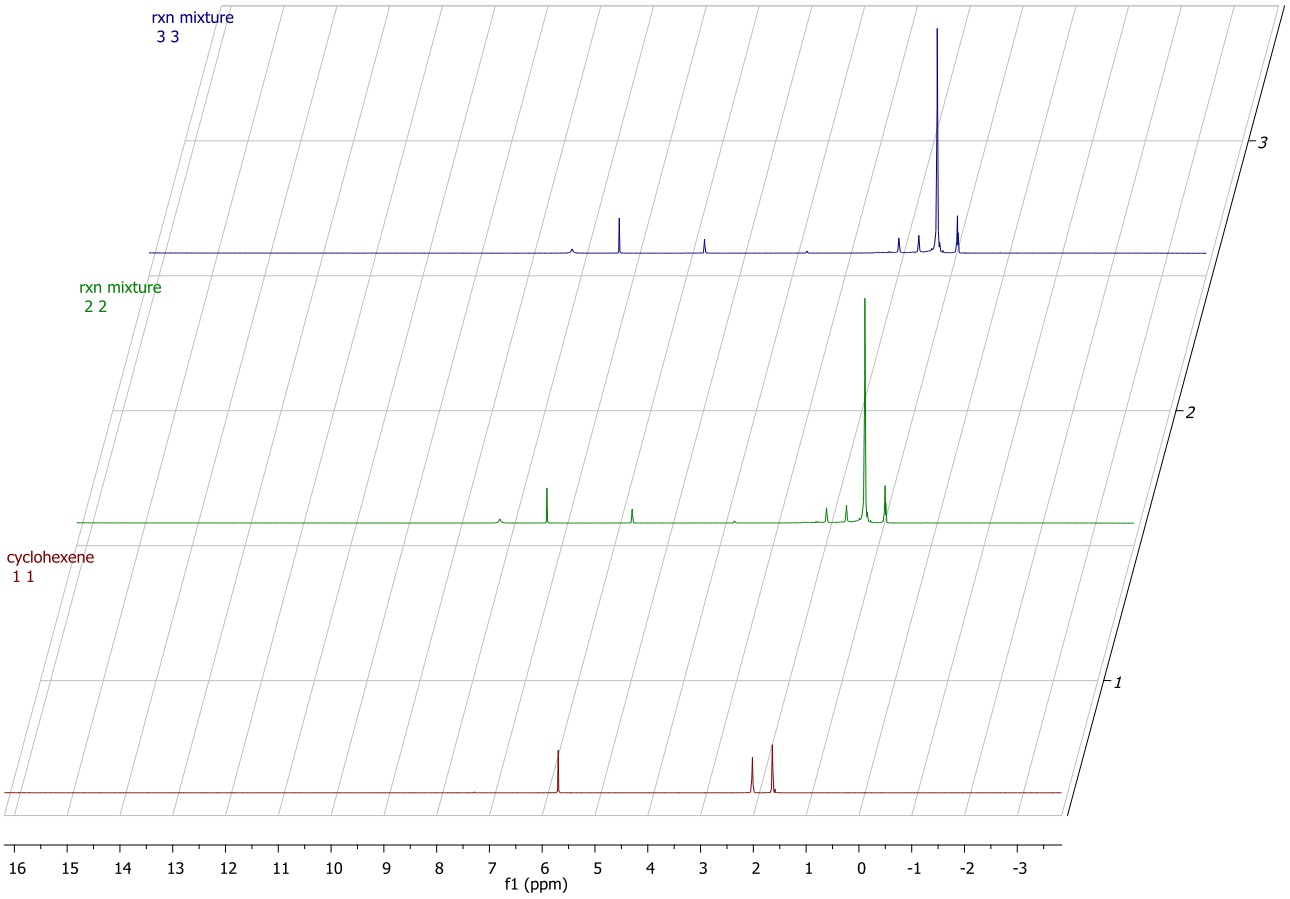

Appendix 4: The ^{1}H NMR spectrum of cyclohexene (spectrum 1) and the reaction mixture with TBHP in decane (spectrum 2), before and after the 72 hours over which the reaction was run.

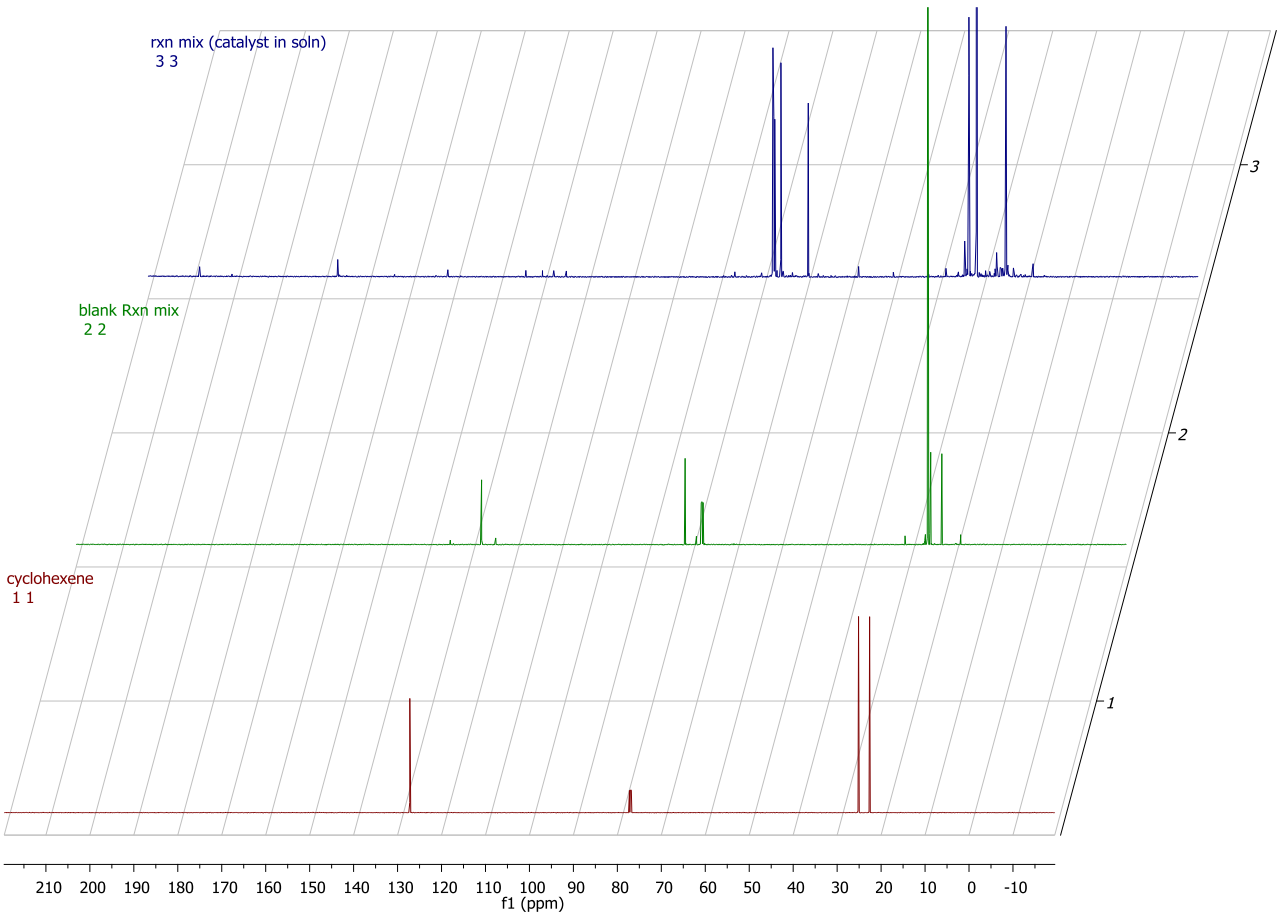

Appendix 5: The ^{13}C NMR spectrum of cyclohexene (spectrum 1), the reaction mixture with TBHP in water, before (spectrum 2) and after (spectrum 3) the 72 hours over which the reaction was run.

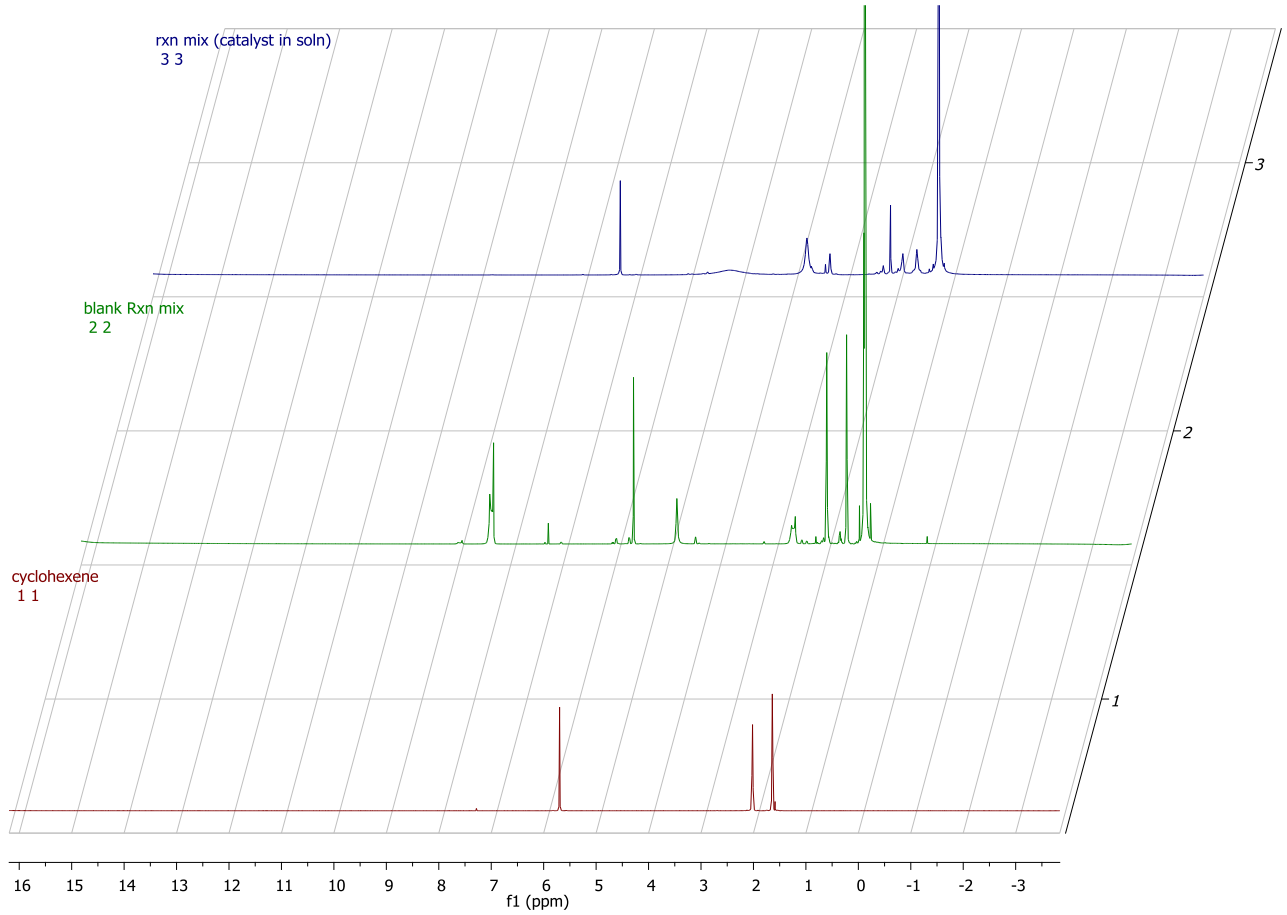

Appendix 6: The ^{1}H NMR spectrum of cyclohexene (spectrum 1), the reaction mixture with TBHP in water, before (spectrum 2) and after (spectrum 3) the 72 hours over which the reaction was run.

Appendix 7: The total number signals for the ^{13}C NMR spectrum of the reaction mixture with TBHP in water after 72 hours.

The peaks were identified using MestReNova Version: 6.0.2-5475, which are provided below:

Reaction mixture:

δ = 207,74; 200,37; 176,32; 163,22; 151,27; 133,52; 129,74; 127,18; 124,31; 85,98; 76,39; 75,50; 75,07; 74,96; 69,28; 57,83; 49,93; 37,96; 33,69; 32,84; 32,73; 31,13; 31,01; 30,89; 26,78; 26,43; 26,31; 26,24; 25,62; 25,32; 25,04; 24,29; 24,22; 23,99; 23,96; 23,86; 22,61; 22,52; 18,12 ppm.

Cyclohexene oxide: (Sigma Aldrich) (http://sdbs.db.aist.go.jp/sdbs/cgi-bin/direct_frame_disp.cgi?sdbsno=1308)

δ = 51,92; 24,18; 19,44 ppm

Cyclohexane-1,2-diol: (Sigma Aldrich)(http://sdbs.db.aist.go.jp/sdbs/cgi-bin/direct_frame_disp.cgi?sdbsno=2416)

δ = 75,61; 33,02; 24,46 ppm

2-cyclohexen-1-one: (Sigma Aldrich)(http://sdbs.db.aist.go.jp/sdbs/cgi-bin/direct_frame_disp.cgi?sdbsno=5498)

δ = 199,65; 150,86; 129,84; 38,13; 25,72; 22,79 ppm

***Tert* butylperoxy-1-cyclohexene:** (Gade & Meder [8])

δ = 133,7; 124,5; 80,0; 76,7; 27,3; 26,8; 25,7; 18,8 ppm

2-cyclohexen-1-ol: (http://sdbs.db.aist.go.jp/sdbs/cgi-bin/direct_frame_disp.cgi?sdbsno=3231)

δ = 130,37; 130,01; 65,43; 32,03; 25,14; 19,25 ppm

Cyclohexene: (Solvent Supplier)(http://sdbs.db.aist.go.jp/sdbs/cgi-bin/direct_frame_disp.cgi?sdbsno=569)

δ = 127,20; 25,10; 22,58 ppm

TBHP: (Sigma Aldrich)

δ = 80,96; 25,73 ppm

Appendix 8: The methodology used for the analysis of the GC-MS data and chromatograms

The results for each catalytic material are presented in the form of speciation curves, which are a combination of line graphs. Each product/reactant is denoted as a separate line graph, which shows the % yield increase of the products and the decrease of reactants over a 24 hour period. The % yields for all products and reactants in each graph were determined by initially using the MassHunter Workstation Software to quantify the area of each of the peaks of interest. This was done using the integration function, where every peak of importance was quantified. The most important peak to integrate was that of the GC standard; 1,2,4-trichlorobenzene, as once the GC standard peak was quantified, it was related to all the other quantified peaks in an effort to standardise any potential differences between the consecutive runs. This was accomplished by dividing the peak area of the peak of interest by that of the peak area of the standard, this was done for both of the duplicates and then averaged. Each run, from 1 to 24, was finally divided by the initial quantification (run 1) of cyclohexene/1,2,4-trichlorobenzene (which would be the maximum amount of cyclohexene) and multiplied by 100 to determine to total % yield for each of the 24 runs.

Error bars are also given, which are simply the difference between the 2 duplicate points for each run.

Examples of the initial chromatograms, whose peaks were quantified to yield the data used, are displayed as the 1st, 12th and 24th runs respectively (Appendix 9, 10 and 11; pg. 116-118). Runs 1, 12 and 24 are displayed to show how the various reactants and products are formed over time. The peaks of interest are labelled on the plots and their peak locations are given in minutes as; Cyclohexene (1,60), tert-Butanol (1,95), $CHCl_3$ (2,42), Cyclohexene oxide (3,23), TBHP (4,06), 2-Cyclohexen-1-one (4,70), 2-Cyclohexen-1-ol (4,82), 1, 2, 4 - Trichlorobenzene (5,53) and Cyclohexane-1,2-diol (6,75). There are minor artefacts in the region of 1,94 to 2,06 and at approximately 3,12, these were analysed extensively and were not found to be anything associated with the reaction and were possibly due to column bleed. The only other area of possible contention, was the peak which closely precedes that of $CHCl_3$ and drops off suddenly, this was also analysed but could not be identified as anything associated with the reaction, as it remained the constant over the entire course of the reaction, neither increasing nor decreasing. The Chromatogram of run 1 is the reaction mixture before the reaction was started, so shows no conversion of cyclohexene. Shifting to the middle of the reaction, the chromatogram of run 12 shows that there is conversion of cyclohexene to cyclohexene oxide, 2-cyclohexen-1-one and 2-cyclohexen-1-ol, with the latter 2 oxidation products both having very low ionisation counts, indicating that they are produced in low concentrations. TBHP can also be observed to be converted into tert-butanol, which would be the by-product after TBHP has reacted with cyclohexene and the metal centre. Finally in the chromatogram of run 24, one can now observe that cyclohexene has been greatly diminished in relation to the standard and cyclohexene oxide has greatly increased terms of ionisation counts, the same trend can be observed for TBHP and tert-butanol. Cyclohexane-1,2-diol can also be observed, indicating that the epoxide is being converted to the diol in the presence of water.

The graphs are plotted as scatter-plots with polynomial trendlines fitted to the data points. The R^2 values are indicated in the legends of the figures to show how representative the specific trendline is of the data points.

The R^2 values for the trendlines of reactants and products with a large % yield, namely; cyclohexene, cyclohexene oxide and cyclohexane-1,2-diol, were all satisfactory as they were all above 0.9, indicating that the trendline was an accurate representation of the data points. The R^2 values for trendlines of the products with a low % yield, namely; 2-cyclohexene-1-one and 2-cyclohexene-1-ol, did not fit the data points to such a high degree, with the R^2 values only being above 0.7. A possible explanation for this was due to the fact that both 2-cyclohexene-1-one and 2-cyclohexene-1-ol only formed in very low amounts initially, which may have been too small to be identified to an accurate degree by the detection limits of the GC system, possibly resulting in the fluctuations between the data points.

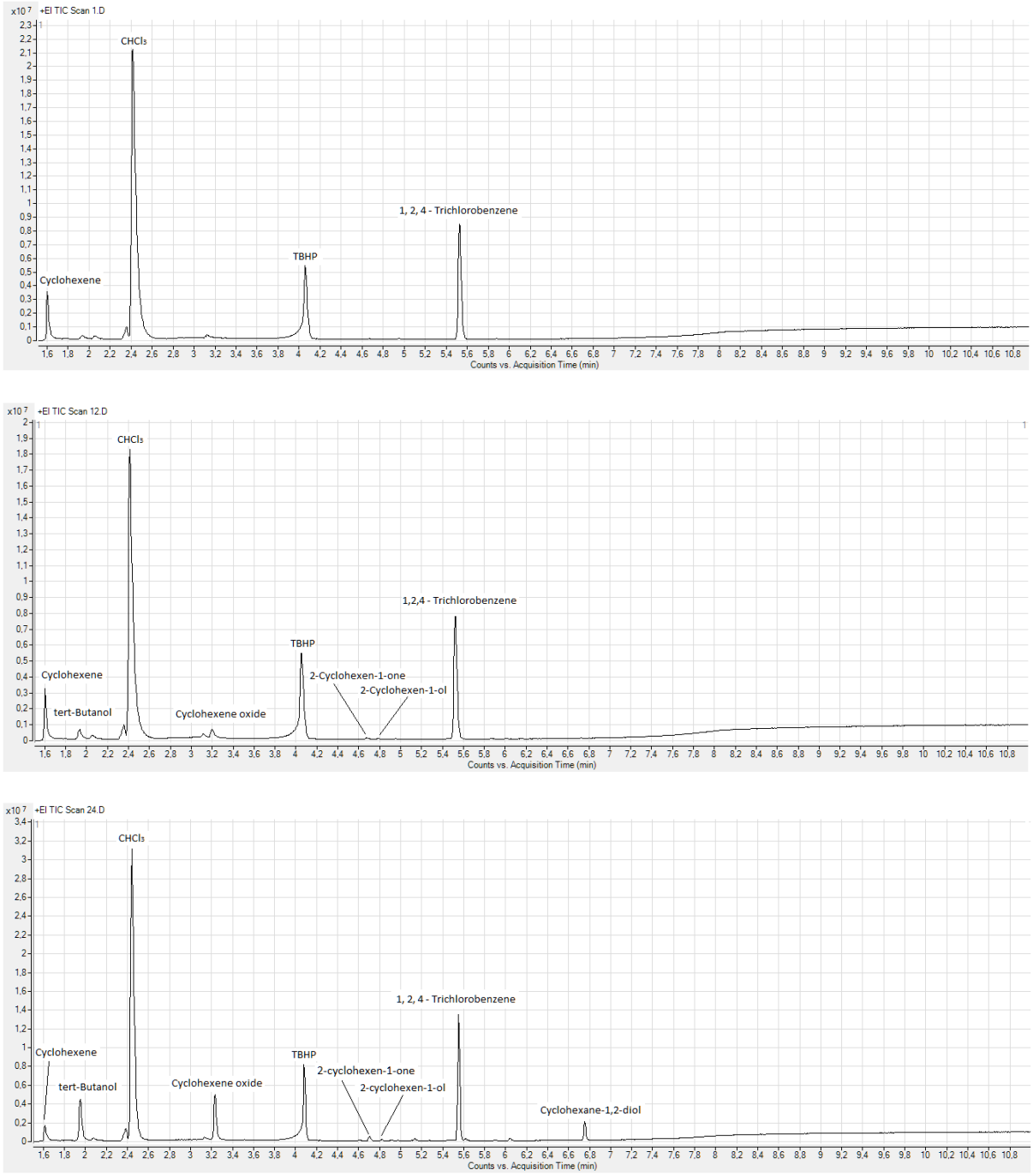

Appendix 9: A comparison of the GC chromatograms for runs 1, 12 and 24 hours, using RU-V1 as a catalyst.

The chromatograms have had the peaks labelled and are plots of the ionisation counts vs acquisition time.

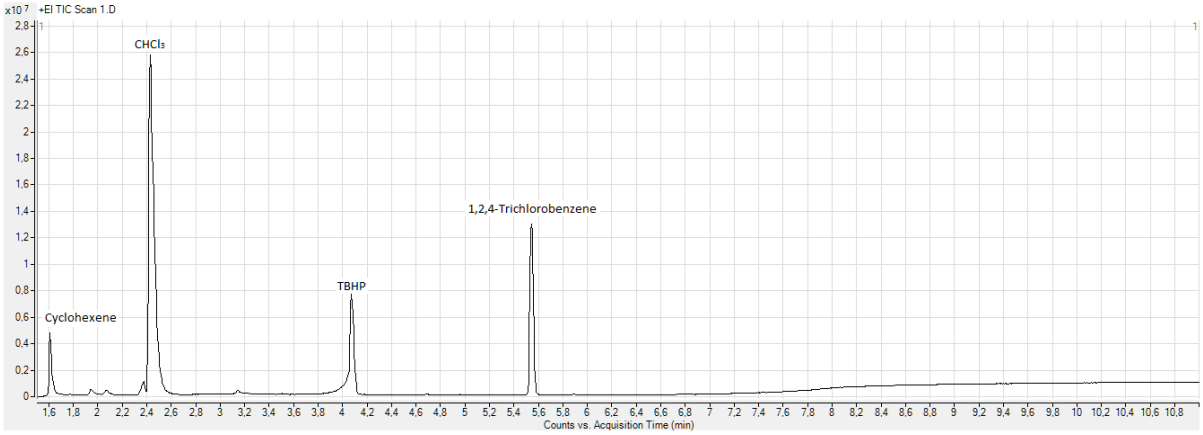

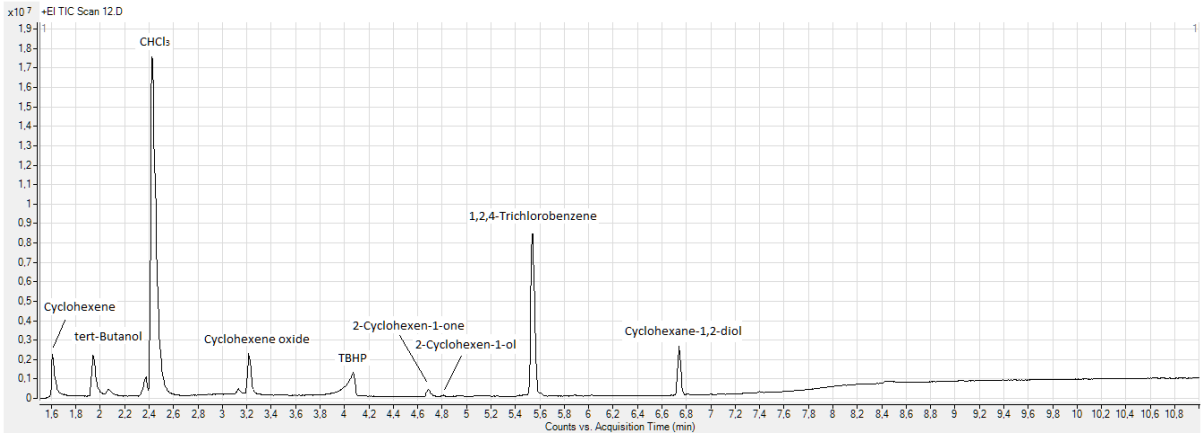

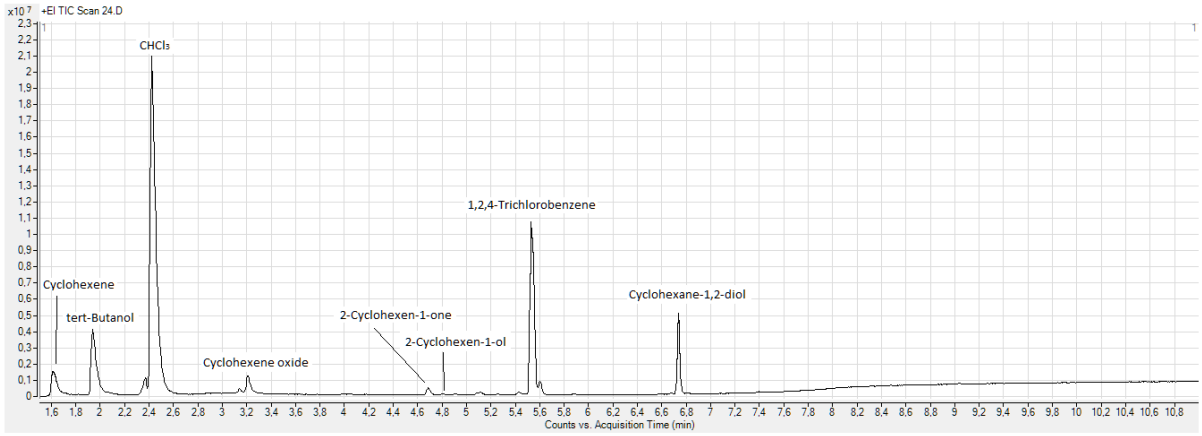

Appendix 10: A comparison of the GC chromatograms for runs 1, 12 and 24 hours, using RU-V2 as a catalyst.

The chromatograms have had the peaks labelled and are plots of the ionisation counts vs acquisition time.

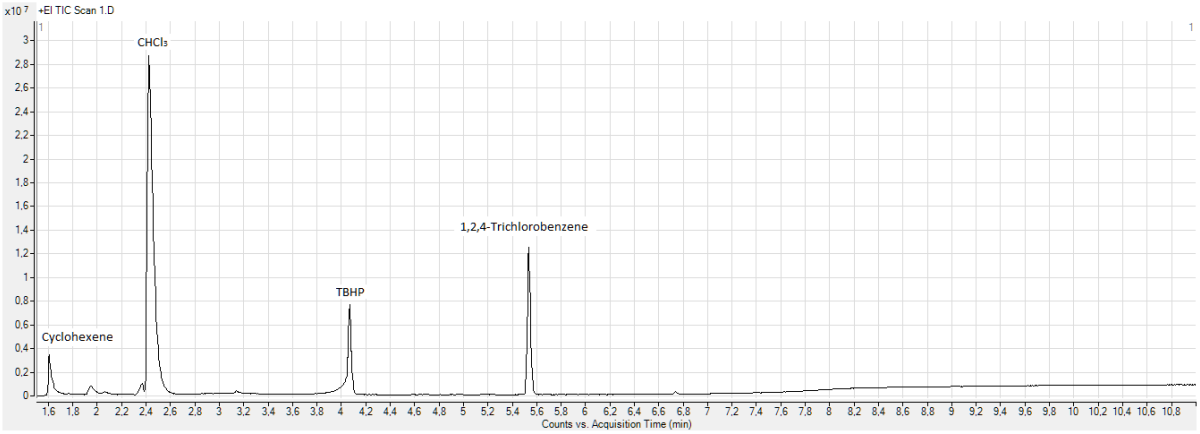

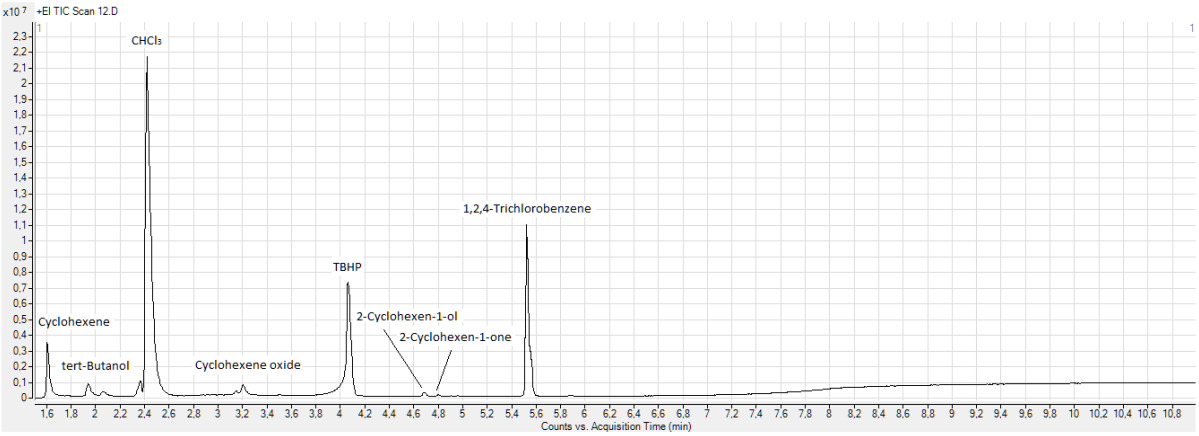

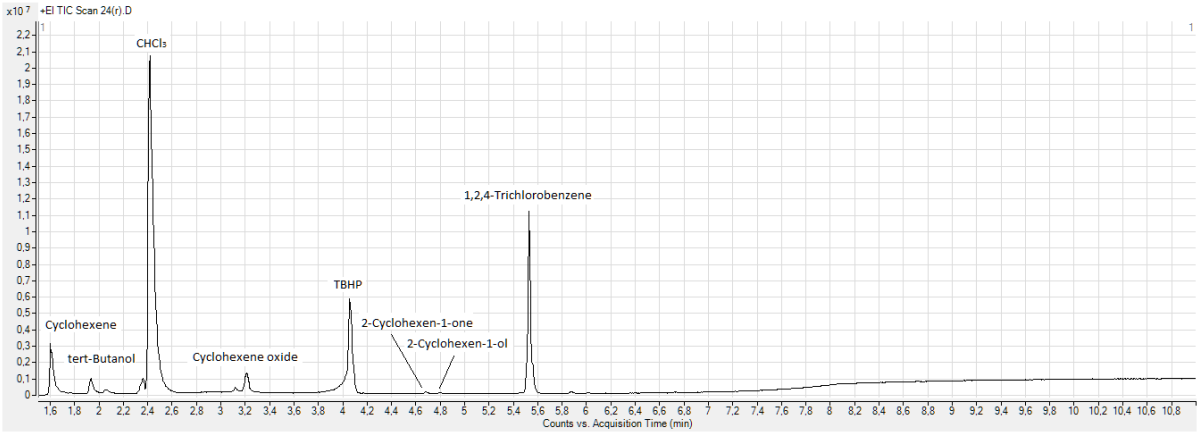

Appendix 11: A comparison of the GC chromatograms for runs 1, 12 and 24 hours , using the solid decavanadate ion as a catalyst.

The chromatograms have had the peaks labelled and are plots of the ionisation counts vs acquisition time.

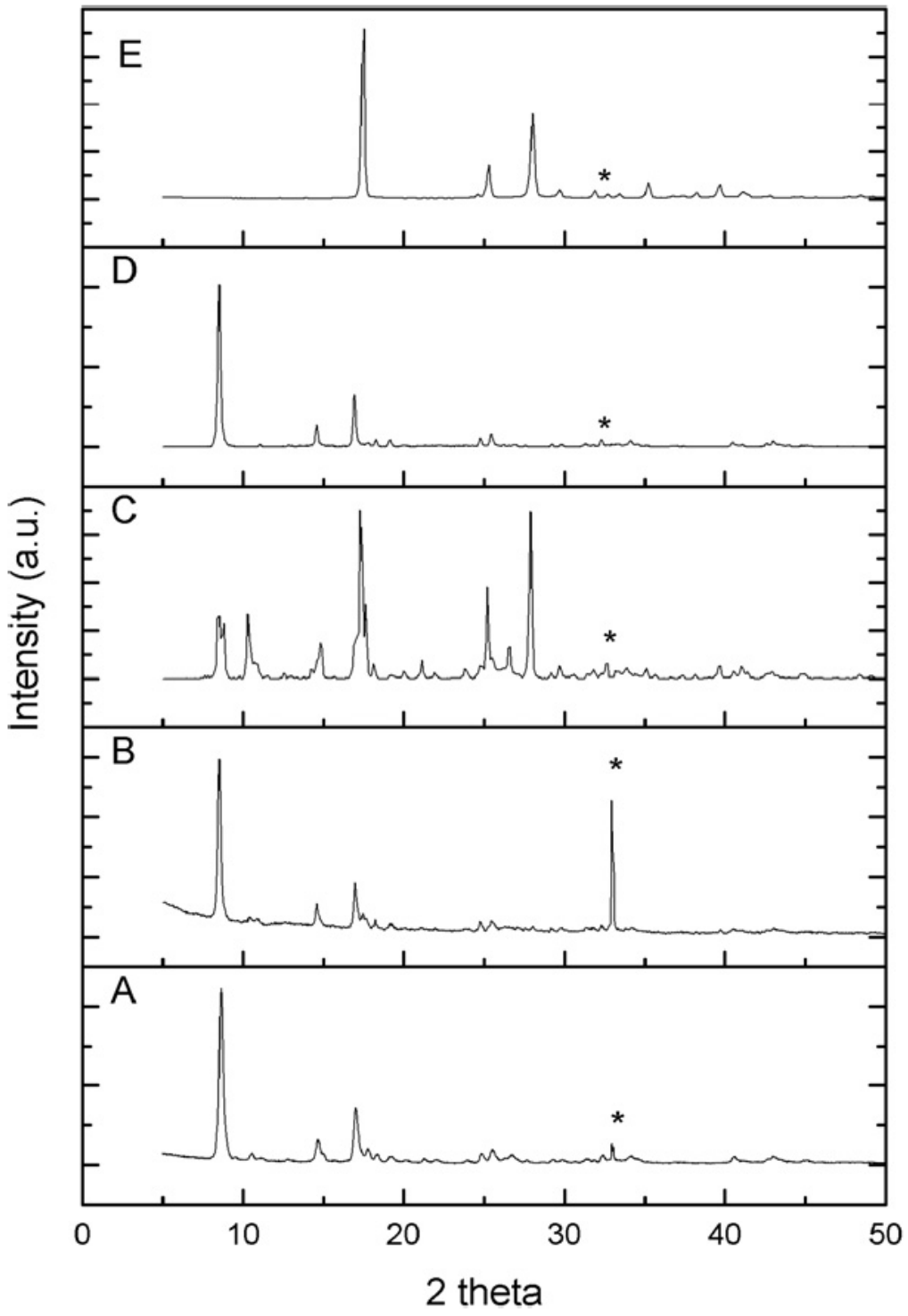

Appendix 12: A comparison taken directly from the study completed by Van der Voort et al, which shows the powder diffraction patterns of MIL-47

A = MIL-47, B = MIL-47 after a reaction with TBHP in decane, C = MIL-47 after a reaction with TBHP in water, D = MIL-47 after regeneration and E = 1,4-benzenedicarboxylic acid. There was a fluctuation in intensity with the peak at 32,9°, due to a background effect from the angle of the sample holder.

IR Absorption Spectrum

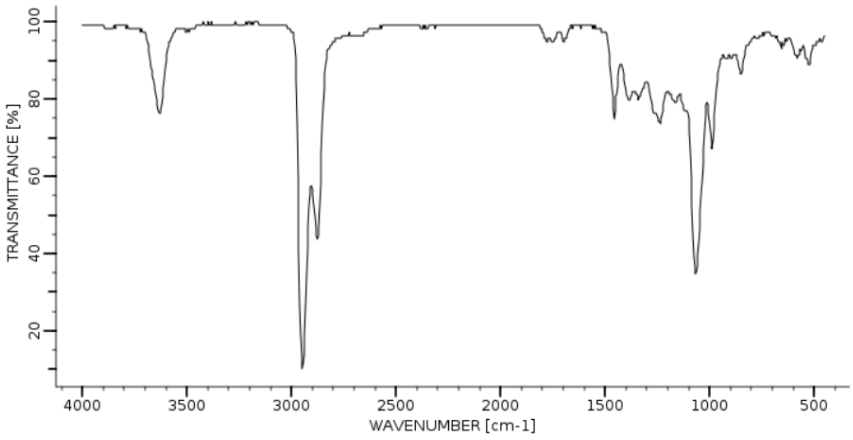

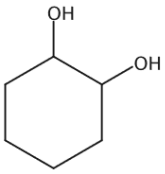

SPECTRUM ID
BR140212

CAS REGISTRY NUMBER
931-17-9

FORMULA
$C_6 H_{12} O_2$

CAS INDEX NAME
1,2-Cyclohexanediol

SPECTROMETER
BIO-RAD DIGILAB FT-IR OR EQUIVALENT

SOURCE
Infrared spectral data from the Bio-Rad/Sadtler IR Data Collection was obtained from Bio-Rad Laboratories, Philadelphia, PA (US). Copyright © Bio-Rad Laboratories. All Rights Reserved.

Appendix 13: The IR absorption spectrum for cyclohexane-1,2-diol taken from the Bio-Rad/Sadtler IR Data Collection.

IR Absorption Spectrum

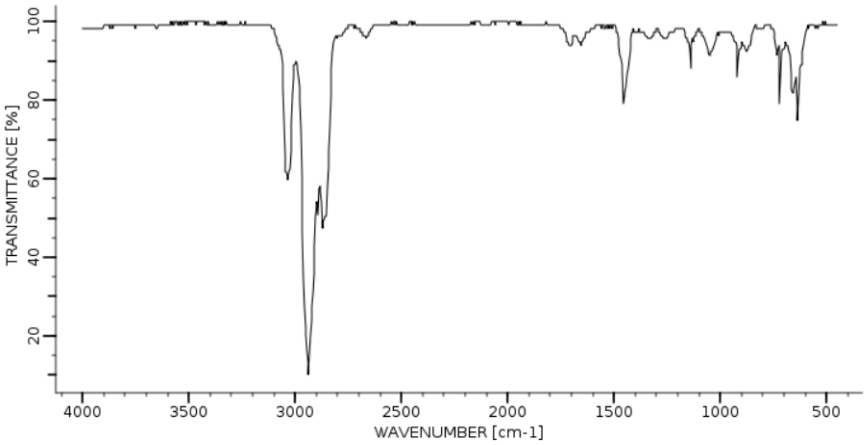

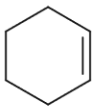

SPECTRUM ID
BR157331

CAS REGISTRY NUMBER
110-83-8

FORMULA
$C_6 H_{10}$

CAS INDEX NAME
Cyclohexene

SPECTROMETER
BIO-RAD DIGILAB FT-IR OR EQUIVALENT

SOURCE
Infrared spectral data from the Bio-Rad/Sadtler IR Data Collection was obtained from Bio-Rad Laboratories, Philadelphia, PA (US). Copyright © Bio-Rad Laboratories. All Rights Reserved.

Appendix 14: The IR absorption spectrum for cyclohexene taken from the Bio-Rad/Sadtler IR Data Collection.

INSTRUMENTATION APPENDIX:

In this section, the detailed descriptions of all the instrumentation used within this thesis are discussed. All of the instruments discussed have their specifications provided in Chapter 2. The references provide here refer to those present at the end of Chapter 2.

Instrument Appendix 1: Elemental Analysis

CHNS analysis is a type of gravimetric analysis where by the sample of interest is heated in the presence of oxygen. Various combustion products, such as carbon dioxide and water vapour are released from the sample and are collected in a number of different traps, each specific to a combustion product. The masses of the combustion products collected can then be used to determine the total mass percentages of carbon, hydrogen, nitrogen and sulphur within the initial sample [11].

ICP-OES and AA are forms of spectroscopy which make use of the specific energy emissions or absorptions made by a sample via photons. The energy of the photons is determined by the change in energy between ground and excited states and this change in energy is dependent on the nature of the atom or ion which is emitting or absorbing it, so can be used to identify specific atoms within a sample, both qualitatively and quantitatively [11]. ICP uses inductively coupled plasma to excite the electrons within the atoms of the sample to higher energy levels, after a short time period, the electron returns to the ground state and in the process, emits electromagnetic radiation with a wavelength specific to the element of interest [11]. The intensity of the radiation emitted can be used to determine the concentration of the element within the sample. AA uses a similar process, but instead of plasma, a flame is used to excite the electron into higher orbitals and the absorption is measured instead of the emission, which is known to have a better signal to noise ratio [12].

Instrument Appendix 2: Vibrational Spectroscopy

Vibrational spectroscopy analyses the vibrational transitions that occur when a molecule absorbs infrared radiation and begins vibrate at a higher energy state. The positions of the vibrational transitions are a reflection of the structure of the molecule and functional groups present and can offer useful insights into the type of binding present. These transitions occur at between 100 and 10000 cm^{-1}, any higher than this and the energy begins to move into the visible and ultra-violet region, where the electrons begin to be excited into higher energy levels [13]. Vibrational transitions can be observed as either infrared or Raman spectra. Infrared spectra are a result of the absorption of a photon in the infrared spectrum, whilst the molecule is in its electronic ground state [13]. Raman spectra make use of a laser which emits radiation over a range of different wavelengths, to polarise the electron density about a molecule. This polarization causes light from the incident beam to be scattered in the both the form of Rayleigh scattering and Raman scattering. Rayleigh scattering is an

elastic scattering process, where the frequency of the scattered radiation is identical to that of the incident radiation [13-14]. Raman scattering is an inelastic scattering process, which is determined by the vibrational frequency of the molecule. The molecule absorbs a portion of energy to become excited to a higher vibrational state, so there is an energy difference between the incident radiation and the scattered radiation [13]. This difference will represent the vibrational frequency of the molecule [13-14].

Instrument Appendix 3: X-Ray Powder Diffraction

When material is defined as being crystalline, the atoms distribute themselves in such a way that a pattern occurs, which is characterised by the ordered repetition of a unit or unit cell. It is possible to determine the size and structural factors of a material by using X-ray powder diffraction. This is done by directing X-radiation at the sample of interest. The interaction of the incident X-radiation with the sample causes an electron from an inner orbital, within the sample atom to be excited to a higher orbital [15]. When relaxation occurs, X-radiation is emitted and interacts with the incident X-radiation, either constructively or destructively. When the radiation interacts constructively, it is said to have been diffracted and it satisfies Braggs law; $n\lambda=2d \sin\theta$, where n is an integer, λ is the wavelength of the incident radiation, d is the distance between 2 successive lattice planes and θ is the angle of the incident radiation to the sample [16]. Braggs law allows for the relation between wavelength of the X-radiation, diffraction angle and distance between two lattice planes (d-spacing) [15][16].

Instrument Appendix 4: Thermogravimetric Analysis

TGA is a technique which measures the change in the mass of a sample over time, where the temperature is programmed to increase at a set rate, under an inert atmosphere [17]. The specific mass losses can be used to confirm an empirical formulae determined by microanalysis, as the FTIR attachment is able to confirm what is being lost at each step and these can be used to identify what was initially present and its relative quantity. An important use for TGA is the determination of how many guest molecules are held within the complex, as this is linked to the pore size, and at what temperature they are released. Both of these properties can be linked to the application which they can be used for, e.g. adsorption of a specific molecule of interest, heterogeneous catalysis, etc. The overall thermal stability of the complex can also be determined with and without the guest molecules. A number of MOFs have their stability linked to the inclusion of their guest molecules, so after these have been released, it is generally seen that the MOF breaks down shortly after, which can be a problem specifically for heterogeneous catalysis and the adsorption and desorption of molecules at elevated temperatures [18].

The nature of the particle size of the sample is an important factor in TGA, as the heating of the sample should be as uniform as possible. For this reason the sample should be in the form of a powder, as this will have the best thermal conductivity [17-19].

Instrument Appendix 5: Differential Scanning Calorimetry

DSC is a thermoanalytical technique, which determines the differences between a sample and a reference material. The sample of interest is entered into a sample pan and the reference material, i.e. an empty sample pan, are heated at the same rate under a controlled temperature program. The objective in power-compensated DSC is to maintain a constant temperature between both the sample and reference material, but for the sample there will generally be processes which alter the energy required. An exothermic process will release energy, so the amount of power required will be reduced, as energy is being released from the sample, whereas the opposite is true for an endothermic process [17]. The difference in power is what is ultimately recorded, and the area of a peak for a given process can be related to the change in enthalpy (ΔH) [19].

Instrument Appendix 6: Gas Chromatography

Gas chromatography is a very useful technique for the separation of compounds which can be volatilised without decomposition, which in this study are volatile organic compounds (VOCs). GC uses 2 phases to achieve separation; the mobile phase, which consists of an inert gas, such as helium, which carries the volatised components through the column and the column itself, which consists of a stationary phase. The stationary phase consists of a coating on the inside of the column that interacts with each of the components, bringing about the separation. Separation in GC is determined by the time upon which a component is retained on the column, which is known as its specific retention time [20]. Each component will have a different retention time, depending on its chemical structure and the chemical structure of the column. There are a number of interactions which can occur between the column and analyte, such as dipole interactions and hydrogen bonding, but it is often difficult to assess each of these interactions individually, so the term 'polarity' is used to simplify the issue. Polarity is a useful in explaining GC separations and retention times, as a column which has a high polarity, such as a PEG column, will retain analytes of a high polarity longer than analytes of a low polarity and the opposite is true of columns with a low polarity [21].

GC-MS is an efficient coupling of 2 techniques into a single instrument to determine the specific mass of the separated products and from the mass, one can determine the identity of the product. It is specifically useful in reactions which form a number of products, as the products will be separated on the column, due to their specific polarities and then will be entered into a mass spectrometry detector, which allows for their identification. Mass spectrometry works by ionising the sample of interest, which causes it to break down into smaller charged fragments [22]. These fragments are separated by an electric or magnetic field, due to the specific amount of charge associated with each fragment and finally analysed by a detector with the capability of detecting charged particles [22]. A fragmentation pattern is built up, as the compound of interest is broken down into smaller fragments and is completed when the compound is completely broken down into the

smallest and most stable fragments [23]. The fragmentation pattern is then compared to a database which has recorded fragmentation patterns for a wide range of different compounds, so the identity of the molecule can be found.

Instrument Appendix 7: Scanning Electron Microscopy – Energy Dispersive X-ray Spectroscopy

SEM is an analytical technique, which uses a beam of electrons to scan over the surface of a material and thereby produce an image. The electron beam interacts with surface of the material to produce secondary and backscattered electrons. Secondary electrons are a product of inelastic scattering, when the primary electron beam has sufficient energy to reach the ionisation potential of the material, a secondary electron will be released [25]. Secondary electrons are used in the production of SEM image. Back-scattered electrons however, are a product of elastic scattering, as they have the same energy as the primary electron beam. They are used in the identification of different elements and their distribution within the material, as their intensity is related to the atomic number of the element present. Samples are generally coated an ultra-thin layer of conducting material, which is most often gold. This allows the electrons that have either interacted with the sample, namely secondary and back-scattered electrons, to be received with a better signal to noise ratio, thereby producing a clearer image [24].

EDX uses back-scattered electrons by using the primary electron beam to 'knock' an electron from one of the inner orbitals within an atom, thereby creating a 'hole'. An electron from an orbital with a higher energy, subsequently drops down to fill the 'hole' and in so doing, releases energy in the form of an x-ray [24]. This x-ray is dependent on the difference between to higher and lower energy levels and this difference is unique to the specific element of interest. Therefore once the x-ray is detected, the element can be identified. EDX is not a quantitative method of analysis, due to the fact that only the surface of the material is scanned and the surface may be inhomogeneous, leading to the release of the x-radiation in any possible direction, which may not be picked up by the detector. The energy differences between orbitals in similar elements can also overlap, so care must be taken in the identification of these elements [24].

Supplementary data:

The excel spread-sheets containing the data used to construct the speciation curves is attached on the accompanying CD.